Quantification of Life-stage Transition Behaviors in Harmful Algae and their Implications for Pelagic and Benthic Distributions

Elizabeth D. Tobin

A dissertation

submitted in partial fulfillment of the

requirements for the degree of

Doctor of Philosophy

University of Washington

2014

Reading Committee:

Dr. Daniel Grünbaum, Chair

Dr. Rose Ann Cattolico

Dr. Evelyn Lessard

Program Authorized to Offer Degree:

School of Oceanography

University of Washington

Abstract

Quantification of Life-stage Transition Behaviors in Harmful Algae and their Implications for Pelagic and Benthic Distributions

Elizabeth D. Tobin

Chair of the Supervisory Committee:
Professor Daniel Grünbaum
School of Oceanography

Harmful algal blooms (HABs) occur when accumulations of algae or algal toxins have adverse impacts on aquatic ecosystems, public health and/or coastal resources. Many of the behavioral and physiological functional traits that regulate HAB dynamics remain poorly understood. Improved understanding of these traits and innovative technologies to detect HAB cells *in situ* are important for assessing future bloom scenarios and establishing appropriate HAB mitigation and management strategies.

Many HAB-forming species exhibit a dual-stage life history, alternating between pelagic and benthic life stages. Rates of transition between pelagic and benthic habitats can regulate cell dispersal and contribute to the timing and severity of HABs. Yet, life stage transitions are among the least understood aspects of HAB dynamics. The focus of this research was to characterize

and quantify behaviors of harmful motile marine algae during life-stage transitions and to assess their influence on pelagic and benthic population distributions.

Two HAB species that commonly occur in the Salish Sea, the fish killing raphidophyte, *Heterosigma akashiwo*, and the toxic dinoflagellate, *Alexandrium catenella*, were the focus of these studies. A combination of field, laboratory and modeling methods were used to elucidate the role of life-stage transitions in bloom dynamics. The primary objectives were to (1) examine benthic emergence characteristics of naturally occurring cysts of *A. catenella* (Chapter 2); (2) quantify strain-specific swimming characteristics during life stage transitions of *H. akashiwo* (Chapters 3 & 4); (3) assess how specific behavioral and physiological traits regulate vertical fluxes and population distributions of *H. akashiwo* (Chapters 3 & 4); and (4) develop a low cost, field-deployable sensor to detect and characterize algal benthic emergence *in situ* (Chapter 5).

The research outcomes indicated that important algal physiological and behavioral traits, including cell survivorship during transitions between life stages, internal regulation of benthic emergence rates, transitional swimming behaviors and post-transition specific growth rates, govern vertical distributions of some harmful algae and the timescales over which HABs form and dissipate. These traits were shown to be largely species and strain dependent, resulting in both species- and region-specific benthic emergence and growth strategies. Results demonstrate that behavioral and physiological traits expressed during life-stage transitions play critical roles in regulating distributions of harmful algal populations. Further, *in situ* detection and monitoring of benthic emergence and other behavioral traits of harmful algae will improve mechanistic understanding of HAB formation and enhance our capacity for successful bloom prediction.

In dedication to my parents,

thank you for your love and support.

Acknowledgements

This doctoral thesis would not have been possible without the support of the many people that I worked and engaged with during my time at the University of Washington, School of Oceanography. I am truly grateful to everyone who assisted me throughout this scientific journey.

First, to my advisor, Danny Grünbaum, thank you for everything that you have done for me. I have learned so much and benefited greatly from the 7 years I spent working in your lab. The intellectual and creative freedom that you provided, and strongly encouraged, allowed me to succeed in my doctoral program and has prepared me for a rewarding interdisciplinary career. Thank you for showing me that I can accomplish anything that I set my mind to.

Thank you to the other members of my thesis committee: Neil Banas, Rose Ann Cattolico, Loveday Conquest, Rita Horner, Evelyn Lessard and Parker MacCready. Each one of your contributions greatly improved this thesis and the intellectual journey that proceeded it. I am especially grateful to Rose Ann, who incorporated me into her lab and provided me with the support and infrastructure required to make this research possible. You have been a wonderful mentor and friend.

Thank you to the members of the Grünbaum lab: Owen, Karen Tansy, Mike and Rachel, and everyone in the Cattolico lab for proving great friendship and support throughout the years. All of you made the lab an enjoyable and fulfilling place to work. A very special thanks to Randy, Tor and Dave in Ocean Engineering, and Jim Postel in Pooled Equipment. The advice, guidance

and assistance that you provided made much of this work possible. I also would like to thank my undergraduate research assistants, Jessica Chess and Colin M. Katagiri, who worked with me for many hours in the field and lab to collect, process and analyze samples.

I have been especially fortunate to make many wonderful friends in graduate school who helped to keep me sane (to the best of their ability). Andrea, Kirsten, Jesse and Alyssa who distracted me from the trials and tribulations of scientific research with wine, dancing, great conversation and a variety of adventures. Karen, my academic sister, who always provided intellectual and emotional support, as well as, amazing baked goods. My husband, Tyler, who always knows how to make me laugh and has proven to be an excellent field hand!

Finally, a big thank you to Chris MacGregor who developed the specialized imaging processing software that was critical to the success of my research. You have been a great friend and collaborator, going above and beyond your computing and programming expertise by spending countless hours in the lab and in the field assisting me with instrument development and deployments. I am very grateful for all that you have done.

Financial support for this research was provided by the National Oceanic and Atmospheric Administration (NOAA) Coastal Ocean Program (#NA04NOS4780273 to R. Horner); NOAA Washington State Sea Grant (#NA040AR170032, # NA10OAR-4170057 to D. Grunbaum, and #NA16RG1044AMO9, # NA07OAR-4170007 to R.A. Cattolico); the NSF, OACIS GK-12, Link Foundation Ocean Engineering and Instrumentation, and the NSF, IGERT Program on Ocean Change Fellowships.

Table of Contents

List of Tables

List of Figures

Chapter 1. Introduction

Harmful algal blooms (HABs) are diverse phenomena that occur when algae produce toxins or accumulate to densities sufficient to be deleterious to other organisms, to damage aquatic ecosystems, to pose risks to public health and/or to threaten aquatic resources [1–4]. HABs have significant ecological and social impacts that affect nearly all coastal environments throughout the US and worldwide [5]. Over the last several decades, HABs are reported to be increasing in frequency, magnitude and intensity [4,6]. The reasons for this apparent increase, and more generally the diverse environmental factors promoting and suppressing HABs, remain poorly understood [7]. Enhancing our ability to manage and mitigate the impacts of HABs requires improved understanding of the mechanisms underlying their occurrence and recurrence.

1. 1 *Dual-stage Life Histories of Many Harmful Algae*

Many HAB-forming algae exhibit a dual-stage life history in which they transition between a pelagic vegetative stage and a benthic resting stage. The benthic resting stage is thought to promote survival during environmental conditions that are unfavorable to growth, to provide refuge from predation, and/or to facilitate long-range transport [8–13]. The benthic resting stage has functions comparable to seed banks in terrestrial plants, with analogous consequences for genetic diversity, fitness and evolution of algal populations [14–16].

Despite having potentially important impacts on HAB timing and severity, transitions between pelagic and benthic stages are among the least studied aspects of bloom dynamics, and their causes and consequences are therefore poorly understood. Rapid transition of pelagic vegetative cells into the benthic resting stage may contribute to bloom termination. Benthic populations may serve as reservoirs that initiate blooms by rapidly reseeding the water column with

vegetative cells when favorable conditions return [17–19]. Hence, transitions into and out of the benthic resting stage may strongly affect the timing, location and magnitude of HABs [20–23].

HAB-forming species may exhibit sexual and/or asexual life history strategies in response to a variety of biotic and abiotic signals, including nutrient limitation, changes in temperature and/or salinity, turbulence, interactions with algicidal bacteria or endogenous regulation [24–30]. Asexual reproduction occurs by binary fission, often producing motile, vegetative cells in the water column. Vegetative cells may enter a temporary benthic resting stage during adverse environmental conditions, from which they revert back to the vegetative stage once conditions again become favorable. Sexual reproduction occurs by the formation and fusion of gametes that produce swimming zygotes, which eventually become dormant as long-term or "over wintering" benthic cysts [31,32].

Transitions between pelagic and benthic habitats often involve significant vertical movements. Vegetative pelagic cells are typically concentrated in the near-surface waters of the photic zone. These cells cannot establish benthic populations until they descend to encounter the benthic substrate. Similarly, benthic cells must ascend to near-surface waters for growth and subsequent bloom development. The timing and rate of these depth changes can have significant impacts on HAB dynamics. Horizontal currents vary in speed and direction over time and with depth. Algal cells cannot swim against these currents and, therefore, can be quickly transported by lateral advection between suitable and unsuitable habitats for survival and growth [8,21,33].

1.2 *Motility in Harmful Algae*

Many HAB-forming algae use active swimming in their pelagic phase to regulate depth and locate growth favorable microenvironments [34–37]. Of the 34 HAB-forming species identified along the U.S. West Coast, 25 are motile [38]. The majority of these motile algae use flagella to propel themselves through the water. Flagella are arranged in various geometries with a variety of beating mechanisms across algal taxa [39,40], resulting in unique swimming modes that can provide potentially valuable diagnostic information for cell identification. Motile algal species have a potential advantage over some non-swimming species because swimming enables cells to regulate their vertical position, and locate nutrients (e.g. chemotaxis) and other resources essential to growth (e.g. phototaxis) that vary across time and space [41,42].

Motile marine algae typically have the capacity to swim substantial vertical distances at speeds up to hundreds of μm s^{-1} [43]. Maximum swimming speeds for many harmful flagellated species have been reported between 100-500 μm s^{-1} [34,36,44–46], providing the potential to cover tens of meters per day. The ability of algal cells to migrate vertically great distances within a 24 hour period has been well documented. Diel vertical migration is one example of this behavior [47,48]. The prevalence of vigorous swimming in HAB-forming algae during the pelagic vegetative stage suggests that behaviors expressed during pelagic-benthic transitions may strongly regulate vertical fluxes. Hence, transitional behaviors could have significant but currently unknown impacts on population-level distributions of HAB-forming species.

1.3 *Variability in Behavioral and Physiological Traits*

Behaviors expressed between pelagic and benthic life stage transitions can be both species- and strain-dependent. For example, *Alexandrium fundyense* (within the *Alexandrium tamarense* species complex) in the Gulf of Maine appears to have an internal mechanism, referred to as an "endogenous clock", that regulates emergence to a specific time of year irrespective of environmental conditions [11,49]. Yet, cysts of the *Alexandrium tamarense* species complex found in sediments in southern France [50] and Puget Sound, WA [51] do not appear to express such a tightly controlled, synchronous emergence behavior. Within *Alexandrium catenella*, strong variation in the timing and rate of benthic emergence has been reported among distinct geographic strains [9,27,52]. Inter-strain variation in cell survivorship, and rates of benthic resting cell formation and emergence have also been reported among strains of the harmful raphidophyte, *Heterosigma akashiwo* [53,54].

Algal swimming can also vary among or within a species of the same genus. Significant differences in maximum swimming speed were observed among three *Alexandrium* species: 474 μm s^{-1} for *A. minutum*, 406 μm s^{-1} for *A. tamarense* and 227 μm s^{-1} for *A. ostenfeldii* [45]. Similar differences in maximum swimming speeds were observed among three strains of another toxic dinoflagellate, *Karenia brevis* [46]. Strain dependent variation in gross swimming speeds of *Heterosigma*: 49–66 μm s^{-1} for strain CCMP452 and 88–119 μm s^{-1} for strain CCAP934-1, from different geographic regions has also been reported [44].

Inter-strain variation in harmful algae has also been documented for several other biological traits, including nutrient acquisition, growth rates, photosynthetic responses, salinity and

temperature tolerance and toxin production [45,52,54–57]. These examples highlight the importance of characterizing and quantifying both inter- and intra-specific variability in harmful algae to better understand diversity in fundamental biological traits and responses to environmental conditions.

1.4 *Examining Biophysical Interactions to Improve HAB Prediction*

Algal swimming behaviors often interact with physical flows to influence cell concentrations and distributions [58–64]. The small size of algal cells, transitions between pelagic-benthic habitats and rapid hour-by-hour variation in mean flow provide significant challenges for following populations of harmful algae in the field. An additional challenge is that harmful species only represent a small fraction (~7%) of known phytoplankton [36]. *In situ* sensors and biophysical models are emerging tools to detect disperse algal populations and study interactions between cell-level behaviors and ambient flows that regulate population distributions [21,65,66]).

Vertical fluxes associated with life-stage transitions are rarely quantified. The only reported example to have integrated transitional swimming to a biophysical model to examine HAB formation is for the toxic dinoflagellate, *Alexandrium fundyense*, in the Gulf of Maine [21,22,67]. This series of studies utilized a numerical circulation model of the Gulf of Maine coupled with a population dynamics model for *A. fundyense* that included fundamental benthic-pelagic transition parameters. These parameters included benthic cyst location and abundance [20], an endogenously regulated benthic emergence factor ("endogenous clock") [11,49], and a mean algal up-swimming velocity determined from laboratory cultures [34]. The model hindcast was successful in reproducing the timing and spatial extent of the 2005 *A. fundyense* bloom,

indicating that both life history and cell swimming parameters were important for generating a realistic simulation of the 2005 bloom [22].

1.5 *Background of Focal Algal Species and Study Region*

The toxic dinoflagellate, *Alexandrium catenella* and the fish-killing raphidophyte, *Heterosigma akashiwo* were the focal algal species of this research. Both HAB-forming species are commonly observed in the estuarine waters of the Salish Sea and other temperate coastal waters worldwide. The Salish Sea is an extensive fjord system that includes the Strait of Georgia (British Columbia, CA) and Puget Sound (Washington, USA) with the Strait of Juan de Fuca being the main connection to the Pacific Ocean. Puget Sound, the focal region of this research, is comprised of a number of interconnected waterways and basins. It is a highly advective region where riverine input, tidal currents and wind-driven currents interact in complex ways to influence circulation [68], and hence, algal transport.

Alexandrium is one of the best studied taxa of harmful cyst-forming dinoflagellates because it is the causative organism of Paralytic Shellfish Poisoning (PSP) [15]. The suite of potent neurotoxins produced by *Alexandrium,* collectively known as saxitoxins, can accumulate in the tissue of filter feeding shellfish to concentrations unsafe for consumption by other organisms, including humans. PSP in the Salish Sea has been attributed to *Alexandrium catenella* and *Alexandrium tamarense* [2,69–71] within the *Alexandrium tamarense* complex (Group 1) [15,72,73]. The research presented herein refers to the focal Puget Sound species as *A. catenella* because *Alexandrium* cysts and cells found in this region have previously been identified as such [69,74,75], and for morphological reasons (e.g., plate structure and chain length) [76]. The dual-

stage life history of *Alexandrium* has been well studied. Benthic populations known as "cysts" are considered to be the initiation sites of harmful *Alexandrium* blooms [20]. Surveys conducted throughout Puget Sound over the last 9 years have identified three persistent, high density *A. catenella* cyst beds, one in Quartermaster Harbor and the other in Bellingham Bay (Fig. 1.1) [75].

Blooms of the raphidophyte, *H. akashiwo,* are associated with kills of wild and pen-reared fish in temperate and subtropical waters worldwide [77–79]. *H. akashiwo* is known to have additional harmful impacts on a wide range of marine organisms from bacteria to invertebrate larvae [80–83]. The finfish aquaculture industry in the Salish Sea has been impacted by *H. akashiwo* since the late 1970's, resulting in millions of dollars in losses to fish [33]. *H. akashiwo* has also been attributed to declining abundance of Fraser River sockeye salmon over the last two decades [77]. The mechanism with which *H. akashiwo* kills fish is still unresolved [78]. However, harmful impacts most often occur during periods of persistent stratification when up-swimming vegetative cells aggregate in low salinity surface waters, accumulating to high surface densities [62,77,84,85]. *H. akashiwo* is also known to have a dual-stage life history, but research on the role of benthic-pelagic life stage transitions on *H. akashiwo* bloom dynamics is limited and has primarily focused on shallow (< 10 m) coastal embayments [10,86–88]. The role of *H. akashiwo* benthic-pelagic life stage transitions in bloom dynamics in deeper estuarine environments, like the Salish Sea, is poorly understood.

1.6 *Study Aims and Chapter Overview*

Collectively, the observations presented in the above sections provide strong evidence that knowledge about how transitional movement behaviors influence algal survival, growth and distributions is critical for improved understanding of HAB dynamics. They also highlight the importance of quantifying both inter- and intra-specific transitional behaviors to improve regional understanding of HAB formation and dissipation. Advancements in *in situ* sensing technologies to regionally detect and quantify real-world behaviors of harmful algae are important for assessing future bloom scenarios and establishing appropriate mitigation and management strategies.

This dissertation aims to deepen our understanding of how cell-level behaviors expressed during pelagic and benthic life stage transitions influence HAB dynamics. The primary questions motivating this research are: (1) How do transitional swimming behaviors influence vertical fluxes? (2) What are the implications of these behaviors for population distributions? (3) How can we enhance our understanding of cell-level behaviors in a way that helps to improve interannual bloom prediction?

The overview of each thesis chapter is described as follows. In Chapter 2, sediments collected from a known benthic cyst reservoir in Quartermaster Harbor, in Puget Sound were used to assess the year-round germination potential and emergence rates of naturally occurring *A. catenella* cysts. Chapters 3 and 4 utilize video-based motion analysis and laboratory techniques to gain insight on the functional traits expressed by *Heterosigma akashiwo* during life stage transitions. In Chapter 3, distinct vertical movement behaviors during pelagic-benthic transition

were identified and quantified, and a simple numerical water column model was used to assess the potential consequences for benthic distributions. Chapter 4 provides quantitative assessment of behavioral and physiological traits expressed by two geographically distinct strains of *H. akashiwo* during emergence from the benthic resting stage and their potential influence on near-surface cell accumulations. Lastly, Chapter 5 describes the development and validation of a novel field-deployable sensor to detect benthic emergence rates and quantify cell-level movement behaviors of planktonic organisms (with a focus on HAB-forming species) *in situ.*

1.7 References

1. Taylor FJR, Haigh R, Sutherland TF (1994) Phytoplankton ecology of Sechelt Inlet, a fjord system on the British Columbia coast. II. Potentially harmful species. Mar Ecol Prog Ser 103: 151–164. doi:10.3354/meps103151.

2. Taylor FJ., Trainer VL (2002) Harmful algal blooms in the PICES region of the North Pacific. B.C. Canada. pp. 156.

3. Cembella AD, Ibarra D, Diogene J, Dahl E (2005) Harmful algal blooms and their assessment in fjords and coastal embayments. Oceanography 18: 158–171. doi:10.5670/oceanog.2005.51.

4. Anderson DM (2007) The ecology and oceanography of harmful algal blooms: Multidisciplinary approaches to research and management. IOC Technical Series 74. UNESCO, Vol. 74. doi:IOC/2007/TS/74.

5. Bauer M (2006) Harmful algal research and response: A human dimensions strategy. In: Bauer M, editor. National Office for Marine Biotoxins and Harmful Algal Blooms, Woods Hole Oceanographic Institution, Woods Hole, MA. p. 58.

6. Anderson DM (1989) Toxic algal blooms and red tides: A global perspective. In: Okaichi, Anderson DM, Nemoto, editors. Environmental Science and Toxicology. Elsevier Science Publishing Co. pp. 11–16. doi:10.1029/95rg00440.

7. Anderson DM, Burkholder JM, Cochlan WP, Glibert PM, Gobler CJ, et al. (2008) Harmful algal blooms and eutrophication: Examining linkages from selected coastal regions of the United States. Harmful Algae 8: 39–53. doi:10.1016/j.hal.2008.08.017.

8. Anderson DM (1997) Bloom dynamics of toxic *Alexandrium* species in northeastern U.S. Limnol Oceanogr 42: 1009–1022. doi:10.4319/lo.1997.42.5_part_2.1009.

9. Hallegraeff GM (1998) Transport of toxic dinoflagellates via ships' ballast water: Bioeconomic risk assessment and efficacy of possible ballast water management strategies. Mar Ecol Prog Ser 168: 297–309. doi:10.3354/meps168297.

10. Imai I, Itakura S (1999) Importance of cysts in the population dynamics of the red tide flagellate *Heterosigma akashiwo* (Raphidophyceae). Mar Biol 133: 755–762. doi:10.1007/s002270050517.

11. Matrai P, Thompson B, Keller M (2005) Circannual excystment of resting cysts of *Alexandrium* spp. from eastern Gulf of Maine populations. Deep Sea Res Part II Top Stud Oceanogr 52: 2560–2568. doi:10.1016/j.dsr2.2005.06.013.

12. Anderson DM, Rengefors K (2006) Community assembly and seasonal succession of marine dinoflagellates in a temperate estuary: The importance of life cycle events. Limnol Oceanogr 51: 860–873. doi:10.4319/lo.2006.51.2.0860.

13. Rengefors K, Karlsson I, Hansson L (1998) Algal cyst dormancy: A temporal escape from herbivory. Proc Biol Sci 265: 1353–1358. doi:10.1098/rspb.1998.0441.

14. Steidinger KA, Garcés E (2006) Importance of life cycles in the ecology of harmful microalgae. In: Graneli E, Turner J., editors. Ecology of Harmful Algae. Berlin: Springer-Verlag, Vol. 189. pp. 37–48.

15. Anderson DM, Alpermann TJ, Cembella AD, Collos Y, Masseret E, et al. (2012) The globally distributed genus *Alexandrium*: Multifaceted roles in marine ecosystems and impacts on human health. Harmful Algae 14: 10–35. doi:10.1016/j.hal.2011.10.012.

16. Holsinger KE (2000) Reproductive systems and evolution in vascular plants. Proc Natl Acad Sci U S A 97: 7037–7042. doi:10.1073/pnas.97.13.7037.

17. Anderson DM, Kulis DM, Binder BJ (1984) Sexuality and cyst formation in the dinoflagellate *Gonyaulax tamarensis*: Cyst yield in batch cultures. J Phycol 20: 418–425. doi:10.1111/j.0022-3646.1984.00418.x.

18. Ishikawa A, Taniguchi A (1996) Contribution of benthic cysts to the population dynamics of *Scrippsiella* spp. (Dinophyceae) in Onagawa Bay, northeast Japan. Mar Ecol Prog Ser 140: 169–178. doi:10.3354/meps140169.

19. Itakura S, Yamaguchi M (2001) Germination characteristics of naturally occurring cysts of *Alexandrium tamarense* (Dinophyceae) in Hiroshima Bay, Inland Sea of Japan. Phycologia 40: 263–267. doi:10.2216/i0031-8884-40-3-263.1.

20. Anderson DM, Stock CA, Keafer BA, Bronzino Nelson A, Thompson B, et al. (2005) *Alexandrium fundyense* cyst dynamics in the Gulf of Maine. Deep Sea Res Part II Top Stud Oceanogr 52: 2522–2542. doi:10.1016/j.dsr2.2005.06.014.

21. McGillicuddy DJ, Anderson DM, Lynch DR, Townsend DW (2005) Mechanisms regulating large-scale seasonal fluctuations in *Alexandrium fundyense* populations in the Gulf of Maine: Results from a physical–biological model. Deep Sea Res Part II Top Stud Oceanogr 52: 2698–2714. doi:10.1016/j.dsr2.2005.06.021.

22. He R, McGillicuddy DJ, Keafer BA, Anderson DM (2008) Historic 2005 toxic bloom of *Alexandrium fundyense* in the western Gulf of Maine: 2. Coupled biophysical numerical modeling. J Geophys Res 113: 1–12. doi:10.1029/2007JC004602.

23. Anderson DM, Keafer BA, Kleindinst JL, McGillicuddy DJ, Martin JL, et al. (2013) *Alexandrium fundyense* cysts in the Gulf of Maine: long-term time series of abundance

and distribution, and linkages to past and future blooms. Deep Sea Res Part II Top Stud Oceanogr. doi:10.1016/j.dsr2.2013.10.002.

24. Itakura S, Nagasaki K, Yamaguchi M, Imai I, Tide R, et al. (1979) Cyst formation in the red tide flagellate *Heterosigma akashiwo* (Raphidophyceae). J Plankton Res 18: 1975–1979. doi:10.1093/plankt/18.10.1975.

25. Mayali X, Franks PJS, Tanaka Y, Azam F (2008) Bacteria-Induced Motility Reduction in *Lingulodinium polyedrum* (Dinophyceae). J Phycol 44: 923–928. doi:10.1111/j.1529-8817.2008.00549.x.

26. Persson A, Smith BC, Wikfors GH, Alix JH (2008) Dinoflagellate gamete formation and environmental cues: Observations, theory, and synthesis. Harmful Algae 7: 798–801. doi:10.1016/j.hal.2008.04.002.

27. Figueroa RI, Bravo I, Garcés E (2005) Effects of nutritional factors and different parental crosses on the encystment of *Alexandrium catenella* (Dinophyceae) in culture. Phycologia 44: 658–670. doi:

28. Figueroa RI, Bravo I, Garcés E (2006) Multiple routes of sexuality in *Alexandrium taylori* (Dinophyceae) in culture. J Phycol 42: 1028–1039. doi:10.1111/j.1529-8817.2006.00262.x.

29. Bravo I, Isabel Figueroa R, Garcés E, Fraga S, Massanet A (2010) The intricacies of dinoflagellate pellicle cysts: The example of *Alexandrium minutum* cysts from a bloom-recurrent area (Bay of Baiona, NW Spain). Deep Sea Res Part II Top Stud Oceanogr 57: 166–174. doi:10.1016/jdsr2.2009.09.003.

30. Imai I, Yamaguchi M (2012) Life cycle, physiology, ecology and red tide occurrences of the fish-killing raphidophyte *Chattonella*. Harmful Algae 14: 46–70. doi:10.1016/j.hal.2011.10.014.

31. Figueroa RI, Rengefors K (2006) Life Cyle and sexuality of the freshwater raphidophyte *Gonyostomum semen* (Raphidophyceae). J Phycol 42: 859–871. doi:10.1111/j.1529-8817.2006.00240.x.

32. Figueroa RI, Garcés E, Bravo I (2007) Comparative study of the life cycles of *Alexandrium tamutum* and *Alexandrium minutum* (Gonyaulacales, Dinophyceae) in culture. J Phycol 43: 1039–1053. doi:10.1111/j.1529-8817.2007.00393.x.

33. Rensel JJE (2007) Fish kills from the harmful alga *Heterosigma akashiwo* in Puget Sound: Recent blooms and review. Prepared by Rensel Associates Aquatic Sciences for the National Oceanic and Atmospheric Administration Center for Sponsored Coastal Ocean Research (CSCOR), Washington, DC (2007): pp. 58.

34. Anderson DM, Stolzenbach K. (1985) Selective retention of two dinoflagellates in a well-mixed estuarine embayment: The importance of diel vertical migration and surface avoidance. Mar Ecol Prog Ser 25: 39–50. doi:10.3354/meps025039.

35. Wada M, Miyazaki A, Fujii T (1985) On the Mechanisms of Diurnal Vertical Migration Behavior of *Heterosigma akashiwo* (Raphidophyceae). Plant Cell Physiol 26: 431–436. doi:10.1111/j.1529-8817.1988

36. Smayda TJ (1997) Harmful Algal Blooms: Their ecophysiology and general relevence to phytoplankton blooms in the sea. Limnol Oceanogr 42: 1137–1153. doi:10.4319/lo.1997.42.5_part_2.1137.

37. Handy SM, Coyne KJ, Portune KJ, Demir E, Doblin MA, et al. (2005) Evaluating vertical migration behavior of harmful raphidophytes in the Delaware Inland Bays utilizing quantitative real-time PCR. Aquat Microb Ecol 40: 121–132. doi:10.3354/ame040121.

38. Horner RA, Garrison DL, Plumley FG (1997) Harmful algal blooms and red tide problems on the U.S. west coast. Limnol Oceanogr 42: 1076–1088. doi:10.4319/lo.1997.42.5_part_2.1076. doi:10.4319/lo.1997.42.5_part_2.1076.

39. Tam D, Hosoi A. (2011) Optimal feeding and swimming gaits of biflagellated organisms. Proc Natl Acad Sci U S A 108: 1001–1006. doi:10.1073/pnas.1011185108.

40. Jahn TL, Votta JJ (1972) Locomotion of protozoa. Annu Rev Fluid Mech 4: 93–116. doi:10.1146/annurev.fl.04.010172.000521.

41. Makoto M W, Nakamura Y, Mori S, Yamochi S (1982) Effects of physico-chemical factors and nutrients on the growth of *Heterosigma akashiwo* hada from Osaka Bay, Japan. Japanese J Phycol 30: 279–288.

42. MacIntyre J, Cullen JJ, Cembella AD (1997) Vertical migration, nutrition and toxicity in the dinoflagellate *Alexandrium tamarense*. Mar Ecol Prog Ser 148: 201–216. doi:10.3354/meps148201.

43. Pedley TJ (1992) Hydrodynamic phemomena in suspensions of swimming microorganisms. Annu Rev Fluid Mech 24: 313–358. doi:10.1146/annurev.fluid.24.1.313.

44. Bearon R., Grunbaum D, Cattolico R. (2004) Relating cell-level swimming behaviors to vertical population distributions in *Heterosigma akashiwo* (Raphidophyceae), a harmful alga. Limnol Oceanogr 49: 607–613. doi:10.4319/lo.2004.49.2.0607.

45. Lewis NI, Xu W, Jericho SK, Kreuzer HJ, Jericho MH, et al. (2006) Swimming speed of three species of *Alexandrium* (Dinophyceae) as determined by digital in-line holography. Phycologia 45: 61–70. doi:10.2216/04-59.1.

46. McKay L, Kamykowski D, Milligan E, Schaeffer B, Sinclair G (2006) Comparison of swimming speed and photophysiological responses to different external conditions among three *Karenia brevis* strains. Harmful Algae 5: 623–636. doi:10.1016/j.hal.2005.12.001.

47. Cullen JJ (1985) Diel vertical migration by dinoflagellates: roles of carbohydrate metabolism and behavioral flexibility. Contrib Mar Sci 27: 135–152.

48. Ralston DK, McGillicuddy DJ, Townsend DW (2007) Asynchronous vertical migration and bimodal distribution of motile phytoplankton. J Plankton Res 29: 803–821. doi:10.1093/plankt/fbm061.

49. Anderson D., Keafer BA (1987) An endogenous annual clock in the toxic marine dinoflagellate *Gonyaulax tamarensis*. Nature 325: 616–617. doi:10.1038/325616.

50. Genovesi B, Laabir M, Masseret E, Collos Y, Vaquer A, et al. (2009) Dormancy and germination features in resting cysts of *Alexandrium tamarense* species complex (Dinophyceae) can facilitate bloom formation in a shallow lagoon (Thau, southern France). J Plankton Res 31: 1209–1224. doi:10.1093/plankt/fbp066.

51. Tobin ED, Horner RA. (2011) Germination characteristics of *Alexandrium catenella* cysts from surface sediments in Quartermaster Harbor, Puget Sound, Washington, USA. Harmful Algae 10: 216–223. doi:10.1016/j.hal.2010.10.002.

52. Joyce LB, Pitcher GC (2006) Cysts of *Alexandrium catenella* on the west coast of South Africa: distribution and characteristics of germination. J Mar Sci 28: 295–298. doi:10.2989/18142320609504165. doi:10.2989/18142320609504165.

53. Han M, Kim Y, Cattolico RA (2002) *Heterosigma akashiwo* (Raphidophyceae) resting cell formation in batch culture: Strain identity versus physiological response. J Phycol 317: 304–317. doi:10.1046/j.1529-8817.2002.01087.x.

54. Powers L, Creed IF, Trick CG (2012) Sinking of *Heterosigma akashiwo* results in increased toxicity of this harmful algal bloom species. Harmful Algae 13: 95–104. doi:10.1016/j.hal.2011.10.007.

55. Fredrickson KA, Strom SL, Crim R, Coyne KJ (2011) Interstrain variability in physiology and genetics of *Heterosigma akashiwo* (Raphidophyceae) from the west coast of North America. J Phycol 47: 25–35. doi:10.1111/j.1529-8817.2010.00942.x.

56. Kremp A, Godhe A, Egardt J, Dupont S, Suikkanen S, et al. (2012) Intraspecific variability in the response of bloom-forming marine microalgae to changed climate conditions. Ecol Evol 2: 1195–1207. doi:10.1002/ece3.245.

57. Lartigue J, Jester ELE, Dickey RW, Villareal TA. (2009) Nitrogen source effects on the growth and toxicity of two strains of the ciguatera-causing dinoflagellate *Gambierdiscus toxicus*. Harmful Algae 8: 781–791. doi:10.1016/j.hal.2008.05.006.

58. Kessler JO (1985) Hydrodynamic focusing of motile algal cells. Lett to Nat 313: 218–220. doi:10.1038/313218a0.

59. Reed C., Amsler CD, Ebeling A. (1992) Dispersal in kelps: Factors affecting spore swimming and competency. Ecology 73: 1577–1585. doi:10.2307/1940011.

60. Donaghay PL, Osborn TR (1997) Toward a theory of biological-physical control of harmful algal bloom dynamics and impacts. Limnol Oceanogr 42: 1283–1296. doi:10.4319/lo.1997.42.5_part_2.1283.

61. Franks PJS (1997) Spatial patterns in dense algal blooms. Limnol Oceanogr 42: 1297–1305. doi:10.4319/lo.1997.42.5_part_2.1283.

62. Bearon RN, Grünbaum D, Cattolico RA (2006) Effects of salinity structure on swimming behavior and harmful algal bloom formation in *Heterosigma akashiwo*, a toxic raphidophyte. Mar Ecol Prog Ser 306: 153–163. doi:10.3354/meps306153.

63. Juhl AR, Trainer VL, Latz MI (2001) Effect of fluid shear and irradiance on population growth and cellular toxin content of the dinoflagellate *Alexandrium fundyense*. Limnol Oceanogr 46: 758–764. doi:10.4319/lo.2001.46.4.0758.

64. Fauchot J, Saucier FJ, Levasseur M, Roy S, Zakardjian B (2008) Wind-driven river plume dynamics and toxic *Alexandrium tamarense* blooms in the St. Lawrence estuary (Canada): A modeling study. Harmful Algae 7: 214–227. doi:10.1016/j.hal.2007.08.002.

65. Villanoy CL, Azanza RV, Altemerano A, Casil AL (2006) Attempts to model the bloom dynamics of Pyrodinium, a tropical toxic dinoflagellate. Harmful Algae 5: 156–183. doi:10.1016/j.hal.2005.07.001.

66. Olson RJ, Sosik HM (2007) A submersible imaging-in-flow instrument to analyze nano- and microplankton: Imaging FlowCytobot: 195–203. doi:10.4319/lom.2007.5.195.

67. Stock CA, McGillicuddy DJ, Solow AR, Anderson DM (2005) Evaluating hypotheses for the initiation and development of *Alexandrium fundyense* blooms in the western Gulf of Maine using a coupled physical–biological model. Deep Sea Res Part II Top Stud Oceanogr 52: 2715–2744. doi:10.1016/j.dsr2.2005.06.022.

68. Sutherland DA, MacCready P, Banas NS, Smedstad LF (2011) A model of study of the Salish Sea esturine circulation. J Phys Oceanogr 41: 1125–1143. doi:10.1175/2011JPO4540.1.

69. Horner R, Greengrove CL, Davies-Vollum KS, Gawel JE, Postel JR, et al. (2011) Spatial distribution of benthic cysts of *Alexandrium catenella* in surface sediments of Puget Sound, Washington, USA. Harmful Algae 11: 96–105. doi:10.1016/j.hal.2011.08.004.

70. Cox AM, Shull DH, Horner RA (2008) Profiles of *Alexandrium catenella* cysts in Puget Sound sediments and the relationship to paralytic shellfish poisoning events. Harmful Alage 7: 379–388. doi:10.1016/j.hal.2007.01.006.

71. Taylor FJ. (1984) Toxic Dinoflagellates: Taxonomic and Biogeographic Aspects with Emphasis on Protogonyaulax. Seafood Toxins, ACS Symposium Series 262. Washington: Am. Chem. Soc. p. 77.

72. Scholin CA, Anderson DM (1994) Identification of group-specific and strain-specific genetic-markers for globally distributed *Alexandrium* (Dinophyceae). 1. Rflp analysis of SSU ribosomal-rRNA Genes. J Phycol 30: 744–754. doi:10.1111/j.0022-3646.1994.00744.x.

73. Lilly EL, Halanych KM, Anderson DM (2007) Species boundaries and global biogeography of the *Alexandrium tamarense* complex (Dinophyceae). J Phycol 43: 1329–1338. doi:10.1111/j.1529-8817.2007.00420.x.

74. Nishitani L, Chew KK (1984) Recent developments in paralytic shellfish poisoning research. Aquaculture 39: 317–329. doi:10.1016/0044-8486(84)90274-6.

75. Greengrove CL, Masura JE, Moore SK, Bill BD, Hay LR, et al. (2012) *Alexandrium catenella* cyst distribution and germination in Puget Sound, WA USA. In: Kim, HG, editor. International Confrence on Harmful Algae 15th Proceedings. Changwong, Korea.

76. Balech E (1995) The genus *Alexandrium halim* (dinoflagellata). Sherkin Island Marine Station. Sherkin Island, Ireland. p. 151. doi:10.2307/3226651.

77. Jack Rensel JE, Haigh N, Tynan TJ (2010) Fraser river sockeye salmon marine survival decline and harmful blooms of *Heterosigma akashiwo*. Harmful Algae 10: 98–115. doi:10.1016/j.hal.2010.07.005.

78. Lewitus AJ, Horner RA, Caron DA, Garcia-mendoza E, Hickey BM, et al. (2012) Harmful algal blooms along the North American west coast region: History, trends, causes and impacts. Harmful Algae. doi:10.1016/j.hal.2012.06.009.

79. Carrasquero-Verde J (1999) Role of associated bacteria in *Heterosigma carterae* toxicity to salmonids. Aquat Toxicol 45: 19–34. doi:10.1016/S0166-445X(98)00089-7.

80. Clough J, Strom S (2005) Effects of *Heterosigma akashiwo* (Raphidophyceae) on protist grazers: Laboratory experiments with ciliates and heterotrophic dinoflagellates. Aquat Microb Ecol 39: 121–134. doi:10.3354/ame039121.

81. Keppler CJ, Hoguet J, Smith K, Ringwood AH, Lewitus AJ (2005) Sublethal effects of the toxic alga *Heterosigma akashiwo* on the southeastern oyster (*Crassostrea virginica*). Harmful Algae 4: 275–285. doi:10.1016/j.hal.2004.05.002.

82. Harvey EL, Menden-Deuer S (2011) Avoidance, movement, and mortality: The interactions between a protistan grazer and *Heterosigma akashiwo*, a harmful algal bloom species. Limnol Oceanogr 56: 371–378. doi:10.4319/lo.2011.56.1.0371.

83. Jeong H, Seong K, Kang N, Yoo Y, Nam S, et al. (2010) Feeding by raphidophytes on the cyanobacterium *Synechococcus* sp. Aquat Microb Ecol 58: 181–195. doi:10.3354/ame01354.

84. Connell L, Jacobs M (1998) Anatomy of a bloom: *Heterosigma carterae* in Puget Sound 1997. Puget Sound Res: 830–834.

85. Hershberger PK, Rensel JE, Matter AL, Taub FB (1997) Vertical distribution of the chloromonad flagellate *Heterosigma carterae* in columns: Implications for bloom development. Can J Fish Aquat Sci 54: 2228–2234. doi:10.1139/f97-131.

86. Portune K, Coyne K, Hutchins D, Handy S, Cary S (2009) Quantitative real-time PCR for detecting germination of *Heterosigma akashiwo* and *Chattonella subsalsa* cysts from Delaware's Inland Bays, USA. Aquat Microb Ecol 55: 229–239. doi:10.3354/ame01292.

87. Shikata T, Nagasoe S, Matsubara T, Yamasaki Y, Shimasaki Y, et al. (2007) Effects of temperature and light on cyst germination and germinated cell survival of the noxious raphidophyte *Heterosigma akashiwo*. Harmful Algae 6: 700–706. doi:10.1016/j.hal.2007.02.008.

88. Shikata T, Nagasoe S, Matsubara T, Yoshikawa S, Yamasaki Y, et al. (2008) Factors influencing the initiation of blooms of the raphidophyte *Heterosigma akashiwo* and the diatom *Skeletonema costatum* in a port in Japan. Limnol Oceanogr 53: 2503–2518. doi:10.4319/lo.2008.53.6.2503.

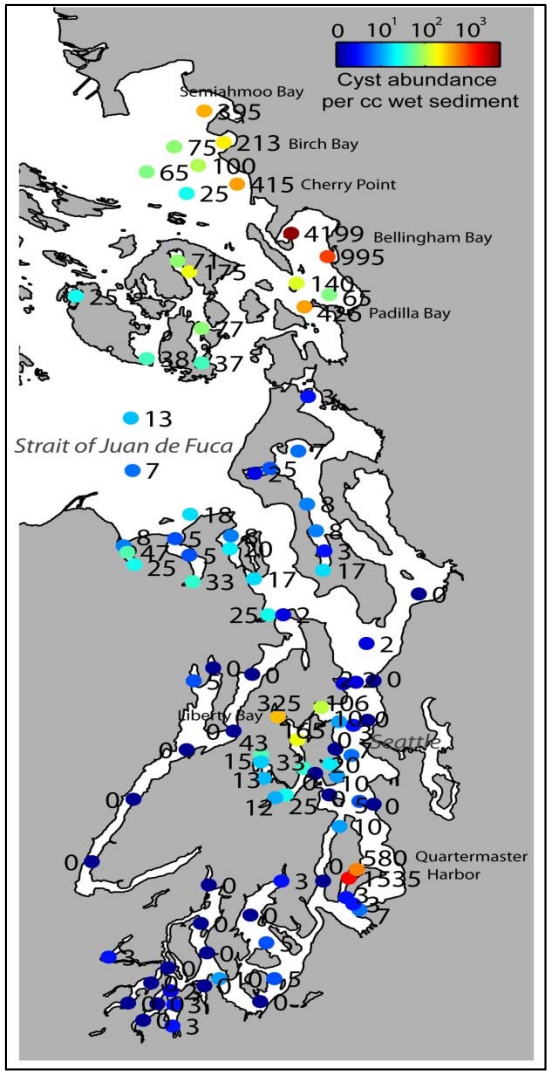

Figure 1.1 *Alexandrium catenella* cyst map for Puget Sound, WA. A survey conducted by the Puget Sound *Alexandrium* Harmful Algal Blooms (PS-AHAB) research team shows cysts abundances for winter 2011. High cysts concentrations occur in Quartermaster Harbor (South) and Bellingham Bay (North). Map source: https://catalyst.uw.edu/workspace/banasn/14943/135346.

Chapter 2. Germination characteristics of *Alexandrium catenella* cysts from surface sediments in Quartermaster Harbor, Puget Sound, Washington, USA.

Elizabeth D. Tobin and Rita A. Horner

School of Oceanography, University of Washington, Seattle WA. 98195-7940

"Reprinted from Harmful Algae, Vol. 10, Tobin, ED and Horner, RA., Germination characteristics of *Alexandrium catenella* cysts from surface sediments in Quartermaster Harbor, Puget Sound, WA, USA, 216-223 (2011), with permission from Elsevier."

2.1 Abstract

The dinoflagellate *Alexandrium catenella* causes frequent outbreaks of paralytic shellfish toxins (PSTs) in Puget Sound, Washington; however, little is known about its basic biology and ecology. Most of what is known is inferred mainly from shellfish toxin records and recent work on cyst distribution and germination potential. We report on a year-long study of cyst dormancy and germination potential based on experiments using surface sediment collected from a shallow embayment, Quartermaster Harbor, in Puget Sound. Cyst abundance in Quartermaster Harbor was 1550-1750 cysts cm^{-3} when sediment was collected in mid-October 2006. Germination experiments set up monthly had germination occur in all months when cysts were provided with adequate growth supporting conditions, in this case, temperature of 13°C and a 12 hour dark: 12 hour light period. Germination rates were highest in May and June when 100% germination occurred within 2 days. Longer incubation periods observed for the first two months of the study (November and December) may indicate a mandatory dormancy period of up to 5 months if the majority of cysts were deposited in the sediments following a late summer bloom that apparently occurred in Quartermaster Harbor in 2006 as indicated by Washington State Department of

Health's toxin records. The data provide no evidence of an endogenous clock restricting germination to a specific annual timeframe for these shallow water cysts. This contrasts with the presence of a circannual endogenous clock, for deep water cysts of *A. fundyense* in the Gulf of Maine. The significance of these results is that germination of the *A. catenella* Puget Sound population appears to be primarily regulated by physiological requirements, but once this requirement is met cysts can germinate rapidly, often within 24 hours, when provided with adequate environmental conditions.

2.2 Introduction

Paralytic shellfish poisoning (PSP), attributed to the dinoflagellate, *Alexandrium catenella* (Kofoid and Swezy) Balech, has a long history in Puget Sound, Washington, causing frequent closures of both commercial and recreational shellfish harvesting [1]. Outbreaks of paralytic shellfish toxins (PSTs) in mollusks have been monitored by the Washington State Department of Health (WDOH) since the 1950s as part of their Biotoxin Monitoring Program, but the biology of *A. catenella* in Puget Sound is not well known. *A. catenella* has a two-stage life cycle with asexual reproduction by binary fission producing motile, vegetative cells in the water column and sexual reproduction resulting from fusion of gametes producing swimming planozygotes that become dormant as non-motile cysts (hypnozygotes) in the sediment. Temporary cysts, sometimes called pellicle or ecdysal cysts, may also be produced by vegetative cells when environmental conditions are unfavorable, but revert to the motile stage when conditions again become favorable. It is thought that cyst formation has contributed to the success of this organism by allowing for an alternation between planktonic and benthic habitats in response to a seasonally variable environment [2–4].

Understanding the mechanisms underlying formation and germination of dinoflagellate cysts is important because cysts are influential in bloom dynamics. Cysts that accumulate in the sediments have the ability to germinate and produce blooms of both benign and harmful dinoflagellate species. The transition into and out of the cyst phase can influence the timing and location of blooms, yet this process remains poorly understood for many dinoflagellate species even though these transitions determine when vegetative cells, and possibly toxins, are present in the water column.

Alexandrium is one of the more well studied harmful cyst-forming dinoflagellates because of its link to PSP [4–8], but germination characteristics of naturally occurring resting cysts of *A. catenella* are not well understood, particularly in Puget Sound. It remains unclear what mechanisms, endogenous or environmental, primarily regulate the timing and rate of germination. Previous studies have reported a wide range of dormancy durations from one week to several months for *A. catenella* from geographically distinct regions [4,6,8]. This range in dormancy durations could represent variability among strains, or be a result of temporal variation. Additionally, the presence of an annual endogenous clock, that may serve to regulate germination to a specific time of year, may be dependent on the location of the benthic population [9,10]. Such variability emphasizes the need to determine specific cyst dynamics for geographically distinct populations.

A survey for *A. catenella* cysts in surface sediments in Puget Sound in early spring 2005 found cysts at 20 of 32 sites sampled (Fig. 2.1) [11]. The highest cyst concentrations were found in

Quartermaster Harbor (station 24, Fig. 2.1) in south central Puget Sound at >12,000 cysts cm^{-3} and Sequim Bay (station 7, Fig. 2.1) along the Strait of Juan de Fuca at ca. 200 cyst cm^{-3}. Preliminary germination studies found that *A. catenella* cysts collected from several sites in Puget Sound, including Quartermaster Harbor, in March and incubated in April and May germinated in 3-6 days. Light was required for germination and highest germination occurred at a temperature near 14°C [12]. A later study from sediment samples collected in January 2006 found no germination in January and February, but did observe germination in March (Hoffer, pers. comm.). In both studies, experiments were observed on days 3, 6, 8 and 10. These preliminary experiments determined the best conditions (light and 13-14°C) to induce germination of *A. catenella* cysts from natural sediment samples, and indicated that populations within Puget Sound may be able to germinate more rapidly than documented strains from other locations. A more in-depth study was necessary to identify year round germination potential and timing of natural cyst populations in Puget Sound. Hence, the objectives of this study were to: (1) identify how quickly germination occurs when conditions that support growth are restored; (2) assess year round germination potential; and (3) determine whether germination of *A. catenella* cysts is regulated primarily by external environmental conditions or endogenous mechanisms.

2.3 Materials and Methods

Sampling site

Quartermaster Harbor (Fig. 2.1 inset) is a shallow, southward facing bay between Vashon and Maury islands and connects over a shallow sill to the southern end of the Main Basin in south Puget Sound, WA. There is a shallow inner bay with an average depth of 6 m connected on the

eastern side to a slightly deeper outer bay with an average depth of 12 m. Our sampling site was at station 54 near the northern end of the outer bay with a water depth of 15 m.

Sampling and experimental design

Surface sediment, predominately composed of silt and sand [11], was collected from Quartermaster Harbor in mid-October 2006 using a van Veen grab sampler. The top 2-3 cm of sediment were collected using a plastic scoop and distributed into 4 resealable plastic bags. The sediment was put in an ice chest and kept cold and in the dark until return to the shore laboratory where the sediment samples, still in the ice chest, were kept in the dark at 4°C until the experiments were set up. The same bag of sediment was used to set up all monthly germination experiments. A 10 mL sediment sample from the same sample bag was fixed with ca. 4% formalin at the start of the time series experiment to determine original cyst abundance.

Experiments were started at the beginning of each month from November 2006 through September 2007. Sediment in the bag was manually mixed prior to setting up each experiment. Two drops, approximately 20 µl [13], of sediment and 4 mL of f/2-Si medium [14] were added to each well of four replicate 12-well plates for a total of 48 individual wells. The well plates were incubated at 13°C on a 12 hour dark: 12 hour light (20 $\mu E/m^2/s$) cycle.

Each individual well was checked for motile, vegetative cells using a dissecting microscope at 25x magnification upon set up, then daily for the first week or until vegetative cells were observed, and once a week thereafter. For each observation the presence or absence of vegetative cells was recorded for each well. Beginning on the first day of observed germination and each

week thereafter, a single well with germinated cells was preserved with ca. 1% formalin. One mL of fresh f/2-Si medium was added to each well every 2-3 weeks, as needed, to replace loss due to evaporation. Each monthly experiment was terminated only after germination had been observed in all of the wells or after 15 weeks under incubation conditions.

Staining and counting of preserved samples

To determine original cyst abundance, cysts in the preserved 10 mL surface sediment sample were counted using epifluorescence microscopy after staining with the fluorochrome primulin [15]. The sediment sample was first sonicated and sieved, then stored in methanol for two days to make the outer cell wall permeable to the stain. Prepared samples were then stained with 1 mL primulin for approximately 1 hour. After staining, the final 5 mL volume was shaken to suspend the sediment. Two 1 mL subsamples were counted in a Sedgwick-Rafter slide using a Zeiss standard microscope equipped with epifluorescence condenser and a filter set comprised of an excitation filter (BP 450-490), a chromatic beam splitter (FT 510) and a barrier filter (LP 520). Cysts exhibited an intense green fluorescence under blue-light excitation. Cysts were counted at 160x magnification, and at the lowest possible dilution based on the amount of sediment. The number of cysts cm^{-3} sediment was calculated [16].

The number of cysts and vegetative cells were determined for the single well sample fixed on the first day of observed germination for each month. Initial staining trials verified that germinated cells stained with primulin alone could not be easily distinguished. Therefore, we added Calcofluor White, a fluorochrome stain that binds to the thecal plates of dinoflagellate vegetative cells as long as motility is inhibited [17], in addition to primulin. Our first two staining attempts

on the preserved well samples for November and January combined the two stains. However, it became apparent that the combined staining method would not work well for the detection of vegetative cells, so we established and tested a method of simultaneously staining for vegetative cells and cysts using only Calcofluor White. The use of the calcofluor stain has previously been tested as an effective method for detection of resting cysts of *Alexandrium* spp. from natural sediments [15].

For the Calcofluor White method, the 4 mL fixed well sample was transferred to a 10 mL centrifuge tube and centrifuged for 15-20 min. The f/2-Si and formalin supernate was discarded, and the remaining sediment was stained with 1 mL of a 10 μg mL^{-1} stock solution of Calcofluor White. The sample was refrigerated for 24 hours, centrifuged, and the stain decanted. The remaining sediment was resuspended in 2 mL deionized water. One mL of sample was put into a Sedgwick-Rafter slide and examined with the epifluorescence microscope under UV excitation at 160x magnification. Both the thecal plates of the vegetative cells and the cyst wall of *A. catenella* were successfully stained, exhibiting bright blue fluorescence, thus making both cysts and vegetative cells easily identifiable in a single sample (Fig. 2.2a, b).

2.4 Results

Staining Methods

Calcofluor White staining alone worked better for preserved samples recovered from the well plates than staining with primulin when both cysts and motile cells were present. The primulin method was effective only for cyst enumeration. When primulin was used alone or in combination, very few vegetative cells were observed and many of those few appeared to be

degraded. To test the effect of the primulin staining method on vegetative cells, we carried out subsequent cell counts on a vegetative culture of *A. catenella*. When treated with the primulin staining method cell concentrations determined from the same culture were approximately 2/3 less when treated with the primulin staining method than those not exposed to the primulin staining method (data not shown here). Additionally, we observed that the primulin stain cannot be used to accurately identify, and hence enumerate, vegetative *Alexandrium* cells since the stain is not picked up by the thecal plates (Fig. 2.2c).

Similar to previous findings [15], we observed that Calcoflour White binds to cyst walls. Subsequent staining trials revealed that the use of Calcofluor White alone effectively stained the cell walls of both cysts and vegetative cells a brilliant blue allowing us to clearly distinguish between them (Fig. 2.2).

Cyst Germination

A. catenella cysts collected from Quartermaster Harbor in mid-October 2006 were able to germinate in all months, November through September (Table 1). In some months germination occurred quite rapidly, within 24 hrs of sediments containing cysts being restored to conditions that support growth. Vegetative cells were not observed in any of the wells on initial set up of the experiments, indicating that germination occurred only after exposure to incubation conditions.

Germination success was defined as the overall portion of wells with germination by the termination of each experiment at 15 weeks. Germination success was nearly 100% for all months except for the November and December experiments, which had overall germination of

25% and 83%, respectively (Table 1). Incubation period was defined as the length of time after wells were restored to growth supporting conditions until germination was observed. Incubation period was only calculated for wells that had germination. Mean incubation period steadily decreased from November (μ = 73 days) to May (μ = 1 day), as did the range (Fig. 2.3).The first day of observed germination ranged from 21 days to $\leq$ 24 hours during the 11 month study (Table 1). Germination occurred more rapidly ($\leq$ 24 hours) in late spring and into summer, April – August, than in the winter months, November - February (Fig. 2.4).

We could not identify the exact number of cysts contained in each well since a sediment volume of approximately 20 µl was added to each, so we estimated the rate of germination based on the portion of the 48 replicate wells that contained vegetative cells on each day of observation. We indicated 50% germination when 24 wells (1/2 of the 48 individual replicates) contained vegetative cells and 95-100% germination when 46-48 wells contained vegetative cells (Table 1). The highest rates of germination occurred in May and June when germination was observed in $\geq$ 89% of the wells within 24 hours under incubation conditions (Fig. 2.4). The lowest rates of germination occurred in November and December. In the November experiment, only 4% (2 wells) had germination occur after approximately 3 weeks under incubation conditions (Fig. 2.4). No further germination was observed for the November experiment until week 10 (mid-January). For the December experiment, only 11% of the individual wells had germination occur after about 2 weeks under incubation conditions, while the majority (26 wells) did not have germination until about weeks 5-6 (mid-January). Germination rates rapidly increased starting in the January experiment when 50% germination was observed within one week and 100%

germination was observed within 2 weeks (Table 2.1). All monthly experiments thereafter, February – September, had nearly 100% germination within one week

Use of a Spearman's rank correlation test showed a significant negative relationship between overall germination success and mean incubation period for the well plates (r_s = -0.635, P = < 0.001, N = 44).

Cell Counts

Cyst abundance was 1550 – 1750 cysts cm^{-3} in the surface sediment in Quartermaster Harbor when the sediment was collected in mid-October, 2006. Cell enumeration from the preserved well samples revealed that not all of the cysts in each well germinated on the first day of observed germination. Also, cyst abundance appeared to be highly variable between replicate wells despite equal volumes of well-mixed sediment being added to each (Table 2.2).
Both vegetative cells and cysts were observed in the preserved well samples for nearly all months except in November which was likely compromised by the primulin staining method.

Of the total number of cells counted in each preserved well sample, the fraction of vegetative cells and the fraction of cysts were determined for each month (Table 2.2). November and January cell counts were excluded because we believe use of the primulin staining method destroyed, severely damaged, or made difficult to identify (see above) most of the germinated cells so the true fraction could not be determined. Comparing the portion of each cell type revealed an interesting seasonal pattern (Table 2.2, shaded values). From spring-early summer (March-June)−when incubation periods were short and germination success was high−the

majority of the total cells counted on the first day of observed germination were cysts (>60 %). While from mid to late summer (July-September), and December, germinated cells made up a larger fraction of the total cells counted (>60 %).

2.5 Discussion

The timing and rate of germination of benthic resting cysts can strongly regulate the location and magnitude of harmful bloom events. In this study, we sought to identify the germination characteristics of naturally occurring resting cysts of the PSP causative organism, *Alexandrium catenella*[1], in Quartermaster Harbor, WA. We found that germination can occur quite rapidly (≤ 24 hours). Our results provide no evidence indicating the presence of a synchronous endogenous clock restricting germination to a specific seasonal window since cysts were able to germinate nearly year round (November-September). Further, our results provide some preliminary evidence that suggests cysts of *A. catenella* may need to fulfill a mandatory dormancy for several months. Hence, cyst germination of *A. catenella* in Puget Sound is likely regulated primarily by physiological requirements and secondarily by environmental conditions

Improved staining protocol

We established a modified protocol of staining with Calcoflour White for the detection and enumeration of *A. catenella* cells from sediment samples. We found that our method of staining with Calcofluor White was effective for simultaneous enumeration of cysts and vegetative cells

[1] *A. catenella*, *A. tamarense* and *A. fundyense* maybe considered varieties of the same species, referred to as the "tamarensis complex" [21,22]. *A. tamarense* has been described in the Pacific Northwest [23] as *Protogonyaulax tamarense*, and *A. fundyense* has been found in the Gulf of Alaska [21]. However, we have chosen to claim *A. catenella* here since the *Alexandrium* cysts and cells found in QMH have previously been identified as such [11,20]. Also, for morphological reasons (e.g., plate structure and chain length) our cell more closely resembles that of *A. catenella* ([24]; previous observations).

of *A. catenella*, while the more commonly used primulin staining protocol was effective only for cyst enumeration. We observed many more vegetative cells when staining was done with Calcofluor White alone. The few vegetative cells observed in the wells treated with the primulin stain appeared to be degraded. Therefore, we believe that one of two steps: the addition of methanol or sonication, in the primulin staining method caused damage to the vegetative cells. Further, our method of staining with Calcofluor White is a more rapid alternative to primulin staining, requiring approximately 24 hours to prepare and stain samples, as opposed to 48-72 hours for primulin. Use of this method is not specific to *Alexandrium* since the calcofluor stain readily binds to cellulose, and therefore should be effective for detection and enumeration of cysts and vegetative cells of other dinoflagellate taxa [17].

Germination potential

A. catenella cysts in the sediments of Quartermaster Harbor, WA, have the ability to germinate within 24 hours after conditions that support growth are restored. In our studies, those conditions were a temperature of 13°C and on a 12 hour dark: 12 hour light (20 μE/m^2/s) period in April through August. Our findings differ from the earlier observations of Hoffer et al. [12] which, under similar incubation conditions, reported germination of *A. catenella* from 10 stations in Puget Sound, WA (including Quartermaster Harbor) took 3 to 6 days in April and May. Differences in the incubation period between our study and previous observations may be explained by differences in the frequency of observations. While Hoffer et al. monitored for vegetative cells only on days 3, 6, 8 and 10, the present study monitored for vegetative cells upon initiation of the experiment and daily thereafter.

In our study, germination occurred more rapidly in the spring and summer months relative to winter months. *A. catenella* germination rates from the shallow waters of Quartermaster Harbor were the highest in May and June and lowest in November and December. This result is the opposite of what was observed for *Alexandrium fundyense* cysts from deep waters in the Gulf of Maine where germination peaked in the winter months (November-February), and declined in the spring/summer months [10]. Despite seasonal variation in incubation periods, *A. catenella* cysts in Puget Sound appear to be able to germinate at any time during the year provided they have fulfilled any dormancy requirement and are provided with the appropriate environmental conditions.

We found that populations of *A. catenella* in Puget Sound can germinate more rapidly than previously thought. Knowing the time to germination for geographically distinct populations is especially important when seeking to accurately predict the timing and location of a subsequent bloom event, and is critical for modeling efforts since ambient conditions that influence bloom development and cell distribution (e.g., wind and tidal currents, mixing and nutrient concentrations) can change rapidly over short time scales (hours to days).

Endogenous regulation of cyst germination

Dinoflagellate cyst germination is regulated by both internal and external environmental factors. A mandatory dormancy period and the presence of a synchronous biological clock are two endogenous factors that may regulate germination [18]. We used the data collected here to gain insight on these two endogenous mechanisms for *A. catenella* in Quartermaster Harbor, WA.

Mandatory Dormancy Period

Considerable variability in dormancy periods has been documented for distinct geographic strains of *A. catenella*. It has been proposed that variation in cyst dormancy requirements among geographic strains of the same dinoflagellate taxon can serve different ecological roles [19]. Longer dormancy requirements provide an effective overwintering strategy, while shorter dormancy requirements allow for rapid transitions between the benthic and planktonic stages. Such variability in dormancy period may also be a result of temporal variation, or location of the benthic population [9].

Our results may indicate the presence of a longer-term dormancy (months) for Puget Sound *A. catenella* cysts. We could not determine the absolute duration of this mandatory dormancy period because it is not known exactly when the cysts were formed, and to the best of our knowledge no phytoplankton samples were collected from Quartermaster Harbor in 2006. However, shellfish toxicity levels can be used as a proxy for vegetative cell concentrations. Earlier research [20] and more recent sampling in 2008 (SoundToxins phytoplankton monitoring records and WDOH toxin records; F. Cox, pers. comm.), found that increases in PSTs in mussels from Quartermaster Harbor paralleled increases in abundance of *A. catenella* in surface waters. Therefore, we used PSP toxin records from Quartermaster Harbor in 2006 to establish a proposed timeframe for *A. catenella* blooms and subsequent cyst deposition.

Washington State Department of Health's Biotoxin Program reported two episodes of high PSTs in Quartermaster Harbor from May – September, 2006 when toxin levels were reported weekly. The first episode of molluscan toxicity began on June 6th, and peaked at a concentration of 1619

μg/100 g on June 13th, after which PSTs declined to nearly undetectable by July 12th. The second episode appeared suddenly on August 16th with the highest levels of PSTs observed for the year (2049 μg/100 g), and steadily declined thereafter. From this toxicity data, we can approximate two bloom periods, early-mid June and early-mid August, in 2006 from which cysts were likely deposited into the surface sediments in Quartermaster Harbor. These probable bloom periods are consistent with previous research that reported two periods of high *A. catenella* abundances in 1981 in mid-June and September [20], and with more recent, 2008-2009, *A. catenella* cell concentrations peaking in late summer months, August-October (SoundToxins phytoplankton monitoring records).

Given these two estimated periods of cyst deposition in Quartermaster Harbor, it is possible that local *A. catenella* populations may have a mandatory dormancy period of up to 5 months (see Fig. 2.5). The longer mean incubation periods and much slower germination rates we observed in the November and December germination experiments could indicate that the majority of cysts were still in their dormancy period during those months. The additional episodes of germination for the November and December experiments, as well as, the shortened mean incubation periods and increased rates of germination starting in January may have marked the end of the maturation period. If *A. catenella* populations from Quartermaster Harbor in fact have a dormancy period on the order of 5 months, cysts that formed following the early summer bloom (early-mid June) would have the potential to germinate around mid-November and cysts that formed following the later summer bloom (early-mid August) would have the potential to germinate around mid-January (Fig. 2.5).

Although it is reasonable to assume we collected surface sediments containing cysts formed from both blooms in 2006, we believe that a larger portion of the cysts collected were formed following the late summer bloom. Higher levels of shellfish toxicity reported for late summer suggest greater vegetative cell abundances, and hence, possible increased cyst deposition at that time. Fewer cysts deposited from the early summer bloom could account for the lower rates of germination observed in the November and December experiments. It is possible that the few portion of wells with germination in the months of November (4%) and December (11%) contained a few cysts deposited from the early summer bloom while the majority of germination, which did not occur until mid-January, occurred from cysts deposited from the late summer bloom.

It remains unclear exactly why overall germination success was lower for the November and December germination experiments, although, it could be associated with the longer incubation periods observed for those months. We found that cysts remaining under incubation conditions for longer periods had significantly lower germination success. Perhaps conditions within the well plates were not suitable for long term cell survival (cyst or vegetative cells) despite replenishing wells with fresh medium. This outcome could be a result of fluctuations in salinity due to medium evaporation from the small volume wells increasing cell mortality and decreasing germination success of cysts still in their dormancy period.

Synchronous Endogenous Clock

The presence of a synchronous biological clock has been reported to restrict cyst germination to a specific seasonal time frame irrespective of the environmental conditions [9]. We found no

evidence of such an endogenous mechanism restricting germination to a specific seasonal window for *A. catenella* cysts from Quartermaster Harbor, since cysts were able to germinate year round (November-September).

The presence of a synchronous biological timing mechanism might best serve deep-water cyst beds that are exposed to fairly constant conditions and lack variation in light and temperature cues as was found for *Gonyaulax tamarensis* cysts collected from deep-water in the Gulf of Maine [9]. *Alexandrium fundyense* cysts collected from several deep-water sites (138 and 150 m) in the Gulf of Maine were found to have a circannual biological clock with an average period of 11 months [10]. In that study, cysts did not germinate in summer to fall even when provided with favorable growth conditions. However, Quartermaster Harbor is a relatively shallow bay with bottom waters that experience seasonal variation in environmental cues that can signal germination (e.g., light, temperature). Thus, the presence of a synchronous biological clock as described above may not be required for *A. catenella* cysts residing in a shallow location such as Quartermaster Harbor.

Our results provide some preliminary evidence indicating *A. catenella* cysts from Quartermaster Harbor have some form of endogenous control over germination apart from a period of mandatory dormancy. Both cysts and vegetative cells were present in the preserved samples for nearly all months, suggesting that either not all of the cysts were viable, or they did not have the same rates of germination. It is likely that many of the cysts counted in the samples preserved on the first day of observed germination were viable, and would have germinated given more time. If true, this would indicate variability in endogenous regulation of germination. Such variability

in emergence of *A. catenella* cysts has previously been reported and possibly reflects genetic variation among individuals from the same population [3,19].

Further, our cell counts from the wells preserved on the first day of observed germination revealed an interesting seasonal emergence pattern that could reflect more synchronous germination in late summer and winter, then in spring/early summer. Cysts made up a larger fraction of the total cells counted in the preserved well samples from March through June, while vegetative cells made up the majority from July-September, and potentially into the winter months. This observation appears to be consistent with recent bloom patterns reported for Quartermaster Harbor where *A. catenella* vegetative cell concentrations peak in late summer months, August-October (SoundToxins phytoplankton monitoring records).

Such seasonal emergence patterns may reflect cells operating under different germination strategies. Individuals might operate under either "tight" or "loose" endogenous control with tight endogenous control having germination patterns more reflective of a synchronous biological clock, while loose endogenous control would allow for rapid inoculation of the water column in response to favorable changes in environmental conditions. The presence of different germination strategies could help to ensure survival of the population [3]. Future work is needed to identify genotypic differences on isolated cysts to confirm the presence of different germination physiology within the population.

Ecological Implications

Puget Sound *A. catenella* populations have the potential to germinate year round, given dormancy requirements and environmental conditions are met. We have found evidence suggesting the presence of a longer-term mandatory dormancy of several months for *A. catenella* cysts in Quartermaster Harbor. Hence, for long-term cysts, excystment appears to be primarily regulated by physiological requirements (the details of which have not yet been identified), while specific environmental cues, such as temperature, light, oxygen and cyst resuspension, appear to be secondary in regulating excystment dynamics. Once physiological requirements are met and bottom water conditions support germination, *A. catenella* cysts have the ability to rapidly reseed the water column with vegetative cells. Such rapid germination rates observed in all months from January through September may help to explain frequent high winter toxin levels in shellfish, especially geoducks, and the necessity for harvest closures at times when motile cells are not expected to be present and have not been looked for in the water column (WDOH toxin records, F. Cox, pers. comm.).

We realize that our suggestions concerning endogenous regulation of germination are speculative, but believe they provide a starting point for more rigorous studies on *A. catenella* cyst germination in Puget Sound. As such, we view our results pertaining to mandatory dormancy as preliminary and suggest that cysts from both shallow embayments such as Quartermaster Harbor (depth < 30 m) and from deep water, such as the main basin (depth ≈ 250 m) be isolated and subject to detailed germination experiments.

2.6 References

1. Trainer VL, Eberhart B-TL, Wekell JC, Adams NG, Hanson L, et al. (2003) Paralytic shellfish toxins in Puget Sound, Washington State. J Shellfish Res 22: 213–223.

2. Anderson DM (1997) Bloom dynamics of toxic *Alexandrium* species in northeastern U.S. Limnol Oceanogr 42: 1009–1022. doi:10.4319/lo.1997.42.5_part_2.1009.

3. Anderson DM (1998) Physiology and Bloom Dynamics of Toxic *Alexandrium* Species, with Emphasis on Life Cycle Transitions. In: Anderson DM, Cembella AD, Hallefraeff GM, editors. Physiological Ecology of Harmful Algal Blooms. Springer-Verlag Berline Heidelberg. pp. 29–48.

4. Hallegraeff GM, Marshall J, Valentine J, Hardiman S (1998) Short cyst-dormancy period of an Australian isolate of the toxic dinoflagellate *Alexandrium catenella*. Mar Freshw Res 49: 415–420.

5. Anderson DM, Stock CA, Keafer BA, Bronzino Nelson A, Thompson B, et al. (2005) *Alexandrium fundyense* cyst dynamics in the Gulf of Maine. Deep Sea Res Part II Top Stud Oceanogr 52: 2522–2542. doi:10.1016/j.dsr2.2005.06.014.

6. Figueroa RI, Bravo I, Garcés E (2005) Effects of nutritional factors and different parental crosses on the encystment and excystment of *Alexandrium catenella* (Dinophyceae) in culture. Phycologia 44: 658–670. doi:10.2216/0031-8884(2005)44[658:eonfad]2.0.co;2.

7. Figueroa RI, Bravo I, Garcés E (2006) Multiple routes of sexuality in *Alexandrium taylori* (Dinophyceae) in culture. J Phycol 42: 1028–1039. doi:10.1111/j.1529-8817.2006.00262.x.

8. Joyce LB, Pitcher GC (2006) Cysts of *Alexandrium catenella* on the west coast of South Africa: distribution and characteristics of germination. J Mar Sci 28: 295–298. doi:10.2989/18142320609504165.

9. Anderson DM, Keafer BA (1987) An endogenous annual clock in the toxic marine dinoflagellate *Gonyaulax tamarensis*. Nature 325: 616–617. doi:10.1038/325616.

10. Matrai P, Thompson B, Keller M (2005) Circannual excystment of resting cysts of *Alexandrium* spp. from eastern Gulf of Maine populations. Deep Sea Res Part II Top Stud Oceanogr 52: 2560–2568. doi:10.1016/j.dsr2.2005.06.013.

11. Horner, R.A., Greengrove CL, Postel FR, Gawel JE, Davies-Vollum KS, Cox A, et al. (2008) *Alexandrium* cysts in Puget Sound, Washington, USA. Proceedings of the 12th International Conference on Harmful Algae. Copenhagen: International Society for the Study of Harmful Algae and Intergovernmental Oceanographic Commission of UNESCO. pp. 196–199.

12. Hoffer S, Horner RA, Greengrove CL (2005) Germination experiments with *Alexandrium catenella* cysts collected from surface sediments in Puget Sound. Third Symposium on Harmful Algae in the U.S. Pacific Grove, CA.

13. Andersen P, Throndsen J (2003) Estimating cell numbers. In: Hallegraeff GM, Anderson DM, Cembella AD, editors. Manual on harmful marine microalgae. Monographs on oceanographic methodology. Paris: UNESCO. pp. 99–129.

14. Guillard RRL, Ryther JH (1962) Studies of marine planktonic diatoms. I. *Cyclotella nana* Hustedt and *Detonula confervacea* Cleve. Can J Microbiol 8: 229–239.

15. Yamaguchi M, Itakura S, Imai I, Ishida Y (1995) A rapid and precise technique for enumeration of resting cysts of *Alexandrium* spp. (Dinophyceae) in natural sediments. Phycologica 34: 207–214.

16. Cox AM, Shull DH, Horner R. (2008) Profiles of *Alexandrium catenella* cysts in Puget Sound sediments and the relationship to paralytic shellfish poisoning events. Harmful Algae 7: 379–388. doi:10.1016/j.hal.2007.01.006.

17. Fritz L, Triemer RE (1985) A rapid simple technique utilizing Calcoflour White M2R for the visualization of dinoflagellate thecal plates. J Phycol 21: 662–664.

18. Rengefors K, Anderson DM (1998) Environmental and endogenous regulation of cyst germination in two freshwater dinoflagellates. J Phycol 34: 568–577. doi:10.1046/j.1529-8817.1998.340568.x.

19. Hallegraeff GM (1998) Transport of toxic dinoflagellates via ships' ballast water: bioeconomic risk assessment and efficacy of possible ballast water management strategies. Mar Ecol Prog Ser 168: 297–309. doi:10.3354/meps168297.

20. Nishitani L, Chew KK (1984) Recent developments in paralytic shellfish poisoning research. Aquaculture 39: 317–329. doi:10.1016/0044-8486(84)90274-6.

21. Scholin CA, Anderson DM (1994) Identification of group-specific and strain-specific genetic-markers for globally distributed *Alexandrium* (Dinophyceae). 1. Rflp analysis of SSU ribosomal-rRNA Genes. J Phycol 30: 744–754. doi:10.1111/j.0022-3646.1994.00744.x.

22. Lilly EL, Halanych KM, Anderson DM (2007) Species boundaries and global biogeography of the *Alexandrium tamarense* complex (Dinophyceae). J Phycol 43: 1329–1338. doi:10.1111/j.1529-8817.2007.00420.x.

23. Taylor FJ. (1984) Toxic dinoflagellates: Taxonomic and biogeographic aspects with emphasis on *Protogonyaulax*. Seafood Toxins, ACS Symposium Series 262. Washington: Am. Chem. Soc. p. 77.

24. Balech E (1995) The genus *Alexandrium* Halim (dinoflagellata). Sherkin Island Marine Station. Sherkin Island, Ireland. p. 151. doi:10.2307/3226651.

Table 2.1 Summary of germination rates and overall germination success in replicate wells for each monthly experiment.

	Time to first day of observed germination	Time to 50% germination (days)	Time to 95-100% germination (days)	Number of wells with germination (N)	Germination success (%)
November	~21	---	---	11	25
December	~14	~35-42	---	38	83
January	5	7	~14	48	100
February	4	4	7	47	98
March	2	2	4- 7	48	100
April	≤ 1	2	3	48	100
May	**≤ 1**	**≤ 1**	**≤ 1**	**48**	**100**
June	**≤ 1**	**≤ 1**	**2**	**48**	**100**
July	≤ 1	1-2	2	48	100
August	≤ 1	1	3	48	100
September	2	3	4	48	100

Table 2.2 Motile cell and cyst enumeration from the representative well sample preserved on the first day vegetative cells were observed for each month of the time-series experiment.

	Day well fixed	Total cells counted	Vegetative	Cysts	Portion vegetative	Portion cysts	Stain
November	21	24	0*	24	----	----	P &CW
December	14	130	127	3	0.98	0.02	CW
January	7	23	3*	20	----	----	P &CW
February	4	81	42	39	0.52	0.48	CW
March	2	71	20	51	0.28	0.72	CW
April	1	126	22	104	0.17	0.83	CW
May	1	91	31	60	0.34	0.66	CW
June	1	122	46	76	0.38	0.62	CW
July	2	111	99	12	0.89	0.11	CW
August	1	46	31	15	0.67	0.33	CW
September	2	3	3	0	1.00	0.00	CW

* Primulin staining method may have destroyed motile cells in the sample. P is primulin stained; CW is Calcofluor White stained**.**

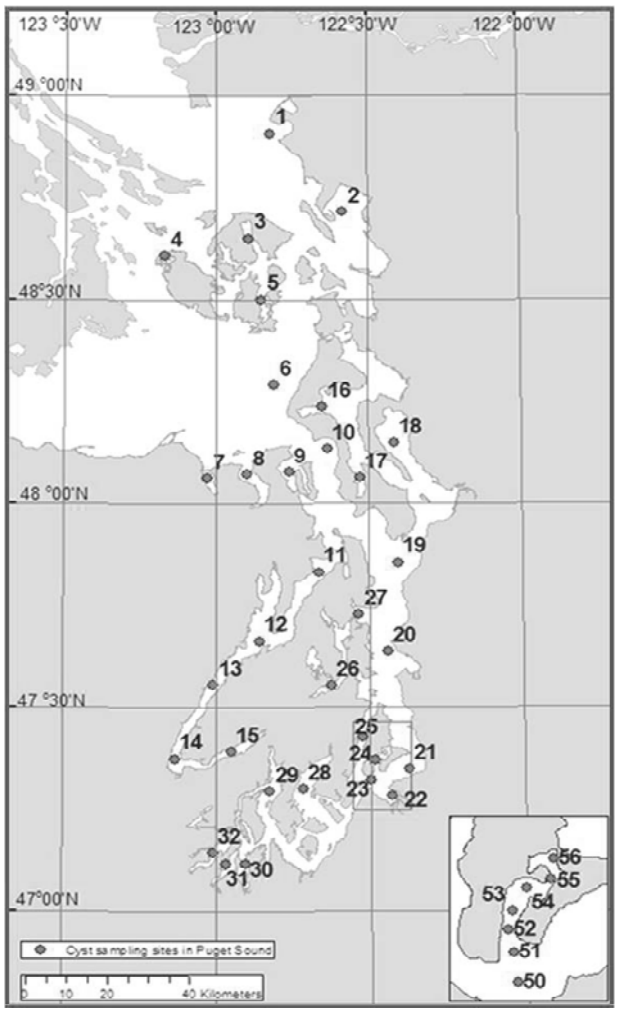

Figure 2.1 Map of Puget Sound, WA including all 2005 cyst survey sites. Inset shows Quartermaster Harbor from an intensive survey there in 2006 with our sampling site, station54.

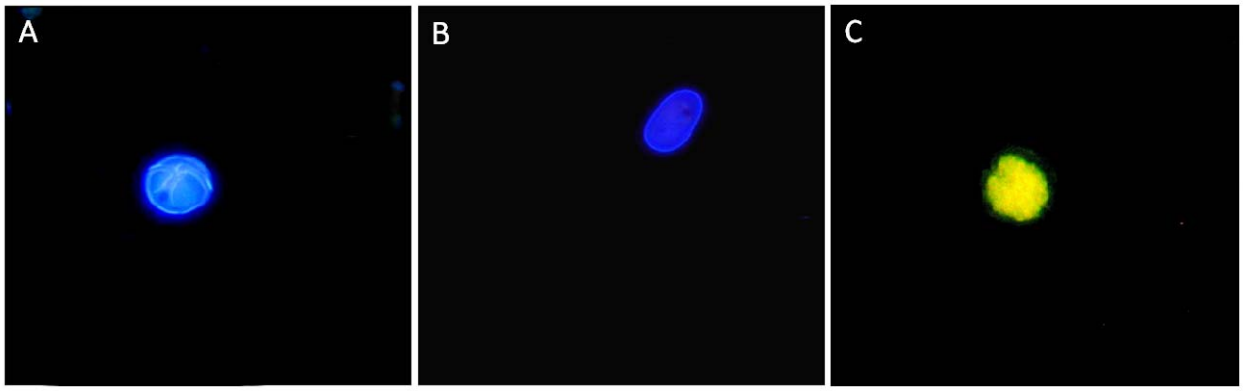

Figure 2.2 Stained *A. catenella* cells. Cells of *A. catenella* from the same incubated and preserved sediment subsample stained with Calcoflour White: vegetative cell (A) and cyst (B), and Primulin: vegetative cell (C).

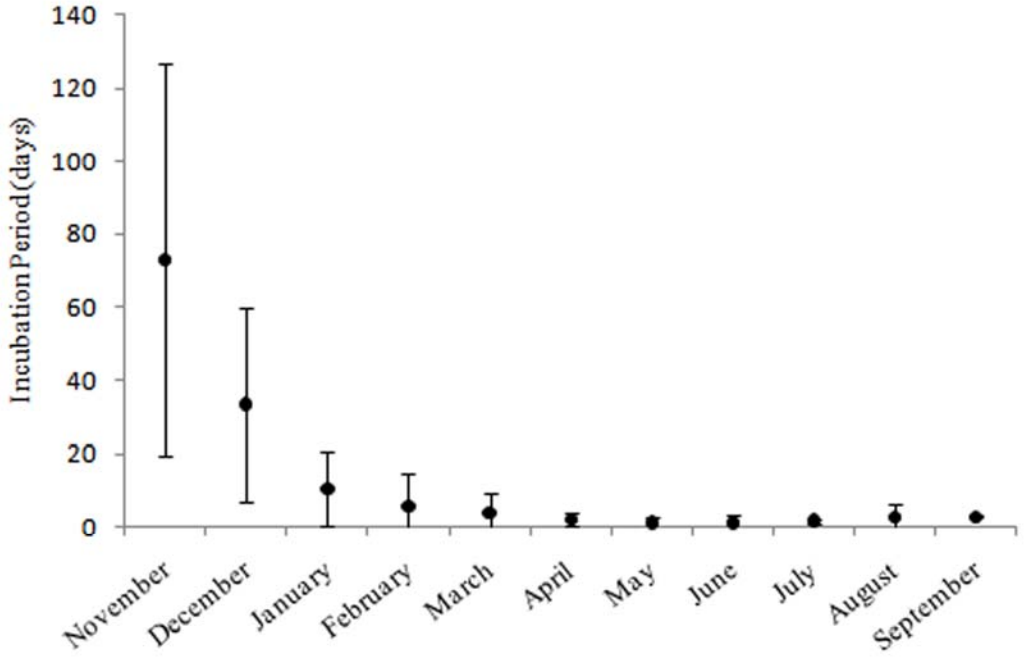

Figure 2.3 *A. catenella* cyst incubation period. The duration of the cyst incubation period (days) for each month of the time-series experiment (November 2006 – Septermber 2007). Center dot marks the mean incubation period for that month and error bars represent ± 2 standard deviations from the mean.

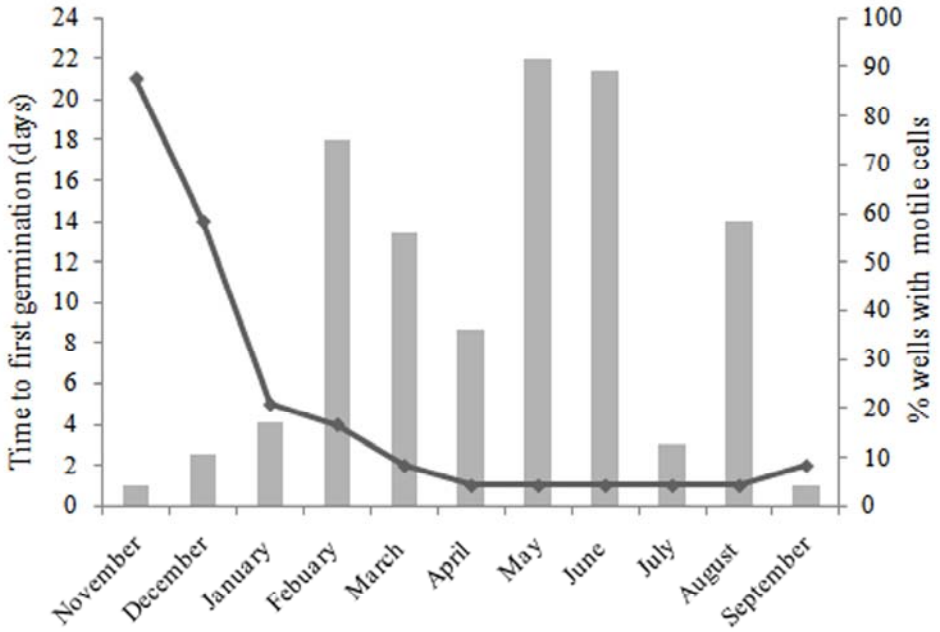

Figure 2.4 Time to first observed germination. The line graph shows time to first observed germination (days) for each month of the time-series experiment (November 2006 – Septermber 2007). The bar graph shows the portion of wells containing vegetative cells on the first day of observed germination.

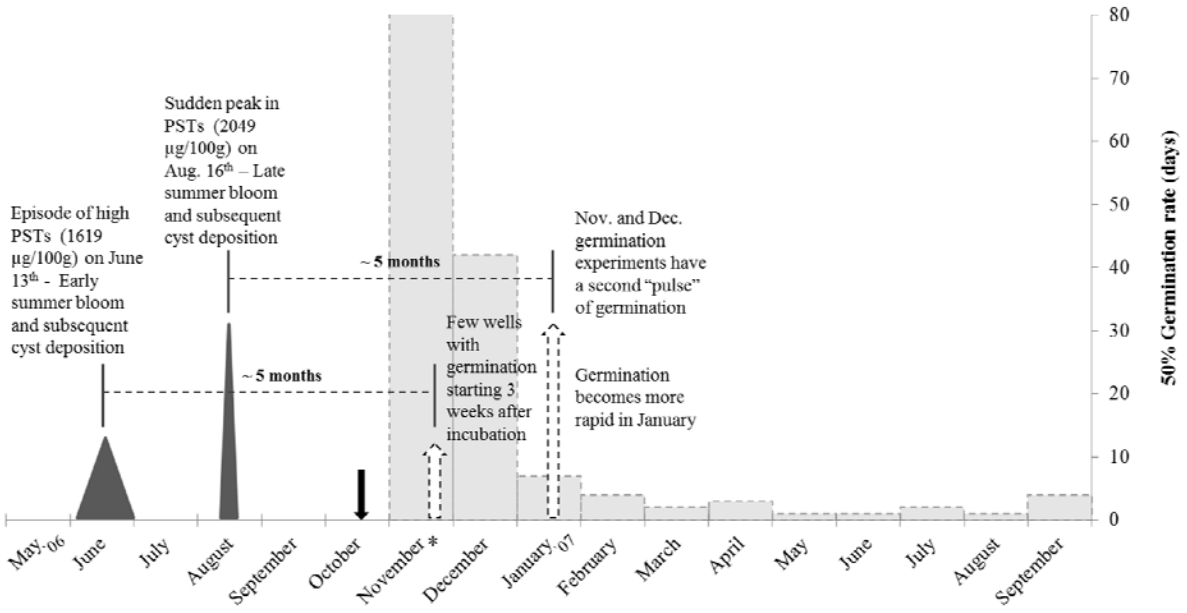

Figure 2.5 *A. catenella* cyst germination timeline. The timeline shows the approximated 5 month mandatory dormancy for *A. catenella* cysts in Quartermaster Harbor, WA. The timeline includes: suggested bloom periods and subsequent cyst deposition as indicated by PST records for summer 2006 (grey triangles), time of sediment collection (black arrow) and earliest episodes of germination (dotted arrows). The shaded bar graph shows time to 50% germination for each month. * November did not reach 50% within 15 weeks under incubation conditions.

Chapter 3. Pelagic-benthic transition of the harmful alga, *Heterosigma akashiwo*: Changes in swimming and implications for benthic cell distributions.

Elizabeth D. Tobin, Daniel Grünbaum, and Rose Ann Cattolico

School of Oceanography, University of Washington, Seattle WA. 98195-7940

"Reprinted from Harmful Algae, Vol. 10, Tobin, ED., Grünbaum, D., Cattolico, RA., Pelagic-benthic transition of the harmful alga, *Heterosigma akashiwo*: Changes in swimming and implications for benthic cell distributions, 619-628 (2011), with permission from Elsevier."

3.1 Abstract

Many harmful algal blooming (HAB) species transition between a vegetative, motile phase in the water column and a dormant, non-motile resting phase in the sediments. These life history transitions potentially regulate the timing, location and persistence of bloom events. Motility promotes aggregation and influences vertical distributions in the water column. However, the contribution of this behavior to benthic distributions of resting cells is currently unknown. We used video-tracking techniques to test the hypothesis that algal cells use active down-swimming during pelagic-benthic transition to favorably influence benthic distributions. In an experimental water column, we monitored cell swimming trajectories of *Heterosigma akashiwo* for 14 days after cells were signaled to enter the benthic resting stage. Using the statistical characteristics of individual cell trajectories, we developed a video-based motion assay to assign each tracked *Heterosigma* cell to one of three cell states known to occur during pelagic-benthic transition: induced motile, transitional and resting. The primary swimming characteristic influencing benthic distribution, net vertical velocity, was essentially the same for all three cell states. Hence, we found no evidence that active down-swimming influences benthic distributions. Our data

suggest that benthic distributions of *Heterosigma* resting cells are similar to distributions of slowly sedimenting passive particles. These observations suggest that *Heterosigma* benthic resting cell distributions can be predicted by modeling the effects of cell sedimentation rates combined with geophysical flow patterns.

3.1 Introduction

Many HAB-forming algae exhibit a dual-stage life history, transitioning between a pelagic vegetative stage and a benthic resting stage. These transitions are among the least understood aspects of HAB dynamics. The benthic stage is thought to promote survival during environmental conditions that are unfavorable to growth, to provide refuge from predation, and/or to facilitate long-range transport [1–6]. Rapid transition of pelagic vegetative cells into the benthic resting stage can contribute to HAB termination, while benthic populations can serve as reservoirs that initiate HABs by rapidly reseeding the water column with vegetative cells when favorable conditions return [7,8]. Hence, transitions into and out of the benthic resting stage may strongly affect the timing, location and magnitude of HABs [9,10].

Transitions between pelagic and benthic habitats often involve significant vertical movements. Vegetative, pelagic cells are typically concentrated in near-surface waters. These cells cannot establish benthic populations until they descend to encounter the benthic substrate, often a depth change of tens of meters. The timing and rate of these depth changes are critical to survival of these cells, because lateral advection in coastal environments can quickly move cells between suitable (usually shallow) benthic habitats and unsuitable (usually deeper) locations. In deep sediments, cells are less likely to experience bottom conditions, principally temperature and

light, conducive to germination and subsequent transition to the vegetative stage. However, the mechanisms that control depth during pelagic-benthic transition, and thus ultimately lead to deposition in the sediments, are poorly understood.

HAB-forming algae commonly use active swimming in their pelagic phase to regulate depth and locate favorable growth conditions [11,12]. Algal swimming often interacts with physical flows to influence cell concentrations and distributions in the water column [13–17]. The prevalence of swimming in HAB-forming algae, together with the apparent importance of resting cell deposition in suitable substrates, suggests the hypothesis that algal cells use active swimming during the pelagic-benthic transition to favorably influence benthic distributions. If so, motility during benthic cyst formation could have important but currently unknown impacts on HAB dynamics.

In this paper, we experimentally test this hypothesis using *Heterosigma akashiwo* as our focal organism. *Heterosigma* is a harmful raphidophyte that forms dense surface blooms associated with kills of wild and pen-reared fish in temperate and subtropical waters worldwide [18,19]. These blooms are often initiated in shallow coastal embayments, but may be advected to deeper waters [3,20–23]. *Heterosigma* has an alternating pelagic-benthic life history [19,24]. Field conditions that signal transition into the benthic resting phase are not well understood. Cell aggregation has been reported to be a preliminary step in the formation of benthic resting cells [24]. These benthic cells had poor survival at higher temperatures (≥ 15°C) in the light. Additional laboratory-based studies have also shown that reduced temperature and dark conditions induce formation and extend survival of benthic resting cells [25,26]. Transition out

of the benthic stage is controlled largely by temperature, with 10°C the approximate lower limit for emergence and ≥15°C required for successful proliferation [3,26–29]. *Heterosigma* exhibits vigorous up-swimming behavior in its vegetative stage, and this swimming behavior has been identified as an important mechanism in bloom formation [17,20,23,30,31].

Little is known about how *Heterosigma's* swimming behaviors influence benthic distributions following HAB termination. In one of the few published studies of *Heterosigma* benthic resting cell formation, Han et al. [26] used microscopy to show that vegetative cells transitioning into benthic resting cells express a distinct "transitional" stage of reduced motility. These transitional cells are characterized by reduced swimming velocity and directionality (rotating in circles or spinning in place) as flagellar movement is lost. Because the ultimate goal of that study was not to characterize cell swimming behaviors, Han et al.'s observations did not establish how cell movements progress from the up-swimming vegetative stage to the non-motile benthic stage, or the consequences of those movements for benthic distributions. Bearon et al. [31] suggested that the oscillatory movement of helical swimming algae like *Heterosigma* could provide useful diagnostic information about the type and state of cells. The existence of a distinct transitional phase identifiable by movement characteristics also suggests that movement-based assays have the potential to identify cell state during pelagic-benthic transition on a cell-by-cell level.

To obtain quantitative information about individual *Heterosigma* cell movements during pelagic-benthic transition, we used a video-based tracking technique to monitor cell swimming in an experimental water column. Similar motion analysis techniques have been used to assess movement behaviors, physiological state and health of algal cells [17,31–33]. We developed statistical methods to classify each tracked cell into one of three physiological states based on

fine scale horizontal movements, and then quantified net vertical movements associated with each state. We then used state-specific vertical movement data to test the hypothesis that *Heterosigma* cells actively influence their benthic distribution by shifting from up-swimming to down-swimming prior to forming benthic resting cells. The specific goals of this study were: (1) to develop a video-based motion assay to identify cell state using swimming characteristics during pelagic-benthic transition, and to verify that assay with traditional microscope techniques; (2) to determine whether *Heterosigma* exhibits distinct state-specific vertical movement behaviors during transition; and (3) to assess the potential consequences of transitional behaviors for benthic distributions of *Heterosigma* resting cells.

3.3 Materials and Procedure

Cell maintenance and resting cell induction

A *Heterosigma akashiwo* strain CCMP452 culture was maintained in 1 L reduced salinity (22‰) artificial seawater O-3 medium [34] and grown to stationary phase (>$2x10^5$ cells mL^{-1}) at 20°C, on a 12 hour dark:12 hour light (50 µmol/m^2/s; LI-COR Inc. LI-250A, NE, USA) photoperiod under continuous rotary agitation (60 rpm). This culture was used to inoculate eighteen 250 mL experimental flasks, each containing 125 mL medium, to $2.5x10^4$ cells mL^{-1}. These sub-cultures were maintained at 15°C on a 12 hour dark: 12 hour light (50 µmol/m^2/s) photoperiod for five days prior to the start of the experiment. Concentrations of cell cultures were determined with a ZBI Coulter Counter (Coulter Electronics, Inc. Hialeah, FL, USA) equipped with a 100µm aperture. On the starting day of the experiment (Day 0), cell concentrations were approximately 6-$8x10^4$ cells mL^{-1} in each flask. To induce *Heterosigma* cells to enter their benthic resting stage on Day 0, the experimental flasks were placed in the dark at 10°C [26]. Because even short

exposures to very low light levels (<0.1 μmol/m^2/s) inhibit resting cell formation [26] (Cattolico unpublished data) each experimental flask was wrapped in foil prior to being stored in the darkened environmental chamber. Preliminary experiments conducted to test the viability of resting cells formed under our induction conditions showed up to 95% survival when these resting cells were activated to return to the vegetative stage after 16 days by restoring light to ~50 μmol/m^2/s and temperature to 20°C (data not shown).

Experimental tank for cell observations

Cell movements were observed in a 190 mm x 140 mm x 60 mm experimental tank constructed with 6 equally spaced replicate partitions (Fig. 3.1). Each partition was filled from the bottom using a peristalitic pump. This method enabled the formation of a two-layer stratified water column that suppressed fluid convection [17]. A halocline was established between a 100 mL bottom layer that had a weakly stratified linear salinity gradient ranging from 30 psu at the base to 26 psu at the top and a 50 mL top layer of modified O-3 medium at 22 psu (Fig. 3.1). The salinity gradient was established with O3 medium (30 psu) diluted with fresh (de-ionized) water to generate the specified salinity structure. Each observation day, 0.5mL of cell culture was taken from two of the 250mL experimental flasks (one flask for partitions 1, 3 and 5, the other for partitions 2, 4 and 6). These cells were added slowly to the top layer of each partition of the tank, so that each top layer contained approximately 7-8x10^2 cells mL^{-1}. Prior to experiments, we used fluorescein added to the top, lower salinity layer to verify that cell addition did not disturb the stratified water column. All cell transfers were performed inside a dark environmental chamber under red light (620-750 nm), to which *Heterosigma* cells do not respond (Lakeman and Cattolico unpublished data; pers. obs.). The experimental tank was then covered with a light-

tight box made of infrared (IR) transmitting acrylic, so that cells could be imaged while excluding visible light. The filming experiments took place within a dark environmental chamber, maintained at 10°C for the duration of the study. Cells were observed on Day 0 and every other day for 14 days by capturing two minute video clips every 30 min for the first 2 hours and hourly for the next 6 hours. A total of 64 video clips from hours 0-5 were analyzed (8 clips for each of the 8 observation days).

Microscope analysis of cell states

Cells exposed to induction conditions were counted under bright field microscopy (400x) in a Palmer-Maloney counting slide and classified into one of three states. To determine cell concentrations, the entire chamber was counted. To classify the portion of cells in each state, cells were counted in each field of view using the grid on the optical lens until ≥ 100 cells were counted. Cells were classified as "induced motile" if they expressed propulsive helical swimming, irrespective of cell shape; as "transitional" if they appeared to have highly reduced swimming capabilities (rotation, twitching or vibration), or had no movement and were aspherical; and as "resting" if they had no movement and were spherical. Sphericity is a robust morphological characteristic of *Heterosigma* cysts formed in culture [24–26]. Non-moving cells that were not spherical were rarely observed. Cell counts were conducted on experimental flasks before loading cells into the experimental tank on each observation day, and were used to calculate the initial cell concentration in the 50 mL top layer at hour 0. To determine final cell distributions (hour 8), the top and bottom layers in the experimental tank were sampled from 4 of the 6 replicate partitions. The entire 50 mL top layer of the stratified water column was extracted and gently mixed, and 10 mL were sub-sampled. A 10 mL sub-sample of the bottom layer was

extracted from a fixed tube pre-positioned at the base of each partition. Cell concentrations for the entire 100 mL bottom layer were also estimated by subtracting the final top layer cell population from the cell population initially added. We placed sampled aliquots into light-excluding test tubes for subsequent counting. Cell concentrations were determined by a ZBI Coulter Counter and verified by light microscopy.

Video analysis of cell motility

Video sequences of cell movement were captured to a computer at 30 frames s^{-1} using an IR sensitive analog camera (Mintron Opitic Industry Co. #MTV-13V8HE) equipped with a Nikon Nikkor 60 mm lens (aperture f/8) and a #8 extension tube. Cells were observed under dark field illumination using two IR LED banks. The camera and light sources were mounted on a computer-controlled motorized platform that moved horizontally across the tank, so lighting and imaging were consistent for all partitions. A SmartRelay controller (6bit Inc., UT, USA) was used to control camera position, filming duration, and lighting from a computer located outside of the environmental chamber. The camera was positioned approximately 22 mm from the tank, providing a field of view approximately 9 mm x 12 mm located entirely within the bottom layer of each partition. Thus, only cells leaving the top layer by downward swimming or passive sinking were imaged and analyzed (Fig. 3.2).

Video processing and path analysis

Pixel positions of the cells in each video clip were determined by video processing using a modified version of the open source video editing package, Avidemux 2.4, to remove background, equalize lighting, threshold frames and set particle size range to clearly resolve

cells. Video was calibrated with a uniform grid of dots with 2.5 mm spacing. Pixel coordinates of cells were converted into physical positions and assembled into 2D cell swimming trajectories with Tracker3D, a MATLAB-based motion-analysis package to track organism movement (Grünbaum unpubl.). High frequency noise was removed from cell trajectories using a short-interval smoothing spline [31,35]. This spline had knot spacing of 30 frames (1 second), which was short enough to resolve oscillations in cell trajectories. Overall direction was defined using a long-interval spline with knot spacing of 225 frames (7.5 seconds) to follow the central axis of each cell's path. Analysis included only cell trajectories longer than 900 frames (30 seconds).

To characterize cell-specific swimming behaviors, splined trajectories were used to calculate five swimming metrics. We defined the oscillatory component of swimming as the difference between the long-interval and short-interval splines. To determine the mean oscillatory speed for each trajectory, we took the time derivative of the oscillatory component to obtain the associated velocities, calculated the roots of the sums of the squares (RSS) of those velocities to obtain oscillatory speed, and finally averaged oscillatory speeds over the entire trajectory. We calculated mean horizontal and mean vertical velocity for each trajectory by taking the time derivative of the long-interval spline (i.e., the central axis) to obtain its instantaneous horizontal and vertical velocity components, and then averaged the vertical velocity components over the entire trajectory. Finally, we calculated gross swimming speed of each trajectory by taking the RSS of the instantaneous velocity components in two dimensions. All mean path statistics were weighted by path duration to avoid biasing in favor of shorter or longer paths.

These swimming metrics, in association with the microscope-based classifications, were the basis of our video-based classification of cell state. We used a Pearson's correlation test to determine whether video-based and microscope-base methods were statistically consistent in establishing the proportion of the population in each state over the duration of the study. The proportion data were normalized using an arcsin transformation.

3.4 Results

Trends in cell state and distribution

Cell concentrations within the sampling flasks at the outset of each filming experiment were nearly identical when determined using the Coulter Counter and the Palmer-Maloney counting chamber (Table 3.1). Both methods verified that modest cell loss occurred during the 14 day experiment (Fig. 3.2a). On Day 0, 99% of the cells were in the induced motile state (Table 3.1). Over successive days, a larger proportion of cells were identified as either transitional or non-motile resting cells. By the end of the experiment (Day 14), 33% of cells were identified as transitional and 54% as non-motile resting cells.

Microscope counts showed that cell concentrations within the experimental tank decreased in the top layer and increased in the bottom layer over successive observation days, indicating that more cells had net downward movement as the population transitioned into the benthic resting phase (Fig. 3.2b, d). Cell concentrations from the sub-sampled (10 mL) bottom layer closely matched concentrations calculated for the entire (100 mL) bottom layer, indicating that the sub-sampled bottom layer counts were representative of the bottom layer population (Fig. 3.2c, d).

Identification and verification of cell states from video-based observations

Pronounced changes in distributions of mean oscillatory speed were observed as the cell population transitioned from predominantly motile cells (Day 0) to mostly non-motile resting cells (Day 14). We used mean oscillatory speed to assign each trajectory to its appropriate cell state[1]. Our assignments were based on the observed changes in mean oscillatory speed for cell trajectories over successive observation days (Fig. 3.3), as well as detailed examination of swimming characteristics of individual trajectories (Fig. 3.4). Mean oscillatory speeds were mostly >9 μm s^{-1} on Day 0, while at the end of the study nearly all mean oscillatory speeds were <9 μm s^{-1} (Fig. 3.3). Hence, we established 9 μm s^{-1} as a lower limit for the oscillatory speed of an induced motile cell. Though resting cells are non-motile, their oscillatory speed is non-zero due to random fluctuations in the net downward trajectory from Brownian motion and/or electronic noise during video acquisition. Therefore, we examined hundreds of individual straight downward moving trajectories, indicative of non-motile sinking cells, and found that none of the trajectories observed had mean oscillatory speeds ≥ 4 μm s^{-1} (Fig. 3.4c). We consequently established 4 μm s^{-1} as an upper limit to the oscillatory speed of a non-motile, resting cell (Fig. 3.3). Some straight downward trajectories, similar to those of resting cells, sank at velocities > 10 μm s^{-1}. Because this sinking velocity implies an unrealistically high density (based on Stokes Flow; see Table 3.2) for a *Heterosigma* cell, these trajectories were almost certainly created by extraneous particles present in the culture medium. We therefore excluded such trajectories from our statistical analysis.

[1] Because our trajectories are two-dimensional projections of three-dimensional helical movements, our calculated oscillatory speeds slightly underestimate three-dimensional speeds. Our assessment thresholds apply to our two-dimensional projected movements. Corresponding thresholds for three-dimensional data are higher by a factor of approximately 2π.

Over the 8 filming experiments, we analyzed a total of 19,307 cell trajectories (Table 3.2). Figure 4 shows typical swimming trajectories for induced motile cells (more convoluted), transitional cells (more regular but lower-amplitude oscillations) and resting cells (nearly straight downward profiles) according to the criteria described above.

Population fraction assigned to each cell state was quantitatively consistent between our video-based assay and microscope counts over successive days (Fig. 3.5a). Both methods were significantly correlated in determining the population fractions assigned to each cell state (Fig. 3.5b). The induced motile cell fractions were strongly correlated ($r = 0.78$, $P < 0.001$), while the transitional and resting cell fractions had slightly weaker associations ($r = 0.54$, $P = 0.001$ and $r = 0.40$, $P = 0.02$, respectively).

Comparison of swimming among cell states

We used the classification assignments based on oscillatory movement to compare the state-specific values of net vertical velocity for each cell trajectory. Mean vertical velocities for each observed state were relatively consistent over the duration of the experiment. As expected, nearly the entire cell population observed in the bottom layer had net downward movement on all days (Fig. 3.6a). The calculated vertical velocities were unimodal and tightly distributed around the mean. Hence, only a very small fraction of the sampled population had net upward movement (Fig. 3.6b).

State-specific swimming statistics averaged over the duration of the experiment showed that induced motile cells had overall higher mean gross speeds (9 ± 4.8 μm s^{-1}) than transitional and

resting cells (6 ± 2.0 μm s^{-1} and 5 ± 1.7 μm s^{-1}, respectively). However, all three states had essentially equal mean downward vertical velocities (Table 3.2).

3.5 Discussion

Cell-level swimming plays a critical role in influencing distributions of algal populations, and hence in HAB dynamics, by modulating cell interactions with physical transport mechanisms in the water column [14,15,17,19,36]. In this study, we developed a video-based motion assay to identify state-specific changes in swimming of the HAB-forming alga *Heterosigma akashiwo* during transition from the vegetative pelagic phase to the dormant benthic phase. We used this assay to assess the implications of swimming for benthic distributions. Our key finding is that, while *Heterosigma* exhibits a succession of distinct swimming modes during pelagic-benthic transition, none of these swimming modes have a strong influence on vertical movement rates. Consequently, our observations suggest that benthic resting cell deposition in natural environments where *Heterosigma* forms HABs can be predicted by modeling the combined effects of *Heterosigma* sedimentation rates and geophysical flow patterns.

Motion-based assay of physiological state

The results reported here demonstrate that quantification of the oscillatory movement of a helically swimming algal cell, as suggested by Bearon et al. [31], is a viable method of identifying cell state (Fig. 3.4). Net movements of *Heterosigma* are predominantly vertical [17,31]; the oscillatory deviations from these net movements are predominantly horizontal. Our video-based assay uses quantitative analysis of these horizontal deviations to infer physiological

state of individual tracked cells, which is a necessary step in comparing state-specific vertical swimming behaviors.

We assessed the accuracy of our video-based motion assay by comparing its assignments of population fraction in each physiological state to assignments made from traditional microscope-based classification. The two methods were significantly correlated when assigning the population to each cell state (Fig. 3.5b). The correlation was strongest for assignment of the induced motile cell fraction of the population and slightly weaker for transitional and resting cell assignments. The weaker association between video and microscope-based assignments of transitional and resting cell fractions is likely due to differences in the resolution with which each method detects fine scale movements. We expected that the resting cell fraction would monotonically increase over time as the cell population was continuously exposed to conditions that signal transition to the benthic resting stage. The results of the video-based assay were more consistent with this expectation than those of the microscope-base assay. The observed decline in the resting cell fraction after Day 8 (Fig. 3.5a, lower) reported from the microscope-based analysis suggests misclassification. Hence, the video-based classification developed in this study may be more accurate than traditional microscope-based classification.

Our video-based approach has some additional advantages over microscope-based methods of detection and enumeration. Video analysis can be conducted more quickly and with less observer training, and can be conducted in the field or even implemented as remote sensing. Another advantage, and the one most crucial to the analysis of this study, is that our video-based assay can classify cell states on a trajectory-by-trajectory basis. This cell-level association between

state and movement is essential to understanding state-specific vertical fluxes at bloom termination. To the best of our knowledge, there is no alternative method to video analysis for simultaneously quantifying cell state and swimming velocity.

Swimming behaviors during pelagic-benthic transition

Our results showed that cells in all three states observed during the transition from motile, vegetative cells to non-motile, resting cells had essentially the same mean downward velocities of approximately 4 μm s^{-1} (Table 3.2). Because swimming plays a key role in benthic-pelagic transition, it is somewhat surprising that we did not observe active down-swimming during the pelagic-benthic life-stage transition. Induced motile cells had mean downward velocity of 4 ± 3.5 μm s^{-1} and mean gross speed of 9 ± 4.8 μm s^{-1}. Vegetative cells of the same *Heterosigma* strain observed under growth-supporting conditions were reported to have mean upward velocities between 35-60 μm s^{-1} and mean gross speeds between 49-66 μm s^{-1} [31]. The difference in gross speeds indicates that induced motile cells have a highly reduced overall swimming capacity compared to vegetative motile cells. The theoretical settling velocity of a *Heterosigma*-sized spherical particle is 3.77 μm s^{-1} (based on Stokes flow, see Table 3.2) which closely matches the mean downward vertical velocities of induced motile cells observed in this study. This result suggests that, even with functional flagella, transitioning cells reached the bottom layer of the tank by passive settling under gravity (Table 3.2).

Slow downward movement and convoluted swimming observed in induced motile cells indicate that transitioning *Heterosigma* cells lose the orientation ability necessary for directional swimming before losing flagellar propulsion. Loss of orientation is unexpected because it is

unclear what, if any, benefits are gained from non-oriented swimming rather than immediate cessation of flagellar activity. It may be there is no benefit to cells, but also little cost. Alternatively, retention of partial flagellar function might allow for faster reversion to the vegetative phase if environmental conditions improve. It is also possible that even undirected swimming positively impacts nutrient uptake, bacterial feeding, or interactions with predators, pathogens and substrate through mechanisms that are still unclear.

The ability of *Heterosigma* cells to enter the resting stage may represent a generalized response to adverse physiological conditions. In addition to our study, prior observations have shown that both nutrient and abiotic stresses can lead to benthic resting cell formation in *Heterosigma* (Lakeman and Cattolico, pers. comm.; pers. obs.) [24,26]. Benthic resting cell formation could act as a temporary refuge from adverse environmental conditions, wherein cells enter a form of stasis mediated by reduced metabolic activity (Cattolico and Deodato, unpublished). Because no single environmental cue strictly triggers the onset of this process, transitional behaviors are likely to be similar in response to a variety of abruptly changing environmental conditions. If so, our study provides highly detailed information concerning swimming behaviors as cells transition between pelagic and benthic stages.

The results from this study provide evidence that *Heterosigma* cells reach the sediments through passive sinking. However, we cannot rule out the possibility that cells use particle attachment or aggregation as an additional means to facilitate rapid downward transport [24]. *Heterosigma* cells often produce an external sticky polysaccharide calyx, which may serve to attach cells to sinking particles or may promote cell aggregation, thus accelerating downward transport

[19,26,37]. A preliminary experiment we conducted to determine whether the presence of sinking particles (glass beads of various sizes) accelerated downward transport of transitioning *Heterosigma* cells did not show an effect of these particles on *Heterosigma* cell transport (data not shown). This result may suggest *Heterosigma* cells do not actively attach to sinking particles to facilitate downward transport during life stage transition. However, it may also reflect artifacts of laboratory conditions due to the type of particles or culture medium. The potential for facilitated sinking using attachment warrants further investigation.

To the best of our knowledge, swimming behaviors of *Heterosigma* cells during pelagic-benthic life stage transition have not been documented in the field. However, it is interesting to consider how our observations might compare to behaviors expressed in their natural environment. For example, different cell morphologies have been observed for *Heterosigma* cells during bloom events [18,21]. It has been suggested that smaller, non-motile cells observed at bloom termination in Puget Sound, WA could represent the resting or pre-resting stage for this organism [21]. Observations of smaller, non-motile cells occurring in natural blooms provides some evidence that cessation of flagellar activity occurs in the water column, resulting in subsequent sedimentation to the benthos as we observed in our experiments.

Implications for benthic distributions

Cell behaviors expressed during pelagic-benthic life-stage transition in dynamic estuarine systems could be of particular importance to bloom reoccurrences by influencing seeding patterns of benthic resting cells. *Heterosigma* cells in the vegetative phase are notably vigorous swimmers with upward speeds of up to 100 μm s^{-1} [31], suggesting that they can potentially

move vertically several meters per day. However, our results show *Heterosigma* cells lose their directed swimming capacity early in transition, apparently before it can serve any significant role in influencing benthic distributions.

Our observations raise important questions concerning *Heterosigma* life history. Why do *Heterosigma* cells not use their considerable swimming capacity to facilitate rapid downward transport during pelagic-benthic transition? What are the dominant mechanisms (in the absence of swimming) by which transitioning cells are transported to the sediments? How frequently do cells encounter benthic habitats suitable for survival and re-emergence?

For perspective on these questions, we developed an idealized numerical water column model to identify the time scales that transitioning cells (initially at the surface, < 1m) require to make contact with sediments at various depths under a range of ecologically relevant vertical mixing rates (Fig 3.7). This model computes the distribution of cells over time and depth as a function of vertical turbulent mixing, downward cell swimming velocity and depth. We used this model to test two alternate behavioral responses: the observed sinking at 4 μm s^{-1}, and hypothetical down-swimming at 100 μm s^{-1}.

We estimated the influence of vertical mixing on *Heterosigma* cells due to turbulent transport using eddy diffusivity, K (m^2/s). Eddy diffusivity varies with depth due to boundary-layer effects and interactions with obstacles such as sediments, biota and seabed topography [38–40]. However, for a rough order-of-magnitude estimate we approximated eddy diffusivity as being constant throughout the water column, and varied that constant over a wide range to reflect

Heterosigma's coastal and estuarine environments (see x-axis of Fig. 3.7). We obtained these varied rates of eddy diffusivity from published data [39,41,42].

Our estimates from the model output show that both depth and speed of net downward movement strongly influence the rate of contact with the sediments (Fig. 3.7). Regardless of *Heterosigma's* downward movement behavior, and under all relevant turbulent mixing conditions, the amount of time to contact the sediments increases strongly and consistently with depth. This outcome is in agreement with the findings of Gaylord et al. who reported sinking depth to be the primary factor influencing macroalgal spore dispersal, except during periods of intense vertical mixing [38,39].

In estuarine environments *Heterosigma* cells are transported by horizontal advection over both shallow and deep sediments. Survival depends on resting cells depositing in shallow sediments that provide the necessary light and temperature conditions required for re-emergence [3,21,43]. Our model output shows hypothetical active down-swimming at 100 μm s^{-1} would likely have only modest effects on contact with shallow sediments (< 60 m) under moderate or intense turbulent mixing (> 4 m^2 s^{-1}). On the other hand, active down-swimming could substantially increase contact rates with deeper sediments relative to turbulent mixing (see Fig. 3.7). The rate of transport suggested by our idealized model would be altered under more stratified conditions, e.g., in the presence of a halocline or thermocline, that limits the mixed layer depth in which cells would be entrained. Nonetheless, our model suggests (somewhat counter-intuitively) that down-swimming might be disadvantageous under certain flow conditions (e.g., those dominated

by vertical turbulent mixing) since active down-swimming increases the relative probability of contacting deeper rather than shallower sediments.

The slow sedimentation that we observed in transitioning cells suggests that benthic distributions of *Heterosigma* resting cells are ultimately controlled by physical processes, with vertical transport dominated by turbulence and horizontal transport dominated by ambient currents. In coastal and estuarine environments changes in mean flow associated with tidal cycles occur frequently while cells are suspended in the water column. Rapid, hour-by-hour variation in speed and direction of mean flow can cause increased variability in abundances and spatial extent of benthic populations, and may partially explain the stochastic nature of *Heterosigma* blooms in such regions [21,44].

In terms of HAB prediction, our observations of *Heterosigma* during transition suggest that simple, physics-driven prediction schemes underlying distribution patterns of *Heterosigma* resting cells are likely to be successful. Future benthic distributions are likely to mirror distributions of slowly sedimenting particles released from current bloom termination sites. Improving our ability to model the location and abundance of these benthic populations will provide the basis for improved interannual bloom prediction.

3.6 References

1. Anderson DM (1997) Bloom dynamics of toxic *Alexandrium* species in northeastern U.S. Limnol Oceanogr 42: 1009–1022. doi:10.4319/lo.1997.42.5_part_2.1009.

2. Hallegraeff GM (1998) Transport of toxic dinoflagellates via ships' ballast water: bioeconomic risk assessment and efficacy of possible ballast water management strategies. Mar Ecol Prog Ser 168: 297–309. doi:10.3354/meps168297.

3. Imai I, Itakura S (1999) Importance of cysts in the population dynamics of the red tide flagellate *Heterosigma akashiwo* (Raphidophyceae). Mar Biol 133: 755–762. doi:10.1007/s002270050517.

4. Matrai P, Thompson B, Keller M (2005) Circannual excystment of resting cysts of *Alexandrium* spp. from eastern Gulf of Maine populations. Deep Sea Res Part II Top Stud Oceanogr 52: 2560–2568. doi:10.1016/j.dsr2.2005.06.013.

5. Anderson DM, Rengefors K (2006) Community assembly and seasonal succession of marine dinoflagellates in a temperate estuary: The importance of life cycle events. Limnol Oceanogr 51: 860–873. doi:10.4319/lo.2006.51.2.0860.

6. Kremp A, Rengefors K, Montresor M (2009) Species specific encystment patterns in three Baltic cold-water dinoflagellates: The role of multiple cues in resting cyst formation. Limnol Oceanogr 54: 1125–1138. doi:10.4319/lo.2009.54.4.1125.

7. Anderson DM, Kulis DM, Binder BJ (1984) Sexuality and cyst formation in the dinoflagellate *Gonyaulax tamarensis*: Cyst yield in batch cultures. J Phycol 20: 418–425. doi:10.1111/j.0022-3646.1984.00418.x.

8. Ishikawa A, Taniguchi A (1996) Contribution of benthic cysts to the population dynamics of *Scrippsiella* spp. (Dinophyceae). Mar Ecol Prog Ser 140: 169–178. doi:10.3354/meps140169.

9. Anderson DM, Stock CA, Keafer BA, Bronzino Nelson A, Thompson B, et al. (2005) *Alexandrium fundyense* cyst dynamics in the Gulf of Maine. Deep Sea Res Part II Top Stud Oceanogr 52: 2522–2542. doi:10.1016/j.dsr2.2005.06.014.

10. He R, McGillicuddy DJ, Keafer BA, Anderson DM (2008) Historic 2005 toxic bloom of *Alexandrium fundyense* in the western Gulf of Maine: Coupled biophysical numerical modeling. J Geophys Res 113: C07040. doi:10.1029/2007JC004602.

11. Anderson DM, Stolzenbach KD (1985) Selective retention of two dinoflagellates in a well- mixed estuarine embayment: The importance of diel vertical migration and surface avoidance. Mar Ecol Prog Ser 25: 39–50. doi:10.3354/meps025039.

12. MacIntyre J, Cullen JJ, Cembella AD (1997) Vertical migration, nutrition and toxicity in the dinoflagellate *Alexandrium tamarense*. Mar Ecol Prog Ser 148: 201–216. doi:10.3354/meps148201.

13. Kessler JO (1985) Hydrodynamic focusing of motile algal cells. Nature 313: 218–220. doi:10.1038/313218a0.

14. Donaghay PL, Osborn TR (1997) Toward a theory of biological-physical control of harmful algal bloom dynamics and impacts. Limnol Oceanogr 42: 1283–1296. doi:10.4319/lo.1997.42.5_part_2.1283.

15. Franks PJS (1997) Spatial patterns in dense algal blooms. Limnol Oceanogr 42: 1297–1305. doi:10.4319/lo.1997.42.5_part_2.1297.

16. Smayda TJ (2002) Turbulence, watermass stratification and harmful algal blooms: An alternative view and frontal zones as "pelagic seed banks." Harmful Algae 1: 95–112. doi:10.1016/S1568-9883(02)00010-0.

17. Bearon RN, Grünbaum D, Cattolico RA (2006) Effects of salinity structure on swimming behavior and harmful algal bloom formation in *Heterosigma akashiwo*, a toxic raphidophyte. Mar Ecol Prog Ser 306: 153–163. doi:10.3354/meps306153.

18. Jack Rensel JE, Haigh N, Tynan TJ (2010) Fraser river sockeye salmon marine survival decline and harmful blooms of *Heterosigma akashiwo*. Harmful Algae 10: 98–115. doi:10.1016/j.hal.2010.07.005.

19. Smayda TJ (1998) Ecophysiology and bloom dynamics of *Heterosigma akashiwo* (Raphidophyceae). In: Anderson. D.M, Cembella AD, Hallegraeff G., editors. Physological Ecology of Harmful Algal Blooms. Springer-Verlag Berlin Heidelberg. pp. 115–131.

20. Handy SM, Coyne KJ, Portune KJ, Demir E, Doblin MA, et al. (2005) Evaluating vertical migration behavior of harmful raphidophytes in the Delaware Inland Bays utilizing quantitative real-time PCR. Aquat Microb Ecol 40: 121–132. doi:10.3354/ame040121.

21. Rensel JJE (2007) Fish kills from the harmful alga *Heterosigma akashiwo* in Puget Sound: Recent blooms and review. Prepared by Rensel Associates Aquatic Sciences for the National Oceanic and Atmospheric Administration Center for Sponsored Coastal Ocean Research (CSCOR), Washington, DC (2007). pp. 58

22. Kempton J, Keppler CJ, Lewitus A, Shuler A, Wilde S (2008) A novel *Heterosigma akashiwo* (Raphidophyceae) bloom extending from a South Carolina bay to offshore waters. Harmful Algae 7: 235–240. doi:10.1016/j.hal.2007.08.003.

23. Yamochi S, Abe T (1984) Mechanisms to initiate a *Heterosigma akashiwo* red tide in Osaka bay. Mar Biol 83: 255–261. doi:10.1007/BF00397457.

24. Tomas CR (1978) *Olsthodiscus luteus* (Chrysophyceae) II. Formation and survival of a benthic stage. J Phycol 14: 314–319. doi:10.1111/j.1529-8817.1978.tb00304.x.

25. Itakura S, Nagasaki K, Yamaguchi M, Imai I, Tide R, et al. (1996) Cyst formation in the red tide flagellate *Heterosigma akashiwo* (Raphidophyceae). J Plankton Res 18: 1975–1979. doi:10.1093/plankt/18.10.1975.

26. Han M, Kim Y, Cattolico RA, Taylor FJR (2002) *Heterosigma akashiwo* (Raphidophyceae) resting cell formation in batch culture: Strain identity versus physiological response. J Phycol 317: 304–317. doi:10.1046/j.1529-8817.2002.01087.x.

27. Shikata T, Nagasoe S, Matsubara T, Yamasaki Y, Shimasaki Y, et al. (2007) Effects of temperature and light on cyst germination and germinated cell survival of the noxious raphidophyte *Heterosigma akashiwo*. Harmful Algae 6: 700–706. doi:10.1016/j.hal.2007.02.008.

28. Shikata T, Nagasoe S, Matsubara T, Yoshikawa S, Yamasaki Y, et al. (2008) Factors influencing the initiation of blooms of the raphidophyte *Heterosigma akashiwo* and the diatom *Skeletonema costatum* in a port in Japan. Limnol Oceanogr 53: 2503–2518. doi:10.4319/lo.2008.53.6.2503.

29. Taylor FJR, Horner R (1994) Red tides and other problems with harmful algal blooms in Pacific Northwest coastal waters. In: Wilson RCH, Beamish RJ, Aitkens F, Bell J, editors. Review of the marine environment and biota of Strait of Georgia, Puget Sound and Juan de Fuca Strait. Canadian Technical Report of Fisheries and Aquatic Sciences. pp. 175–186.

30. Hershberger PK, Rensel JE, Matter a L, Taub FB (1997) Vertical distribution of the chloromonad flagellate *Heterosigma carterae* in columns: implications for bloom development. Can J Fish Aquat Sci 54: 2228–2234. doi:10.1139/f97-131.

31. Bearon RN, Grunbaum D, Cattolico RA (2004) Relating cell-level swimming behaviors to vertical population distributions in *Heterosigma akashiwo* (Raphidophyceae), a harmful alga. Limnol Oceanogr 49: 607–613. doi:10.4319/lo.2004.49.2.0607.

32. Iken K, Amsler CD, Green SP, Mcclintock JB (2001) Qualitative and quantitative studies of the swimming behaviour of *Hincksia irregularis* (Phaeophyceae) spores: Ecologicla implications and parameter for quantitative swimming assays. Phycologia 40: 359–366.

33. Mayali X, Franks PJS, Tanaka Y, Azam F (2008) Bacteria-induced motility reduction in *Lingulodinium polyedrum* (Dinophyceae). J Phycol 44: 923–928. doi:10.1111/j.1529-8817.2008.00549.x.

34. McIntosh L, Cattolico RA (1978) Preservation of algal and higher plant ribosomal RNA integrity during extraction and electrophoretic quantitation. Anal Biochem 91: 600–612. doi:10.1016/0003-2697(78)90546-8.

35. Bearon RN, Grünbaum D (2008) From individual behaviour to population models: A case study using swimming algae. J Theor Biol 251: 679–697. doi:10.1016/j.jtbi.2008.01.007.

36. Erga SR, Dybwad M, Frette Ø, Lotsberg JK, Aursland K (2003) New aspects of migratory behavior of phytoplankton in stratified waters : Effects of halocline strength and light on *Tetraselmis* sp. (Prasinophyceae) in an artificial water column. Limnol Oceanogr 48: 1202–1213.

37. Cattolico RA, Boothroyd J, Gibbs S (1976) Synchronous growth and plastid replication in the naturally wall-less alga *Olisthodiscus luteus*. Plant Physiol 57: 497–503. doi:10.1104/pp.57.4.497.

38. Gaylord B, Reed DC, Raimondi PT, Washburn L, McLean SR (2002) A physically based model of macroalgal spore dispersal in the wave and current-dominated nearshore. Ecology 83: 1239–1251.

39. Gaylord B, Reed DC, Washburn L, Raimondi PT (2004) Physical–biological coupling in spore dispersal of kelp forest macroalgae. J Mar Syst 49: 19–39. doi:10.1016/j.jmarsys.2003.05.003.

40. Rosman JH, Monismith SG, Denny MW, Koseff JR (2010) Currents and turbulence within a kelp forest (*Macrocystis pyrifera*): Insights from a dynamically scaled laboratory model. Limnol Oceanogr 55: 1145–1158. doi:10.4319/lo.2010.55.3.1145.

41. Lavelle JW, Cokelet ED, Cannon GA. (1991) A model study of density intrusions into and circulation within a deep, silled estuary: Puget Sound. J Geophys Res 96: 16779–16800. Available: http://doi.wiley.com/10.1029/91JC01450.

42. Mickett JB, Gregg MC, Seim HE (2004) Direct measurements of diapycnal mixing in a fjord reach—Puget Sound's Main Basin. Estuar Coast Shelf Sci 59: 539–558. doi:10.1016/j.ecss.2003.10.009.

43. Portune K, Coyne K, Hutchins D, Handy S, Cary S (2009) Quantitative real-time PCR for detecting germination of *Heterosigma akashiwo* and *Chattonella subsalsa* cysts from Delaware's Inland Bays, USA. Aquat Microb Ecol 55: 229–239. doi:10.3354/ame01292.

44. Connell L, Jacobs M (1998) Anatomy of a bloom: *Heterosigma carterae* in Puget Sound 1997. In Puget Sound Research. Vol. 98: 830–834.

45. Wada M, Miyazaki A, Fujii T (1985) On the mechanisms of diurnal vertical migration behavior of *Heterosigma akashiwo* (Raphidophyceae). Plant Cell Physiol 26: 431–436. doi:10.1111/j.1529-8817.1988.tb04452.x.

Table 3.1 Cell concentrations and fractions of the population in each state determined from the experimental flasks used for cell loading on each observation day. Cell concentrations are consistent between the ZBI Coulter Counter and the Palmer-Maloney (PM) counting chamber.

Day	Induced motile (%)	Transitional (%)	Resting (%)	Coulter (cell/ml)	PM (cell/ml)
0	98.6	1.3	0.0	64365	71280
2	75.4	24.1	0.5	73790	62800
4	78.9	15.9	5.1	84720	78400
6	64.2	11.5	24.2	69870	60600
8	47.5	10.7	41.8	69730	70800
10	31.4	27.0	41.6	67380	62200
12	13.4	46.2	40.4	71460	75800
14	13.3	32.8	53.8	62520	65600

Table 3.2 Mean swimming statistics over the 8 days of observation for the three cell states (± 2 SD). All swimming statistics were weighted by path length.

	Induced Motile	Transitional	Resting	Vegetative Motile[1]	Settling Velocity*
Mean Oscillatory Speed (μm s^{-1})	14 ± 6.1	7 ± 2.1	4 ± 0.9		
Mean Gross Speed (μm s^{-1})	9 ± 4.8	6 ± 2.0	5 ± 1.7	49-66	
Mean Vertical Velocity (μm s^{-1})	- 4 ± 3.5	- 4 ± 2.2	- 4 ± 1.8	35-60	3.77
Mean Horizontal Velocity (μm s^{-1})	5 ± 4.1	2 ± 1.7	1 ± 0.6		
N	5712	5161	8434		

[1] Swimming statistics for vegetative motile cells were obtained from Bearon et al. [31]. * Settling velocity was calculated using Stokes flow: $V_s = \frac{2}{9}\frac{(\rho_p - \rho_f)}{\mu} g R^2$. Where ρ_p = 1.105 g cm^{-3} [45], ρ_f = 1.025 g cm^{-3} at a salinity of 28 psu, R = 5 μm, μ = 1.376 x 10^{-3} at a salinity of 28 psu and temperature of 10°C.

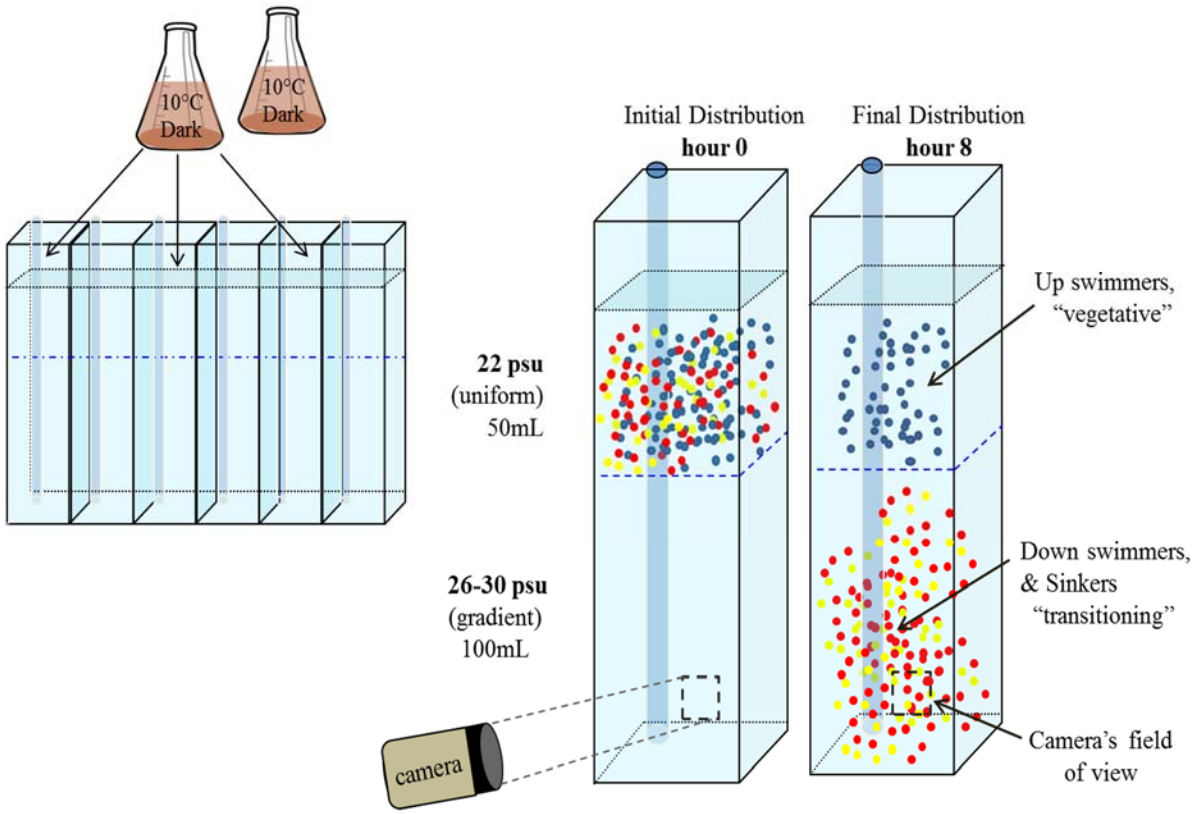

Figure 3.1 Schematic of the experimental filming tank. Experimental tank divided into 6 replicate partitions to which cells were added (left). Detail of the 2-layer water column in a single partition showing expected initial and final cell distributions (right). Cells were added to the top layer of each partition, using two of the experimental flasks at the start of each observation day. At hour 0, cells are present only in the top layer. The 2-layer structure inhibits mixing of water between layers, so all cells observed in the bottom layer entered by swimming down or sinking out of the top layer.

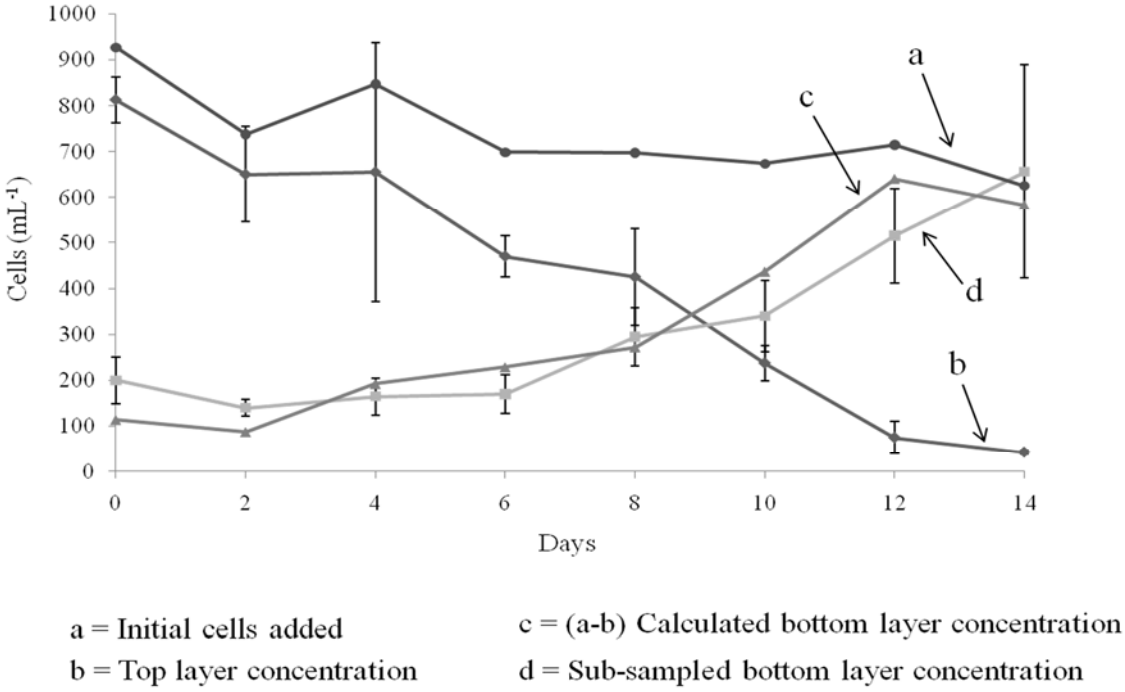

Figure 3.2 Cell concentrations within the experimental tank determined by microscopy on successive days of observation. (a) Initial cell concentration (hour 0) added to the top layer. (b) Final cell concentrations (hour 8) remaining in the top layer. (c) Final cell concentrations in the bottom layer, estimated from the difference between initial and final cell concentrations in the top layer. (d) Final cell concentrations sub-sampled from the bottom layer (hour 8).

Figure 3.3 Examples of scatter plots showing changes in distributions of mean oscillatory speed in cell trajectories between the start and end dates of the experiment. Mean oscillatory speeds were mostly >9 μm s^{-1} (>0.009 mm s^{-1}) on Day 0, when the majority of cells were in the induced motile state (top). The majority of mean oscillatory speeds were <9 μm s^{-1} by the end of the 14 day study (bottom). 4 μm s^{-1} was established as the upper threshold to classify "resting" cells. Paths falling between these thresholds were classified as "transitional" cells. For example, on Day 6 (middle), both video classification and microscope counts showed all three physiological states were present.

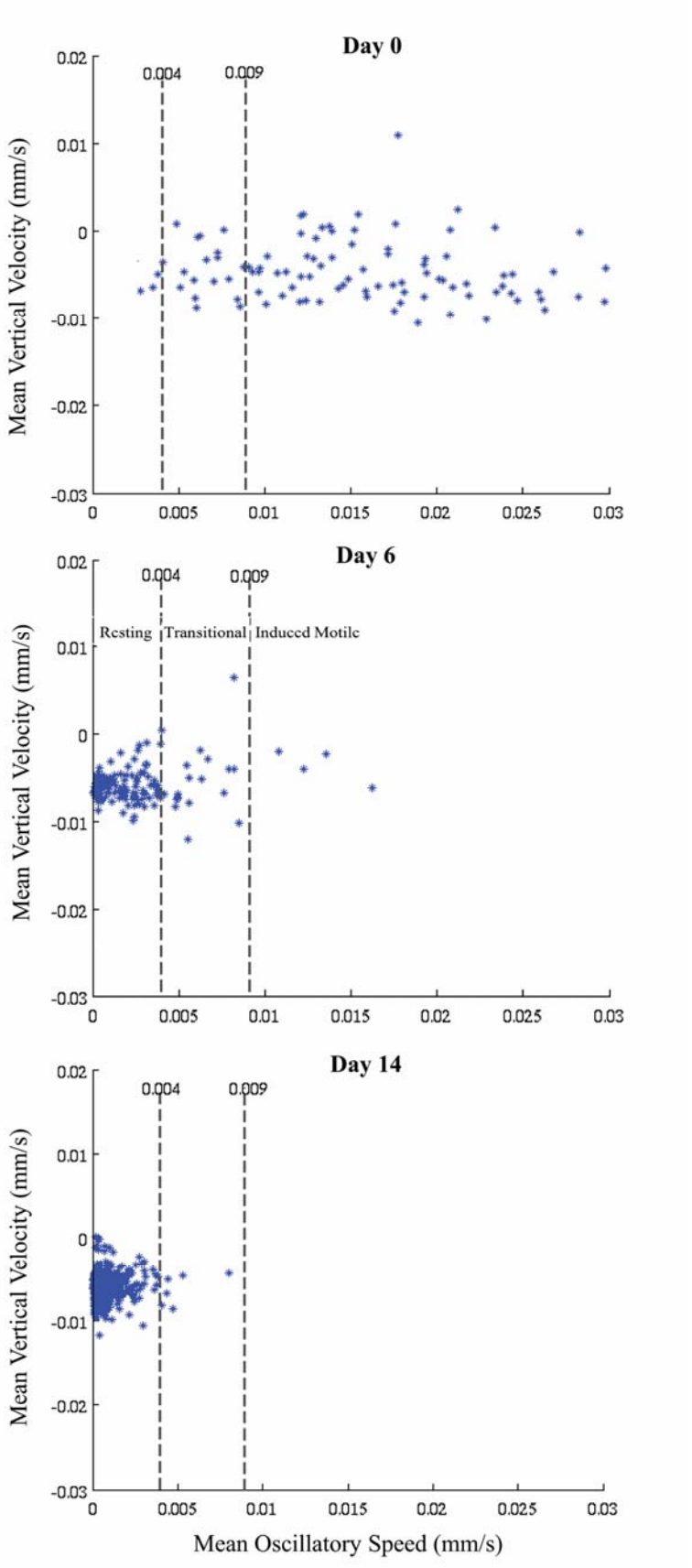
Day 0
Day 6
Day 14
0.004
0.009
Resting
Transitional
Induced Motile
Mean Vertical Velocity (mm/s)
Mean Oscillatory Speed (mm/s)
0.02
0.01
0
-0.01
-0.02
-0.03
0
0.005
0.01
0.015
0.02
0.025
0.03

Figure 3.4 Typical swimming profiles for the three cell states. Example trajectories (left plots) and their associated oscillatory component of swimming (right plots) from the same 2 minute video clip captured on Day 8. Mean oscillatory speed of each distinct profile falls within the selected thresholds used to assign trajectories to the appropriate cell state: (a) induced motile cell, (b) transitional cell, (c) resting cell (see Fig. 3 for details).

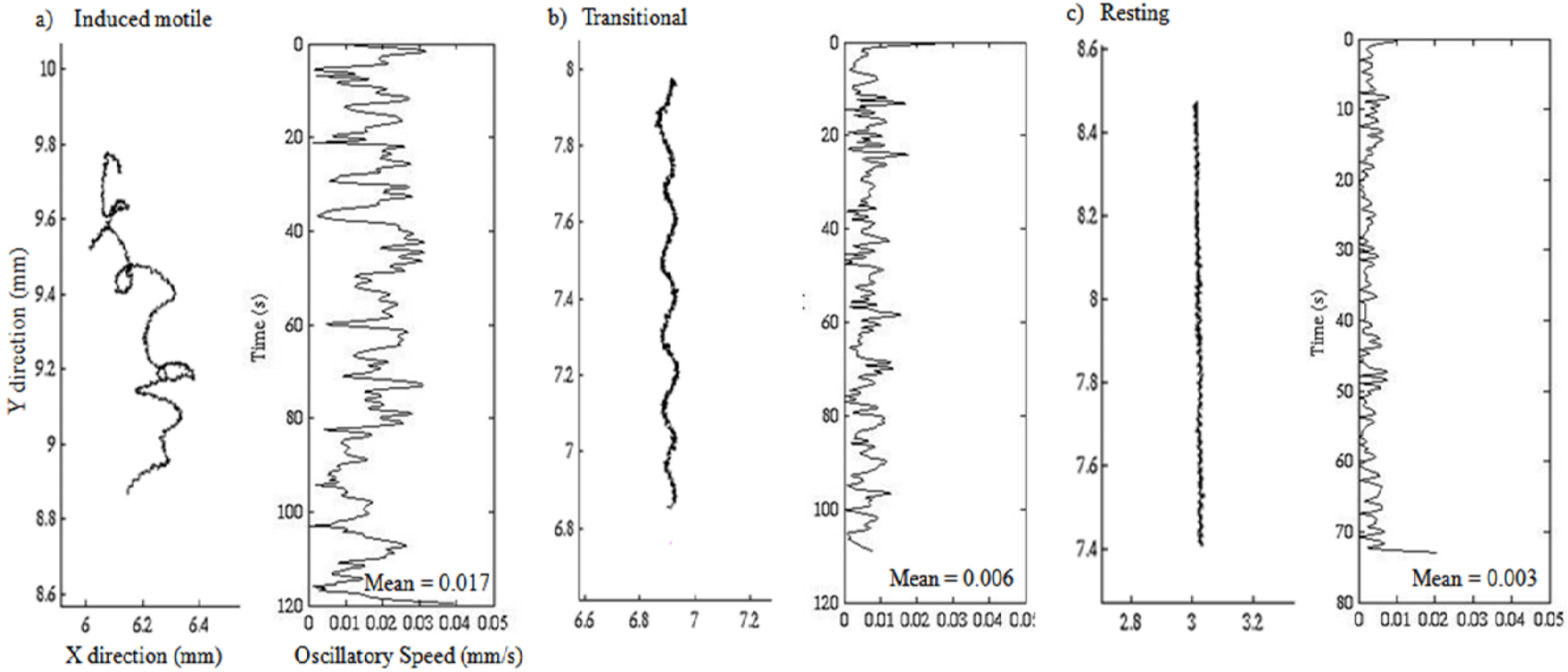
a) Induced motile
b) Transitional
c) Resting
Y direction (mm)
X direction (mm)
Time (s)
Oscillatory Speed (mm/s)
Mean = 0.017
Mean = 0.006
Mean = 0.003

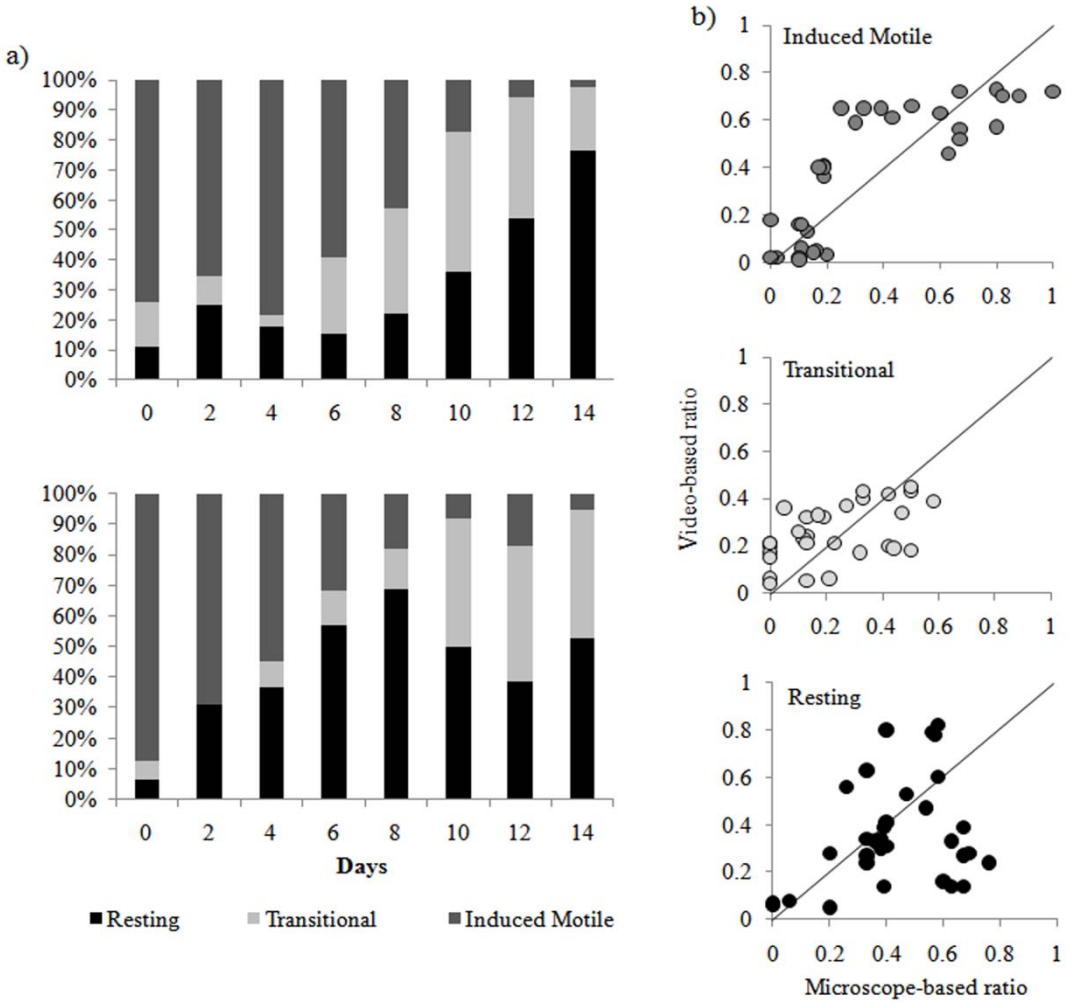

Figure 3.5 Proportion of cells observed in each state for the two enumerations methods. Stacked bar graphs (a) show the population fraction of induced motile, transitional and resting cell states from the bottom layer of the experimental water column for successive observation days according to both enumeration methods used in the study, video-based motion analysis (upper) and microscope-based counts (lower). Correlation plots show the association between the two enumeration methods (b) for the fraction of induced motile cells (upper, $r = 0.783$, $P < 0.001$, $N = 32$), transitional cells (middle, $r = 0.543$, $P = 0.02$, $N = 32$) and resting cells (lower, $r = 0.403$, $P = 0.001$, $N = 32$). Correlation coefficients and P-values were calculated using proportion data normalized by arcsin transformation.

Figure 3.6 Line graphs of mean vertical velocities (a) among induced motile (dot-dash), transitional (dash) and resting (solid) cells for each observation day. Error bars represent standard error. Box plots show the spread of mean vertical velocities for induced motile (b) and transitional cells (c) over successive observation days. The box defines the lower (0.25) and upper (0.75) quartiles and the middle line indicates the median. The whiskers show the range of the 10 and 90 percentiles. The dotted lines separate net upward from net downward movement.

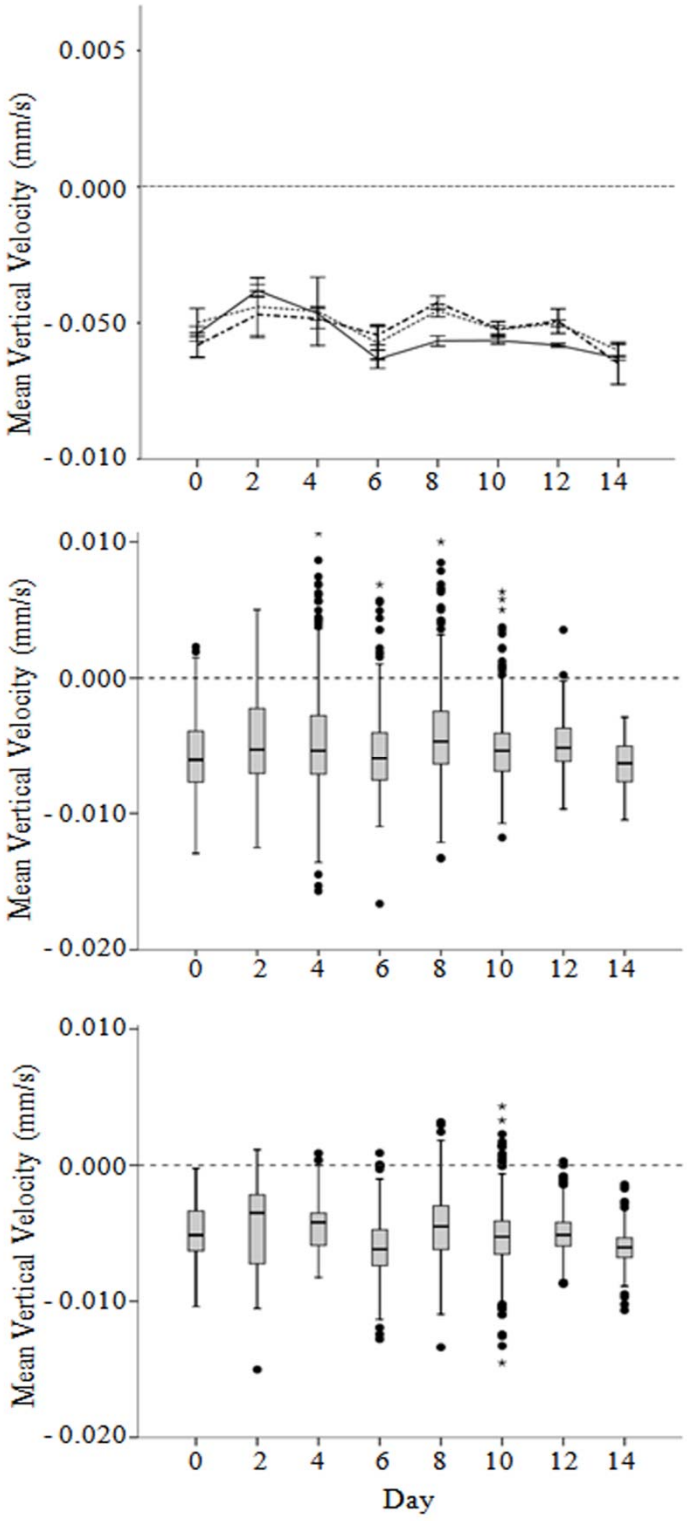
Mean Vertical Velocity (mm/s)
0.005
0.000
- 0.050
- 0.010
0 2 4 6 8 10 12 14
Mean Vertical Velocity (mm/s)
0.010
0.000
- 0.010
- 0.020
0 2 4 6 8 10 12 14
Mean Vertical Velocity (mm/s)
0.010
0.000
- 0.010
- 0.020
0 2 4 6 8 10 12 14
Day

Figure 3.7 Contour plots showing estimated median first contact times with the sediments for (a) passively sinking and (b) hypothetical down-swimming transitional cells under a range of relevant water column depths (m) and turbulent mixing conditions (eddy diffusivity, *K*). Contact times are indicated by time (days) until 50% of the cells have encountered sediments at least once (i.e., the median day of first contact with sediments). Each contour line from dark blue (< 1 day to reach the bottom) to dark red (30+ days to reach the bottom) represents a one day increment.

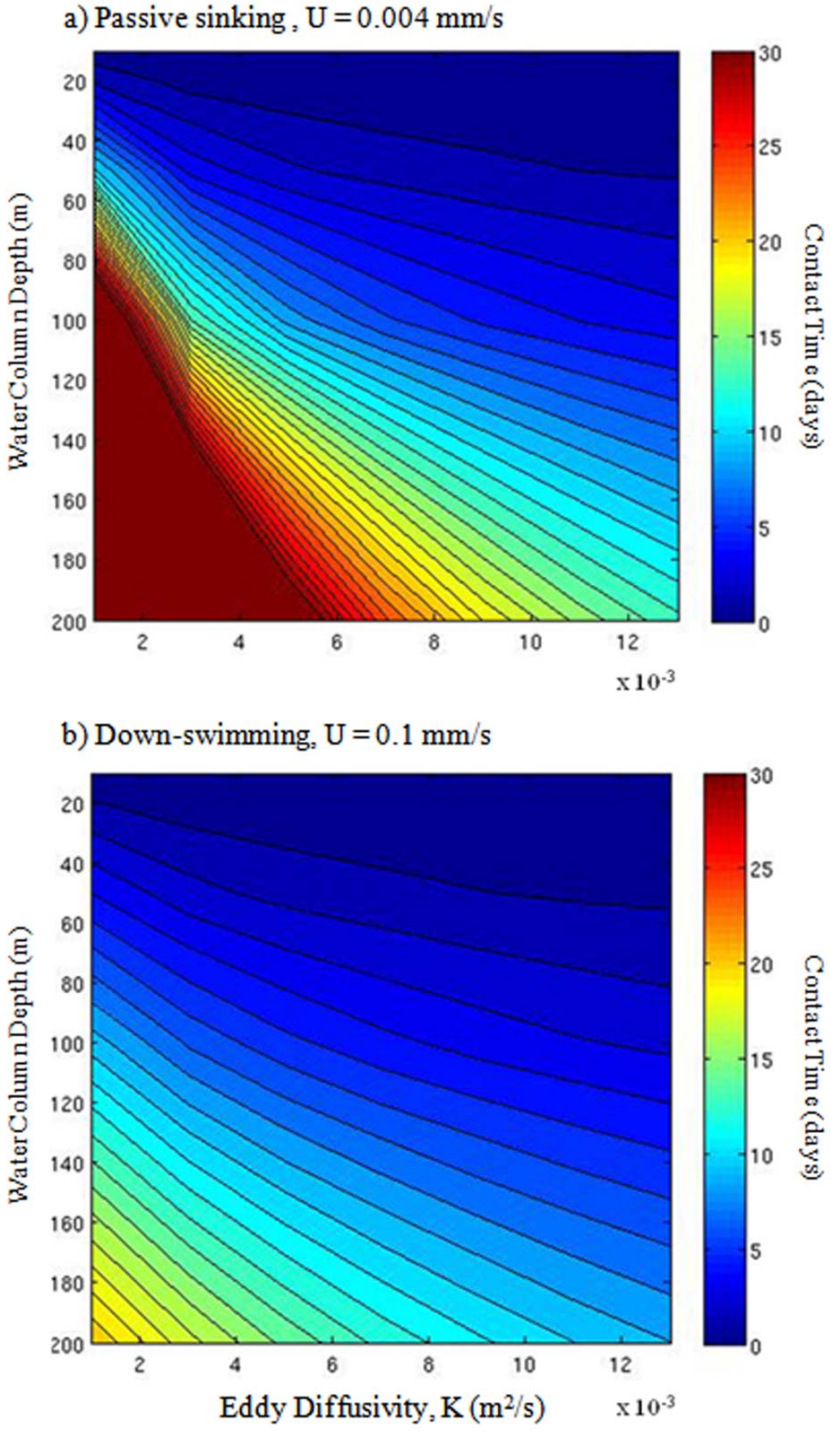
a) Passive sinking , U = 0.004 mm/s
Water Column Depth (m)
20
40
60
80
100
120
140
160
180
200
2
4
6
8
10
12
x 10-3
Contact Time (days)
30
25
20
15
10
5
0
b) Down-swimming, U = 0.1 mm/s
Water Column Depth (m)
Eddy Diffusivity, K (m2/s)
x 10-3
Contact Time (days)

Chapter 4. Behavioral and physiological changes during benthic-pelagic transition in the harmful alga, *Heterosigma akashiwo*: Potential for rapid bloom formation.

Elizabeth D. Tobin[1]*, Daniel Grünbaum[1], Johnathan Patterson[2] and Rose Ann Cattolico[2]

1 School of Oceanography, University of Washington, Seattle, Washington, United States of America.

2 Department of Biology, University of Washington, Seattle, Washington, United States of America.

"Reprinted from *PLOS one*, Vol. 8.10, Tobin, ED., Grünbaum, D., Patterson, J., Cattolico, RA., Behavioral and physiological changes during benthic-pelagic transition in the harmful alga, *Heterosigma akashiwo*: Potential for rapid bloom formation, e76663 (2013), open-access online publication."

4.1 Abstract

Many species of harmful algae transition between a motile, vegetative stage in the water column and a non-motile, resting stage in the sediments. Physiological and behavioral traits expressed during benthic-pelagic transition potentially regulate the timing, location and persistence of blooms. The roles of key physiological and behavioral traits involved in resting cell emergence and bloom formation were examined in two geographically distinct strains of the harmful alga, *Heterosigma akashiwo.* Physiological measures of cell viability, division and population growth, and cell fatty acid content were made using flow cytometry and gas chromatography – mass spectrometry techniques as cells transitioned between the benthic resting stage and the vegetative pelagic stage. Video-based tracking was used to quantify cell-level swimming behaviors. Data show increased temperature and light triggered rapid emergence from the resting stage and initiated cell swimming. Algal strains varied in important physiological and behavioral traits,

including survivorship during life-stage transitions, population growth rates and swimming velocities. Collectively, these traits function as "population growth strategies" that can influence bloom formation. Many resting cells regained the up-swimming capacity necessary to cross an environmentally relevant halocline and the ability to aggregate in near-surface waters within hours after vegetative growth supporting conditions were restored. Using a heuristic model, we illustrate how strain-specific population growth strategies can govern the timescales over which *H. akashiwo* blooms form. Our findings highlight the need for identification and quantification of strain-specific physiological and behavioral traits to improve mechanistic understanding of bloom formation and successful bloom prediction.

4.2 Introduction

Harmful algal blooms (HABs) occur when algal cells produce toxins or accumulate to densities sufficient to be deleterious to other organisms, causing damage to aquatic ecosystems and/or risks to public health [1–4]. Many behavioral and physiological functional traits that regulate HAB dynamics remain poorly understood. Improved understanding of these traits to help manage and mitigate HAB impacts is a current priority of basic and applied research [5].

Many HAB-forming species exhibit a dual-stage life history, in which they alternate between a pelagic vegetative stage and a benthic resting stage (e.g., cysts, resting spores or temporary resting cells). Transitions between these stages have potentially important impacts on bloom dynamics. Rapid transition of pelagic cells into the benthic resting stage can contribute to HAB termination [6,7]. Conversely, some HABs are thought to initiate when benthic cells return to the vegetative state and rapidly repopulate the water column [8,9]. This process typically requires

benthic cells to increase metabolic activity, to emerge from the sediments and ascend toward the surface of the water column, and finally to undergo rapid cell division to form population densities characteristic of blooms. Despite this potentially causal role in bloom dynamics, life stage transitions are among the least understood aspects of HAB dynamics.

Cell transitions between benthic and pelagic environments often include depth changes that are associated with changes in environmental characteristics (e.g., depth, temperature and light) and may significantly influence diverse aspects of algal cell biology. One aspect involves cell swimming behaviors. Many HAB-forming algal species are capable of rapid vertical migration (e.g., tens of meters within 24 hours) [10–12]. Because resting cells occupy benthic habitats that may not provide optimal conditions for cell division, vigorous swimming behaviors expressed during benthic-pelagic transition may be critical to cell survival by regulating vertical fluxes to the photic zone.

Cell physiology (e.g., metabolic processes and maintenance of energy reserves) represents another aspect of algal cell biology influenced by benthic-pelagic life stage transitions. Presently, little is known concerning the relationship between changing physiological cues and the metabolic requirements for either cell survival during the benthic resting stage, or for active swimming during benthic emergence. It is well established that polyunsaturated fatty acids (PUFAs) are essential in maintaining cellular membrane integrity and function during adverse changes in environmental conditions [13,14]. Neutral lipid reserves have been reported to provide an important energy source that supports algal motility [15]. These diverse contributions

to cellular processes suggest the hypothesis that fatty acid content and composition play a central role in successful algal life stage transitions.

In this study, we examined physiological and behavioral traits thought to regulate benthic emergence and surface bloom formation in the harmful raphidophyte, *Heterosigma akashiwo* (Hada) Hada. Blooms of this alga have been associated with fatalities of wild and pen-reared fish in temperate and sub-tropical waters [16,17]. Dense near-surface aggregations and rapid population growth are considered key determinants of the ecological impacts of *H. akashiwo* blooms [17–19]. *H. akashiwo* is capable of growing in salinities ranging from < 10 psu to 40 psu [20,21]. Cells exhibit vigorous up-swimming behavior in the vegetative stage [22] and readily swim across strong haloclines. In laboratory studies, Bearon et al. observed that *H. akashiwo* cells were capable of crossing a 28 to 8 psu halocline with only a modest decrease in swimming speeds [23]. Halocline-crossing behavior has been hypothesized to be an important mechanism in bloom formation that promotes high-density surface aggregations [10,23,24]. Consistent with this hypothesis, *H. akashiwo* blooms often initiate in shallow coastal regions or inland marine waterways that are characterized by strong seasonal stratification [17,18,25–27].

H. akashiwo cell transition out of the benthic stage ("emergence") is regulated largely by temperature and light [28]. Environmental observations suggest that the approximate lower limit for benthic emergence is 10°C, and that 15°C is required for rapid population growth [1,16,25,28–30]. Division rates of vegetative *H. akashiwo* cells are regulated by environmental conditions such as light, temperature, salinity and nutrient concentrations, and typically range

from 0.2 – 1.0 divisions per day [21,31–34]. However, higher division rates (up to ~4.0 div day^{-1}) have been reported [16].

Interstrain variability in vegetative cells of *H. akashiwo* has been observed for a suite of physiological and behavioral parameters (e.g., photosynthetic rates, salinity and temperature tolerance, nitrogen sourcing, growth rates, toxin production and swimming speeds [22,33,34]), suggesting that traits expressed during pelagic and benthic transitions may also be strain-specific. Selection among traits is often associated with metabolic trade-offs that may lead to diversity in survival strategies [35]. For this reason, we evaluated physiological and behavioral traits during benthic-pelagic transitions in two *H. akashiwo* strains that are distinct geographically (west Atlantic and east Pacific, repectively) and genetically (Black and Cattolico, unpublished data).

The specific goals of this study were: *a*) to quantify strain-specific rates of benthic emergence, population growth and up-swimming in *H. akashiwo*; *b*) to gain insight into the roles of fatty acid reserves in *H. akashiwo* benthic-pelagic transitions; and *c*) to integrate these traits into a conceptual framework to assess their implications for timescales of *H. akashiwo* bloom formation. To accomplish these goals, cell viability, cell division and population growth, fatty acid content and cell-level swimming were characterized and quantified as key physiological and behavioral traits in *H. akashiwo* resting cell emergence and bloom formation.

4.3 Materials and Methods

Resting cell induction/activation

Heterosigma akashiwo cultures, strains CCMP 452 (Narragansett Bay, RI, USA, 1952) and UWC 13.03 (Salish Sea, U.S.A/C.A, 2003), were maintained in 2.8 liter Fernbach flasks containing 1.0 liter f/2 medium without silica (f/2-Si) [36]. Cultures were grown to stationary phase (>$2x10^5$ cells mL^{-1}) at 20°C, on a 12 hour light, 12 hour dark (50 µmol m^{-2} s^{-1}) photoperiod with continuous rotary agitation (60 rpm). These cells were used to inoculate 250 mL experimental flasks at a density of $1x10^4$ cells mL^{-1}. Each flask contained 125 mL f/2-Si medium and were fitted with silicone sponge plugs (Bellco Glass, Vineland, NJ, USA.). Triplicate sub-cultures for each strain were maintained at 15°C on a 16 hour light: 8 hour dark (50 µmol m^{-2} s^{-1}) photoperiod. After 5 days at 15°C, cell concentrations within each experimental flask were approximately 2-$4x10^4$ cells mL^{-1}.

To induce *H. akashiwo* cells to enter the benthic resting stage, the experimental flasks were wrapped in aluminum foil and placed in the dark at 10°C for 18 days [28,37]. Resting cells were then signaled to "activate" (i.e., exit stasis) by unwrapping the experimental flasks and exposing them to a 16 hour light, 8 hour dark (20 µmol m^{-2} s^{-1}) photoperiod and temperature of 12°C. These environmentally relevant activation conditions represent typical spring/summer bottom water conditions of shallow embayments (< 20 m) within the Salish Sea (Department of Ecology, Marine Water Quality Monitoring Program: http://www.ecy.wa.gov/programs/eap/mar_wat/moorings.html). The experimental flasks were unwrapped during hour 6 of the light period (L6) and, therefore, were exposed to 10 hours of continuous light during the 1st photoperiod.

Experimental filming tank

Cells were placed in 6 equally spaced replicate filming chambers within a 300 mm x 240 mm x 50 mm experimental tank to observe cell swimming behaviors. Each chamber contained a two-layer stratified water column established using a peristaltic pump. A weak salinity gradient was established within each layer to suppress fluid motion. The top layer consisted of 100 mL f/2-Si medium diluted with double distilled fresh water to establish a salinity gradient of 17 to 15 psu, and the bottom layer had 350 mL diluted f/2-Si medium to form a gradient of 35 to 30 psu (Fig. 4.1). The halocline formed between these two layers had a salinity jump of 13 psu.

On each observation day, 0.5-1 mL of the CCMP 452 resting cell culture and 2-4 mL of the UWC 13.03 resting cell culture were subsampled from each of the 250 mL experimental flasks, and cells of each strain were added to 3 replicate filming chambers. Using a syringe, the cells were added slowly to the bottom of the tank through a fixed tube pre-positioned at the base of each chamber, ensuring that each chamber received approximately $1x10^4$ cells.

Cell sampling for physiological measurements

Cells were subsampled from experimental culturing flasks to determine cell state (vegetative vs. resting), viability, population growth and neutral lipid content. Measurements on vegetative cells ("vegetative control") were taken on cells subsampled just prior to induction into the resting stage ("day -18"). Resting cell measurements were taken after the 18 day induction period ("day 1"). Subsequent measurements were taken on subsamples of activated cell cultures ("days 2-5") to monitor cell state, viability and population growth. Subsamples were collected consistently at

L6 of the 16 hour light: 8 hour dark photoperiod (Fig. 4.2). All measurements, except cell state, were made with a BD Accuri C6 flow cytometer (BD Biosciences, San Jose, CA, USA).

Cell state was determined using bright field microscopy (Zeiss Axioskop 2 plus, Carl Zeiss Microscopy, LLC, USA) under 400x magnification in a Palmer-Maloney counting chamber from subsamples recovered from the experimental flasks. Cells were classified as "vegetative" if they expressed propulsive helical swimming, irrespective of cell shape, or had no movement and were aspherical. Cells were classified as "resting" if they had no movement and were spherical [28,37].

Cell viability and population growth

Cell viability was measured using the live/dead SYTOX-Green stain (Invitrogen Molecular Probes, Carlsbad, CA, USA). A 990 µL aliquot of subsampled cell culture was put into a 1.5 mL black microcentrifuge tube (Lite Safe Micro-Tubes, Research Products International Corp., Mount Prospect, IL, USA) containing 10 µL 50 µM SYTOX-Green working solution prepared by diluting 5 µL 5 mM SYTOX-Green solution with 495 µL f/2-Si medium. The microcentrifuge tubes were inverted 4 times and incubated for 10 min at 20°C. Flow cytometric measurements were made by adding 500 µL of the stained culture to a 5 mL glass test tube. Fluorescence of unstained cells was measured concurrently for background subtraction and to determine the cell concentration. Triplicate 500 µL samples were analyzed with the Accuri C6 flow cytometer. The SYTOX-stained samples were excited at 488 nm and emission was detected at 533 nm (±30 nm). Two wash cycles were run between sample types to eliminate cross-contamination.

Cell densities were measured from subsamples recovered from the experimental culture flasks and population density of viable cells was used to calculate specific growth rates (*k*) for each day after cells were signaled to activate (days 2-5; Table 4.1). Counts were also conducted on cell subsamples collected from each chamber of the experimental filming tank at the end of each 20-hour observation period (Fig. 4.2). The entire 100 mL top layer was extracted from each chamber, gently mixed, and a 10 mL aliquot was collected. A 10 mL aliquot of the bottom layer was recovered from a fixed tube pre-positioned at the base of each chamber (Fig. 4.1). The counts were used to determine the mean proportion of cells distributed within the bottom 10 mL and within the entire 100 mL top layer of the water column based on total number of viable cells added.

Cell division (DNA quantification)

DNA content of recently activated *H. akashiwo* cells was monitored in a separate experiment to identify DNA synthesis as a precursor of cell division. Resting cell induction and activation was completed for triplicate sub-cultures of both strains using the same protocols described above. DNA content of *H. akashiwo* cells was measured immediately after resting cells were signaled to activate, and every hour over a 20 hour period. The relative amount of DNA cell^{-1} was determined by sub-sampling 1 mL of cell culture from the experimental flasks and placing a 495 µL aliquot into a 1.5 mL black microcentrifuge tube containing 5 µL of 50 µM Vybrant DyeCycle Green Stain (Invitrogen Molecular Probes, Carlsbad, CA, USA) working solution. The working solution was prepared by diluting 990 µL 5 mM Vybrant DyeCycle Green Stain with 10 µL f/2-Si. A 500 µL aliquot of cell culture was placed into an empty black microcentrifuge tube to serve as an unstained control. The microcentrifuge tubes were inverted 4 times and incubated

for 30 min. The stained and unstained cells were transferred into 5 mL glass tubes for flow cytometric measurements. The Vybrant DyeCycle Green stained samples and unstained controls were excited at 488 nm with emission detected at 533 nm (±30 nm) by the Accuri flow cytometer. To determine the average DNA content per cell at each time point, the mean background fluorescent signal (FL1-A) of unstained samples was subtracted from the mean fluorescent signal of stained samples. The mean signal was standardized by dividing each value by $1x10^5$.

Cell lipid and fatty acid content

Flow cytometric measurements of cell neutral lipid content were made by placing 990 µL aliquots of subsampled cell culture into a 1.5 mL black microcentrifuge tube containing 10 µL 1.25 µM BODIPY 505/515 solution. The solution was prepared by first dissolving 10 mg BODIPY 505/515 stock powder (Invitrogen Molecular Probes, Carlsbad, CA, USA) with 8.06 mL 99% DMSO to make a 5mM BODIPY 505/515 working solution, and then 30 uL of the 5mM working solution was diluted with 10 µL f/2-Si medium. The microcentrifuge tubes were inverted 4 times and incubated for 30 min at 20°C. A 500 µL aliquot of cell culture was placed into an empty black microcentrifuge tube to serve as an unstained control. Stained and unstained cells were transferred into 5 mL glass tubes, and flow cytometric measurements were made in the dark following the same protocol described above. The BODIPY 505/515 stained samples and unstained controls were excited at 488 nm and emission was detected at 533 nm (±30 nm).

Fatty acid profiles for vegetative and resting cells were obtained in a separate experiment using a GC-MS sub-microscale method [39]. Triplicate sub-cultures for CCMP 452 and UWC 13.03 *H.*

akashiwo strains were grown to a concentration of ~$1x10^5$ cells mL^{-1} and induced into the resting stage as described above. Vegetative cells were sampled immediately prior to resting cell induction. 100 mL samples were collected from each culture flask, placed into screw-threaded clear glass centrifuge tubes (Fisher Scientific, Hampton, NH, USA), and centrifuged at 5000 rpm for 20 minutes at 4°C in a Sorvall RC-5 superspeed refrigerated centrifuge (Fisher Scientific). The cell pellets were resuspended with 250 µL f/2-Si medium, combined into a single 30 mL centrifuge tube and immediately flash frozen in liquid nitrogen and stored at -80°C until lyophilization. The triplicate samples were lyophilized using a Labconco Freezone 2.5 (Labconco, Kansas City, MO, USA) over a 48 hour period. Sample tubes were capped and stored at -20 °C. The tubes were allowed to come to room temperature prior to analysis.

The cell pellets were processed and analyzed following the GC-MS sub-microscale protocol [38]. Briefly, samples were standardized by adding a surrogate mixture with known concentration of C11:0 and C17:0 triglycerides to each sample tube. Each sample was transesterified using methanolic boron trifluoride, followed by a two-step phase separation (brine and isooctane) to extract the fatty acids. The isoocatane layer was transferred to a sample tube and an internal standard of deuterated aromatics was added ("Revised SV Standard", Restek, Bellefonte, PA, USA). The samples were immediately analyzed using a HP 5890 gas chromatograph equipped with an HP 5971A mass spectrometer (Agilent) and lipid quantification was performed against a 27-component external standard ("NLEA Fame Mix", Restek, Bellefont, PA, USA). Two separate runs of this experiment were conducted.

Video capture of cell swimming behaviors

Video observations of cell movements occurred immediately after the resting cells were exposed to the activation conditions (day 1 at L6; filming hour 0) and continued for 5 consecutive days (Fig. 4.2). Video sequences of cell movements were captured to a computer at 10 frames s^{-1} using a Logitech Quickcam Pro900 (infra-red (IR) filter and stock lens removed) that was in a modified housing equipped with a Nikon Nikkor 60 mm lens (aperture f/8) and a #8 extension tube. Cells were observed under dark field illumination using an IR (960 nM) LED bank. The camera and light sources were mounted in a fixed orientation on a computer-controlled motorized platform that moved horizontally and vertically across the tank, to ensure lighting and imaging were consistent at all positions in all replicate filming chambers. The experimental filming tank and automated camera system were located within a temperature- and light-controlled environmental chamber. The environmental chamber was set to the activation conditions described above. A SmartRelay controller (6bit Inc., UT, USA) was used to control camera position, filming duration, and lighting from a computer located outside of the environmental chamber.

Cell movement behaviors were observed at four vertical positions within each replicate chamber. The camera was positioned approximately 100 mm from the tank, providing a field of view (FOV) of approximately 9 mm x 12 mm. The bottom FOV extended upward 2 mm from the base of the tank. The below-halocline FOV was centered about 100 mm above the base. The in-halocline FOV was centered 200 mm above the base. The above-halocline FOV was centered 40 mm above the halocline (240 mm above the tank base). Video clips of 120 seconds duration were captured for each FOV in each replicate chamber at 1 hour intervals over a 19 hour period

(hour 0 – hour 19) on each day of observation. The data reported here represent 40 video clips analyzed from the first two days of observation (day 1 and day 2).

Video processing and swimming path analysis

Pixel positions of the cells in each video clip were determined by video processing using a modified version of the open source video editing package, Avidemux 2.4, to remove background, equalize lighting, threshold frames and set the particle size range to clearly resolve cells [37]. Video was calibrated using a uniform grid of dots with 2.5 mm spacing. Pixel coordinates of cells were converted into physical units and assembled into 2D cell swimming trajectories with Tracker3D, a MATLAB-based motion-analysis package to track organism movement (Grünbaum, unpublished). High frequency noise was removed from cell trajectories using a short-interval smoothing spline [22,39]. This spline had knot spacing of 15 frames (1.5 seconds), which was short enough to accurately resolve oscillations in cell trajectories [37]. Overall direction was defined using a long-interval spline with knot spacing of 150 frames (15 seconds) to follow the central axis of each cell's path. Analysis included only cell trajectories longer than 240 frames (24 seconds).

The splined trajectories were used to characterize cell swimming behaviors. Three swimming metrics (mean vertical velocity, mean horizontal velocity and gross speed) were calculated, as described by Tobin et al. [37]. Gross speed was defined as the total two-dimensional movement along the central axis of a trajectory. Net vertical velocity was defined as the average velocity in the vertical over the length of the trajectory. Mean path statistics were weighted by path duration to avoid biasing in favor of shorter or longer paths.

4.4 Results

Cell viability and population growth

Strain-specific differences in survivorship and resting cell activation rates were observed in the experimental flasks as *H. akashiwo* cells transitioned between benthic and pelagic life-stages. After the 18-day induction period, 99% of cells in both strains had entered the resting stage and no motile cells were observed (Table 4.1). Survivorship during resting cell formation was higher for CCMP 452 than for UWC 13.03. Mean cell concentrations within the experimental sampling flasks decreased by 65% for CCMP 452 and 89% for UWC 13.03, and resting cell viabilities were 94% and 51%, respectively. CCMP 452 cells had a faster rate of activation from the resting stage. When cells were signaled to activate, 17% (CCMP 452) and 4% (UWC 13.03) activated within 24 hours. However, an equal proportion (60%) of both cell populations activated by the end of the study.

The two *H. akashiwo* strains displayed different rates of population growth within the experimental flasks immediately following activation (Table 4.1). Within 24 hours, CCMP 452 had a positive population growth rate (0.85 div day^{-1}) while the UWC 13.03 population continued to decline (-0.40 div day^{-1}). However, the UWC 13.03 culture had a sudden increase in the population growth rate (1.74 div day^{-1}) after 72 hours under activation conditions (day 4). Although the daily population growth rates differed between the two strains, the average population growth rate over the 5 days under activation conditions was nearly equal for CCMP 452 (0.44 div day^{-1}) and UWC 13.03 (0.41 div day^{-1}) cells.

Cell counts from the top layer and bottom 10 mL of each water column within the experimental tank provided estimates of vertical cell distributions. The mean proportion of cells in the top layer and bottom 10 mL at end of each observation 20-hour period was generally less than 100% (Table 4.1). For three days of observation (days 1, 2 and 4) the mean proportions of cells in the two layers was greater than 100% for CCMP 452, indicating that more cells were in the chambers at the end of the observation period than had been initially added. This increase suggested that cell division had occurred within the experimental tank.

Cell division

A Vybrant DyeCycle Green DNA assay provided evidence suggesting that recently activated cells in the experimental flasks may be able to divide within a few hours after exposure to activation conditions. Change in the fluorescent DNA signal cell^{-1} appeared to follow a circadian rhythm, increasing and subsequently decreasing in strength for both *H. akashiwo* strains over the first photoperiod under activation conditions. The lowest fluorescent signal was observed 4 hours after resting cell activation was initiated. It then increased at least 2-fold during the transition from the light to the dark period and declined again within the 20 hours of observation (Fig. 4.3). This change in the DNA fluorescent signal cell^{-1} indicated that DNA synthesis was occurring and oscillation in DNA concentration cell^{-1} supports the view that cells were dividing. While the overall pattern of change in the fluorescent signal was similar for both strains, the relative strength of the signal differed between strains (UWC 13.03 was nearly an order of magnitude greater than observed for CCMP 452).

Fatty acid and neutral lipid content

To examine lipid reserves in vegetative and resting life-stages, neutral lipid and total fatty acid content in *H. akashiwo* cells within the experimental culture flasks were measured using the fluorescent dye BODIPY 505/515 and GC-MS, respectively. Mean neutral lipid content cell^{-1} showed a greater than 2-fold decline as cells entered the resting stage. Both neutral lipid content and cell motility were tightly associated with cell state for both strains of *H. akashiwo* (Fig. 4.4). A Spearman's rank correlation showed that both mean neutral lipid content cell^{-1} and population motility had a significant, positive correlation with time under activation conditions ($r = 0.676$ and 0.824, respectively, $N = 65$, $p = < 0.001$), indicating that cell swimming capacity and lipid synthesis are quickly and synchronously restored upon activation from the resting stage. GC−MS analysis showed a significant change in total fatty acid cell^{-1} as both CCMP 452 and UWC 13.03 cells entered into the resting stage. Resting cells had significantly less total fatty acid cell^{-1} than vegetative cells (Student's t-test: $N = 3$, $p < 0.05$). This result was observed for both strains in the two independent experimental runs. Vegetative cells of UWC 13.03 had 137.1±30 pg cell^{-1} (run 1) and 376.1±106 pg cell^{-1} (run 2), and resting cells had 18.2±3 pg cell^{-1} (run 1) and 23.4±4 pg cell^{-1} (run 2). For CCMP 452, vegetative cells had 68.5±15 pg cell^{-1} and 108.3±19 pg cell^{-1}, and resting cells had 35.4±12 pg cell^{-1} and 22.3±3 pg cell^{-1} for runs 1 and 2, respectively. These values represent a decrease of 87% (run 1) and 94% (run 2) per cell for UWC 13.03, and 48% (run 1) and 79% (run 2) for CCMP 452. Although, GC-MS analysis shows that UWC 13.03 vegetative cells have higher total fatty acid content than vegetative CCMP 452 cells, the UWC 13.03 cells lost significantly more fatty acid content during resting cell formation. As a result, the resting cells of both strains had similar amounts of total fatty acid.

To assess whether fatty acid composition shifts between vegetative and resting life-stages, total fatty acid profiles of CCMP 452 and UWC 13.03 were compared. A broad distribution of fatty acids from C12:0 to C 22:6 was observed (Fig. 4.5). In the vegetative stage, predominant fatty acids included C14:0, C16:0, C16:1, C18:4/5 and C20:5. Shifts in fatty acid profiles of resting cells were similar for both *H. akashiwo* strains. Resting cells showed either a decline or no change in the relative proportion of most fatty acids types, including predominant vegetative fatty acids C16:0, C16:1 and C18:4/5. However, a significant increase in PUFAs C20:5 and C22:6 was observed, indicating that the relative proportion of long-chain unsaturated fatty acids increased in resting cells compared to vegetative cells (Fig. 4.5).

Cell swimming behaviors and vertical distributions

Video observations revealed that emergence from the resting stage occurred rapidly after resting cells were signaled to activate. Within one hour, swimming cells of both strains were observed in the in below-halocline and in-halocline FOVs. However, UWC 13.03 cells were observed above the halocline 1-2 hours earlier than CCMP 452 cells, indicating that UWC 13.03 cells were able to cross the halocline before CCMP 452 cells (Fig. 4.6, day 1). Decreasing (but non-zero) swimming path counts within the bottom FOV over time indicated that newly emerged cells continued to leave the bottom of the chamber and swam up into the water column throughout the light period (Fig. 4.6).

Cell distributions within the experimental tank were similar on both days of video observation. However, the flux of cells into the water column appeared to be higher on day 2 than on day 1 (Fig. 4.6, day 2 - shaded region). Microscope-based observations revealed that all resting cells

within the experimental culture flasks did not activate at the same time, indicating previously-emerged vegetative cells co-occurred with resting cells in the experimental culture flasks on days 2-5. Hence, cells added to the tank on day 2 included both life-stages, and the greater flux of cells observed within the first two hours on day 2 could be accounted for by motile cells that had emerged on the previous day.

To distinguish between these co-occurring cell types in our video observations, we classified cell swimming trajectories as "newly emerged" or "previously emerged" based on the time period over which the swimming paths were observed. All swimming paths observed on day 1 were classified as "newly emerged". On day 2, swimming paths observed in the water column during the first two hours of observation were classified as "previously emerged", and paths observed during the rest of the filming period (hours 3-20) were classified as "newly emerged".

Vertical velocity distributions were significantly different between the two cell classifications in all FOVs except the in-halocline FOV for CCMP 452 (Two-sample Kolmogorvo-Smirnov test, Table 4.2; Fig. 4.7). For both strains, previously emerged cells had faster net upward swimming velocities (CCMP 452 = 19.3 μm/s, UWC 13.03 = 35.3 μm/s) compared to newly emerged cells (CCMP 452 = 7.4 μm/s, UWC 13.03 = 11.4 μm/s).

Newly emerged UWC 13.03 cells generally exhibited faster swimming rates than newly emerged CCMP 452 cells. The maximum gross speed observed for UWC 13.03 was 90 μm s^{-1} and the maximum upward velocity was 87 μm s^{-1}, more than two times greater than for CCMP 452 (45 μm s^{-1} and 36 μm s^{-1}, respectively). Comparisons of mean vertical velocities (Fig. 4.8) showed

UWC 13.03 had significantly faster upward vertical velocities, 12.7 μm s^{-1} on day 1 and 15.2 μm s^{-1} on day 2, than CCMP 452 (7.2 μm s^{-1} and 5.9 μm s^{-1}, respectively) prior to reaching the halocline (Mann-Whitney U test). However, mean vertical velocities were not statistically different between the two strains at the halocline, indicating that the presence of the halocline reduced vertical velocities of UWC 13.03 cells.

Newly emerged *H. akashiwo* cells expressed different swimming behaviors in light vs. dark periods. In both strains, net upward vertical velocities were observed in the light period, but in the dark period net vertical velocities were generally near zero (Fig. 4.9). The proportion of upward- and downward-directed swimming cells differed between the light and dark periods (Chi-square test for comparison of proportions, test statistics: Table 4.3). In both CCMP 452 and UWC 13.03, 60-70% of swimming cells in the water column had upward-directed swimming during the light period, while the proportions of upward and downward swimmers were nearly equal during the dark period (Fig. 4.9).

4.5 Discussion

Quantifying physiological and behavioral characteristics that influence algal cells' rates of benthic emergence and vertical fluxes to the upper water column is critical for understanding the basic timescales over which *H. akashiwo* harmful algal blooms form. A key finding was that cells of *H. akashiwo* can rapidly emerge from the benthic resting stage, regain the swimming capacity necessary to cross environmentally relevant haloclines, and undergo cell division within hours after growth supporting conditions are restored. We also observed pronounced strain-specific variation in important physiological and behavioral traits, including survivorship during

life-stage transitions and post-transition specific growth rates and swimming behaviors. Collectively, these traits function as strain-specific "population growth strategies" that govern timescales of potential *H. akashiwo* bloom formation.

Strain-specific variation in life-stage transitions and growth

Greater cell survivorship and activation rates suggest that CCMP 452 was more successful at transitioning into and out of the benthic resting stage than UWC 13.03. UWC 13.03 had significantly higher mortality during life stage transitions and exhibited a slower rate of activation compared to CCMP 452. These results suggest that strains of *H. akashiwo* which are more successful at transitioning between life stages (e.g., CCMP 452) could supply a higher inoculum of vegetative cells into the water column, compared to strains with reduced survivorship (e.g., UWC 13.03).

Population growth rates immediately after activation from the resting stage also differed between the two strains. The CCMP 452 population density nearly doubled within 24 hours of exposure to activation conditions, while UWC 13.03 showed an initial decline. Although daily population growth rates differed between the two strains, their average population growth rates over the 5 days of observation were nearly equal. This outcome suggests that initial growth responses may not be representative of long-term population growth. Our average population growth rate (0.40 div d^{-1}) is consistent with long-term growth rates observed for vegetative cells of both *H. akashiwo* strains under the environmental conditions tested in this study (E.T., unpublished data).

Two lines of evidence suggest that *H. akashiwo* cells were able to undergo cell division rapidly − within 24 hours − after activation from the resting stage. First, flow cytometry cell counts from the subsamples collected from both the experimental flasks and the video observation tank showed that more CCMP 452 cells were present after 24 hours then were originally present (see Table 4.1, day 1). Second, DNA analysis indicated that DNA synthesis − a precursor to cell division – may have occurred in both strains of *H. akashiwo*. The approximately 2-fold increase in the DNA signal per cell observed near the light/dark transition for both strains provides preliminary evidence that a subset of the cell population was preparing to divide. Cell size is often used in combination with DNA content to infer that cell division has taken place. Unfortunately, since the sampled *H. akashiwo* cultures contained mixed life stages (both resting and vegetative), the cell size data in our observations were not statistically informative.

We observed that DNA dye signal strength differed between strains. The DNA signal cell^{-1} was nearly an order of magnitude greater in UWC 13.03. The reason for this variance in the relative signal strength is not presently known. Preliminary experiments suggest that distinct strains of *H. akashiwo* may have dissimilar levels of mitochondrial DNA (Black and Cattolico, unpublished data). Whether the total DNA complement also varies among strains is currently under investigation. Alternatively, unidentified strain-specificity in fluorochrome uptake or variation in the number of dead or dying cells within the cell cultures could have affected the relative fluorescent intensities [40].

The cell cycle in vegetative *H. akashiwo* displays a circadian rhythm that is regulated by photoperiod [31,41]. Satoh et al. reported that *H. akashiwo* (strain NIES 6) required a minimum

6 hour light period for cell division to occur [41]. If this requirement applies across strains and physiological states, then our experimental post-emergence conditions were suitable for rapid onset of division. It is unclear why population growth lagged in UWC 13.03 despite the evidence for DNA synthesis. A possible explanation is that recently activated cells advanced through S phase but failed to complete cell division. This interpretation of weakened physiological condition associated with life-stage transitions is consistent with our observations of higher mortality in UWC 13.03.

Role of neutral lipids in life-stage transitions and motility

Neutral lipid and fatty acid content per cell in *H. akashiwo* changed with physiological state. Both BODIPY 505/515 neutral lipid and GC-MS assays demonstrated that *H. akashiwo* resting cells have significantly less total lipid content than vegetative cells. UWC 13.03 cells lost significantly more fatty acid content during resting cell formation than CCMP 452. Consequently, cells of both strains had a similar amount of total fatty acid (~20-30 pg $cell^{-1}$) when they reached the resting state. It is possible this fatty acid content approximates a minimum threshold required to ensure survival during and emergence from the resting stage.

We observed shifts in fatty acid composition between the two life-stages. In both strains, the relative proportion of long-chain fatty acids was higher in resting cells compared to vegetative cells, suggesting that *H. akashiwo* cells appeared to selectively retain some PUFAs over other fatty acid types during resting cell formation. A significant change was particularly noted for eicosapentaenoic acid (C20:5), a fatty acid found in unusually high amounts in *H. akashiwo* cells [42]. This long chain fatty acid represented approximately 15 % of the total fatty acids in

vegetative cells, increased to approximately 28 % of the total fatty acids in resting cells. Our results are consistent with the hypothesis that fatty acid composition plays an integral role in successful algal life stage transitions. PUFAs are particularly important for building photosynthetic membranes [43] and are necessary for modification of cellular and organelle membranes during changes in environmental conditions [14,44,45]. For example, eicosapentaenoic acid has been hypothesized to contribute to the maintenance of "optimal membrane fluidity… under low temperature or high hydropressure conditions" [46]. Retention of PUFAs in *H. akashiwo* resting cells may represent a more generalized response to decreased temperature that is often associated with the benthic environment, thus further promoting survival while the alga is in a metabolically down-regulated state (Deodato and Cattolico, unpublished data).

It is generally recognized that neutral lipids serve as energy stores available for maintaining critical metabolic processes [14,47], suggesting they may be important energy sources for cell motility. We found that both neutral lipid content and motility have a positive association with activation from the resting stage. Consistent with our findings, close associations between lipid content and cell motility have been reported in zoospores of the kelp, *Pterygophora californica* [15] and in multiple strains of the dinoflagellate, *Karenia brevis* [48]. Although, we cannot determine whether lipids are being catabolized to provide energy for swimming, our data do indicate that endogenous lipid stores and motility are closely coupled in time.

Swimming behaviors during benthic-pelagic transition

Increased temperature (12°C) and light (20 μmol m^{-2} s^{-1}) triggered *H. akashiwo* resting cells to transition out of the benthic stage and to regain motility. Our video observations revealed that

cells of both strains began to swim up into the water column within an hour after these growth supporting conditions were restored. Newly emerged UWC 13.03 cells exhibited significantly faster mean upward swimming velocities prior to reaching the halocline than newly emerged CCMP 452 cells. This observation is consistent with previous studies on *H. akashiwo* swimming behaviors. Bearon et al. (2004) reported differences in gross swimming speeds for geographically distinct strains of *H. akashiwo*: CCMP 452 (49–66 μm s-1) and CCAP 934-1 (88–119 μm s-1). Helical swimming modes were different across five strains of *H. akashiwo* based on 2D observations and 3D model simulations [49]. Such interstrain variations in *H. akashiwo* swimming behaviors likely correspond to morphological and/or physiological differences which have not yet been identified.

Newly emerged *H. akashiwo* cells quickly reacquired swimming capacity sufficient to cross an environmentally relevant halocline (a 13 psu salinity jump). UWC 13.03 cells showed a significant decrease in mean vertical velocity at the halocline, so that both strains had similar mean vertical velocities within the halocline (see Fig. 4.8). However, UWC 13.03 cells were nonetheless observed above the halocline 1-2 hours before CCMP 452 cells. This result indicates that more vigorous upward swimming by UWC 13.03 cells prior to reaching the halocline enabled them to transit the entire experimental water column more quickly than CCMP 452 cells. Differences in time needed for cells of each *H. akashiwo* strain to reach near-surface layers could be greatly magnified when emergence occurs at the greater depths typical of natural habitats.

Both *H. akashiwo* strains changed mean vertical velocity between the light and dark. In the light, cells expressed faster, net upward velocities while net vertical velocities were near zero in the

dark. These differences were a result of proportional shifts in swimming direction. More cells swam upward in the light, while the number of upward and downward swimming cells was nearly equal in the dark. Our findings are similar to that of Wada et al. (1985) who reported that *H. akashiwo* (strain OHE-1) had more upward directed movement in the light than in the dark [50]. Contrary to our findings, however, Wada et al. reported a distinct downward vertical migration during the dark period, inferred from cell distributions within unstratified 15 mL tubes. Our video observations, in stratified water columns that suppress water motion, did not indicate a shift in vertical population distribution between light and dark periods.

Population growth strategies and timescales of H. akashiwo HAB formation

Our results show that *H. akashiwo* exhibits pronounced strain-specific variation in key physiological and behavioral traits, including survivorship during life-stage transitions, specific growth rates, and swimming behaviors. Collectively, these traits may function as "population growth strategies" that potentially regulate timescales of *H. akashiwo* HAB formation. The CCMP 452 strain exhibited enhanced survivorship coupled with higher rates of resting cell activation and cell division. This "survive and divide" strategy may indicate that energy reserves are used to enhance cell survival during the benthic resting stage and rapid onset of cell division. The UWC 13.03 strain exhibited reduced survivorship and a lag in growth, but had significantly faster upward swimming behavior following benthic emergence. This "swim-first" strategy may indicate that energy reserves are used to fuel swimming, allowing newly emerged cells to quickly reach near-surface waters to acquire energy via photosynthesis to divide.

To gain insight into how these population growth startegies could regulate timescales of bloom formation, we generated a simple, heuristic model of *H. akashiwo* benthic emergence and near-

surface bloom formation (Fig. 4.10). Strain-specific measurments were used to simulate the "survive and divide" (CCMP 452) and "swim-first" (UWC 13.03) population growth strategies, to explore how these strategies influence the rates of near-surface cell accumulations. Prior vegetative populations of CCMP 452 and UWC 13.03 cells were at assumed densities of $5x10^5$ cells L^{-1}, a typical *H. akashiwo* HAB density in the Salish Sea. Mortality rates observed during resting cell formation were applied to calculate benthic population densities of viable resting cells. Rates of resting cell activation were then applied over a 4 day period and each "cohort" of cells was tracked as they emerged from the sediments. The transit time (based on the observed mean vertical velocities; see Fig. 4.8) was calculated as cell cohorts swam upward into a 12 m water column, and each cohort's growth occurred according to the rates (k) measured in this study (see Table 4.1). Additionally, we assumed that: 1) activated cells immediately and synchronously swim to the surface; 2) the depth of the halocline is fixed; and, 3) cells are retained within the surface layer once they cross the halocline. Mortality rates due to predation or pathogens were neglected. Our simplified model is therefore an examination of population growth potential that may not be realized under real-world conditions.

Under these assumptions, model results suggest that the size of the cell inoculum into the water column − a function of benthic viable resting cell density and activation rate – most strongly determines the timescales over which blooms can potentially form. The "survive and divide" strategy of CCMP 452 facilitated a greater flux of cells into the water column, and subsequently this strain increased in near-surface population density more rapidly than UWC 13.03 (Fig. 4.10). Based on our calculations for a 12 m water column, the "swim-first" strategy enabled the UWC 13.03 cells to reach the surface layer in 22 hours, approximately half the time it took

CCMP 452 cells (39 hours). However, near-surface accumulation of UWC 13.03 cells occurred at a much slower rate than CCMP 452. He et al. (2008) used a biophysical numerical modeling approach to reach a similar conclusion about the central role of cell inoculum size in bloom dynamics of the harmful dinoflagellate, *Alexandrium fundyense,* in the Gulf of Maine [9].

While our findings clearly demonstrate that physiological and behavioral traits can regulate bloom formation, environmental characteristics that were omitted from our simplified model can also affect *H. akashiwo* HABs timescales. Algal swimming interacts with physical flows to influence cell concentrations and distributions in the water column [23,39,51–55]. For example, cells can be transported by horizontal advection from ambient currents that may vary in speed and direction with depth. Vertical mixing of cells by turbulence also varies with depth, due to boundary-layer effects and interactions with obstacles such as sediments, biota and seabed topography [56–58]. Hence, horizontal and vertical transport processes also strongly affect the time required for cells to migrate through the water column [37]. Biological controls such as predation, competition and viral infection can further limit *H. akashiwo* cell abundance and distribution [59–62].

Our findings suggest that distinct *H. akashiwo* strains utilize diverse population growth strategies that potentially influence bloom dynamics. Such phenotypic diversity is widespread among many species of algae and likely facilitates survival under a wide range of environmental conditions. It is generally understood that algal strains under long-term culture may express traits that are a result of selective pressures experienced under culture conditions [63]. Hence, our observations may not reflect the precise pre-culture characteristics of the observed strains, and do not capture

the full diversity of *H. akashiwo* in natural ecosystems. We believe that our data nonetheless provides interesting ecological insights into how *H. akashiwo* strains may express alternate responses to the same environmental signals. Our observations suggest that distinct strategies utilized by *H. akashiwo* strains may reflect habitat-specific trade-offs between physiological and/or behavioral traits. The diversity and potential adaptive value of population growth strategies across geographically distinct strains of *H. akashiwo* are currently unknown but are an important priority for future research.

4.6 References

1. Taylor FJR, Horner R (1994) Red tides and other problems with harmful algal blooms in Pacific Northwest coastal waters. In: Wilson RCH, Beamish RJ, Aitkens F, Bell J, editors. Review of the marine environment and biota of Strait of Georgia, Puget Sound and Juan de Fuca Strait. Canadian Technical Report of Fisheries and Aquatic Sciences. pp. 175–186.

2. Taylor FJ., Trainer VL (2002) Harmful algal blooms in the PICES region of the North Pacific. B.C. Canada. pp. 1–156.

3. Cembella A, Ibarra D, Diogene J, Dahl E (2005) Harmful algal blooms and their assessment in fjords and coastal embayments. Oceanography 18: 158–171. doi:10.5670/oceanog.2005.51.

4. Anderson DM (2007) The ecology and oceanography of harmful algal blooms: Multidisciplinary approaches to research and management. IOC Technical Series 74. UNESCO, Vol. 74. doi:IOC/2007/TS/74.

5. Ramsdell J, Anderson D, Glibert P (2005) Harmful algal research and response: A national environmental science strategy 2005-2015 Washington, DC, Vol. 33. pp. 1-96.

6. Ishikawa A, Taniguchi A (1996) Contribution of benthic cysts to the population dynamics of *Scrippsiella* spp. (Dinophyceae). Mar Ecol Prog Ser 140: 169–178. doi:10.3354/meps140169.

7. Itakura S, Yamaguchi M (2001) Germination characteristics of naturally occurring cysts of *Alexandrium tamarense* (Dinophyceae) in Hiroshima Bay, Inland Sea of Japan. Phycologia 40: 263–267. doi:10.2216/i0031-8884-40-3-263.1.

8. Anderson DM, Stock CA, Keafer BA, Bronzino Nelson A, Thompson B, et al. (2005) *Alexandrium fundyense* cyst dynamics in the Gulf of Maine. Deep Sea Res Part II Top Stud Oceanogr 52: 2522–2542. doi:10.1016/j.dsr2.2005.06.014.

9. He R, McGillicuddy DJ, Keafer BA, Anderson DM (2008) Historic 2005 toxic bloom of *Alexandrium fundyense* in the western Gulf of Maine: Coupled biophysical numerical modeling. J Geophys Res 113: C07040. doi:10.1029/2007JC004602.

10. Yamochi S, Abe T (1984) Mechanisms to initiate a *Heterosigma akashiwo* red tide in Osaka bay. Mar Biol 83: 255–261. doi:10.1007/BF00397457.

11. Cullen JJ (1985) Diel vertical migration by dinoflagellates: roles of carbohydrate metabolism and behavioral flexibility. Contrib Mar Sci 27: 135–152.

12. Ralston DK, McGillicuddy DJ, Townsend DW (2007) Asynchronous vertical migration and bimodal distribution of motile phytoplankton. J Plankton Res 29: 803–821. doi:10.1093/plankt/fbm061.

13. Uttaro AD (2006) Biosynthesis of polyunsaturated fatty acids in lower eukaryotes. IUBMB Life 58: 563–571. doi:10.1080/15216540600920899.

14. Guschina I, Harwood JL (2009) Algal lipids and effect of the environment on their biochemistry. Lipids in Aquatic Ecosystems. New York: Springer. pp. 1–24. doi:10.1007/978-0-387-89366-2_1.

15. Reed DC, Brzezinski MA, Coury DA, Graham WM, Petty RL (1999) Neutral lipids in macroalgal spores and their role in swimming. Mar Biol 133: 737–744. doi:10.1007/s002270050515.

16. Smayda TJ (1998) Ecophysiology and bloom dynamics of *Heterosigma akashiwo* (Raphidophyceae). In: Anderson. D.M, Cembella AD, Hallegraeff G, editors. Physological Ecology of Harmful Algal Blooms. Springer-Verlag Berlin Heidelberg. pp. 115–131.

17. Rensel JJE, Haigh N, Tynan TJ (2010) Fraser river sockeye salmon marine survival decline and harmful blooms of *Heterosigma akashiwo*. Harmful Algae 10: 98–115. doi:10.1016/j.hal.2010.07.005.

18. Rensel JJE (2007) Fish kills from the harmful alga *Heterosigma akashiwo* in Puget Sound: Recent blooms and review. Prepared by Rensel Associates Aquatic Sciences for the National Oceanic and Atmospheric Administration Center for Sponsored Coastal Ocean Research (CSCOR), Washington, DC (2007): pp. 1-58.

19. Taylor FJR, Haigh R (1993) The ecology of fish-killing blooms of the chloromonad flagellate *Heterosigma* in the Strait of Georgia and adjacent waters. Dev Mar Biol: 1993.

20. Tomas CR (1978) *Olisthodiscus luteus* (Chrysophyceae) II. Formation and survival of a benthic stage. J Phycol 14: 314–319. doi:10.1111/j.1529-8817.1978.tb00304.x.

21. Haque SM, Onoue Y (2002) Effects of salinity on growth and toxin production of a noxious phytoflagellate, *Heterosigma akashiwo* (Raphidophyceae). Bot Mar 45: 356–363. doi:10.1515/bot.2002.036.

22. Bearon RN, Grunbaum D, Cattolico RA (2004) Relating cell-level swimming behaviors to vertical population distributions in *Heterosigma akashiwo* (Raphidophyceae), a harmful alga. Limnol Oceanogr 49: 607–613. doi:10.4319/lo.2004.49.2.0607.

23. Bearon RN, Grünbaum D, Cattolico RA (2006) Effects of salinity structure on swimming behavior and harmful algal bloom formation in *Heterosigma akashiwo*, a toxic raphidophyte. Mar Ecol Prog Ser 306: 153–163. doi:10.3354/meps306153.

24. Hershberger PK, Rensel JE, Matter AL, Taub FB (1997) Vertical distribution of the chloromonad flagellate *Heterosigma carterae* in columns: Implications for bloom development. Can J Fish Aquat Sci 54: 2228–2234. doi:10.1139/f97-131.

25. Imai I, Itakura S (1999) Importance of cysts in the population dynamics of the red tide flagellate *Heterosigma akashiwo* (Raphidophyceae). Mar Biol 133: 755–762. doi:10.1007/s002270050517.

26. Handy SM, Coyne KJ, Portune KJ, Demir E, Doblin MA, et al. (2005) Evaluating vertical migration behavior of harmful raphidophytes in the Delaware Inland Bays utilizing quantitative real-time PCR. Aquat Microb Ecol 40: 121–132. doi:10.3354/ame040121.

27. Kempton J, Keppler CJ, Lewitus A, Shuler A, Wilde S (2008) A novel *Heterosigma akashiwo* (Raphidophyceae) bloom extending from a South Carolina bay to offshore waters. Harmful Algae 7: 235–240. doi:10.1016/j.hal.2007.08.003.

28. Han M, Kim Y, Cattolico RA, Taylor FJR (2002) *Heterosigma akashiwo* (Raphidophyceae) resting cell formation in batch culture: Strain identity versus physiological response. J Phycol 317: 304–317. doi:10.1046/j.1529-8817.2002.01087.x.

29. Shikata T, Nagasoe S, Matsubara T, Yamasaki Y, Shimasaki Y, et al. (2007) Effects of temperature and light on cyst germination and germinated cell survival of the noxious raphidophyte *Heterosigma akashiwo*. Harmful Algae 6: 700–706. doi:10.1016/j.hal.2007.02.008.

30. Shikata T, Nagasoe S, Matsubara T, Yoshikawa S, Yamasaki Y, et al. (2008) Factors influencing the initiation of blooms of the raphidophyte *Heterosigma akashiwo* and the diatom *Skeletonema costatum* in a port in Japan. Limnol Oceanogr 53: 2503–2518. doi:10.4319/lo.2008.53.6.2503.

31. Cattolico RA, Boothroyd J, Gibbs S (1976) Synchronous Growth and Plastid Replication in the Naturally Wall-less Alga *Olisthodiscus luteus*. Plant Physiol 57: 497–503. doi:10.1104/pp.57.4.497.

32. Herndon J, Cochlan WP (2007) Nitrogen utilization by the raphidophyte *Heterosigma akashiwo*: Growth and uptake kinetics in laboratory cultures. Harmful Algae 6: 260–270. doi:10.1016/j.hal.2006.08.006.

33. Martinez R, Orive E, Laza-Martinez A, Seoane S (2010) Growth response of six strains of *Heterosigma akashiwo* to varying temperature, salinity and irradiance conditions. J Plankton Res 32: 529–538. doi:10.1093/plankt/fbp135.

34. Fredrickson KA, Strom SL, Crim R, Coyne KJ (2011) Interstrain variability in physiology and genetics of *Heterosigma akashiwo* (Raphidophyceae) from the west coast of North America. J Phycol 47: 25–35. doi:10.1111/j.1529-8817.2010.00942.x.

35. Litchman E, Klausmeier CA, Schofield OM, Falkowski PG (2007) The role of functional traits and trade-offs in structuring phytoplankton communities: Scaling from cellular to ecosystem level. Ecol Lett 10: 1170–1181. doi:10.1111/j.1461-0248.2007.01117.x.

36. Guillard RRL, Ryther JH (1962) Studies of marine planktonic diatoms. I. *Cyclotella nana* Hustedt and *Detonula confervacea* Cleve. Can J Microbiol 8: 229–239.

37. Tobin ED, Grünbaum D, Cattolico RA (2011) Pelagic-benthic transition of the harmful alga, *Heterosigma akashiwo*: Changes in swimming and implications for benthic cell distributions. Harmful Algae 10: 619–628. doi:10.1016/j.hal.2011.04.014.

38. Bigelow NW, Hardin WR, Barker JP, Ryken SA, Macrae AC, Cattolico RA (2011) A comprehensive GC-MS sub-microscale assay for fatty acids and its applications. J Am Oil Chem Soc 88: 1329–1338. doi:10.1007/s11746-011-1799-7.

39. Bearon RN, Grünbaum D (2008) From individual behaviour to population models: A case study using swimming algae. J Theor Biol 251: 679–697. doi:10.1016/j.jtbi.2008.01.007.

40. Darzynkiewicz Z (2011) Critical aspects in analysis of cellular DNA content. Curr Protoc Cytom: 1–9. doi:10.1002/0471142956.cy0702s52.

41. Satoh E, Watanabe M, Fujii T (1987) Photoperiodic Regulation of Cell Division and Chloroplast Replication in *Heterosigma akashiwo*. Plant Cell Physiol 28: 1093–1099.

42. Bigelow N, Barker J, Ryken S, Patterson J, Hardin W, Barlow S, Deodato C, Cattolico RA (2013) *Chrysochromulina* sp.: A proposed lipid standard for the algal biofuel industry and its application to diverse taxa for screening lipid content. Algal Res 2: 385–393. doi:10.1016/j.algal.2013.07.001.

43. Solovchenko AE (2012) Physiological role of neutral lipid accumulation in eukaryotic microalgae under stresses. Russ J Plant Physiol 59: 167–176. doi:10.1134/S1021443712020161.

44. Cohen Z, Khozin-Goldberg I, Adlerstein D, Bigogno C (2000) The role of triacylglycerol as a reservoir of polyunsaturated fatty acids for the rapid production of chloroplastic lipids in certain microalgae. Biochem Soc Trans 28: 740–743.

45. Olofsson M, Lamela T, Nilsson E, Bergé JP, del Pino V, et al. (2012) Seasonal variation of lipids and fatty acids of the microalgae *Nannochloropsis oculata* grown in outdoor large-scale photobioreactors. Energies 5: 1577–1592. doi:10.3390/en5051577.

46. Okuyama H, Orikasa Y, Nishida T (2008) Significance of antioxidative functions of eicosapentaenoic and docosahexaenoic acids in marine microorganisms. Appl Environ Microbiol 74: 570–574. doi:10.1128/AEM.02256-07.

47. Eltgroth ML, Watwood RL, Wolfe GV (2005) Production and cellular localization of neutral long-Chain lipids in the haptophyte algae *Isochrysis galbana* and *Emiliania huxleyi*. J Phycol 41: 1000–1009. doi:10.1111/j.1529-8817.2005.00128.x.

48. McKay L, Kamykowski D, Milligan E, Schaeffer B, Sinclair G (2006) Comparison of swimming speed and photophysiological responses to different external conditions among three *Karenia brevis* strains. Harmful Algae 5: 623–636. doi:10.1016/j.hal.2005.12.001.

49. Gurarie E, Grünbaum D, Nishizaki MT (2011) Estimating 3D movements from 2D observations using a continuous model of helical swimming. Bull Math Biol 73: 1358–1377. doi:10.1007/s11538-010-9575-7.

50. Wada M, Miyazaki A, Fujii T (1985) On the mechanisms of diurnal vertical migration behavior of *Heterosigma akashiwo* (Raphidophyceae). Plant Cell Physiol 26: 431–436. doi:10.1111/j.1529-8817.1988.tb04452.x.

51. Kessler JO (1985) Hydrodynamic focusing of motile algal cells. Nature 313: 218–220. doi:10.1038/313218a0.

52. Donaghay PL, Osborn TR (1997) Toward a theory of biological-physical control of harmful algal bloom dynamics and impacts. Limnol Oceanogr 42: 1283–1296. doi:10.4319/lo.1997.42.5_part_2.1283.

53. Franks PJS (1997) Spatial patterns in dense algal blooms. Limnol Oceanogr 42: 1297–1305. doi:10.4319/lo.1997.42.5_part_2.1297.

54. Smayda TJ (2002) Turbulence, watermass stratification and harmful algal blooms: an alternative view and frontal zones as "pelagic seed banks." Harmful Algae 1: 95–112. doi:10.1016/S1568-9883(02)00010-0.

55. Durham WM, Stocker R (2012) Thin phytoplankton layers: Characteristics, mechanisms, and consequences. Ann Rev Mar Sci 4: 177–207. doi:10.1146/annurev-marine-120710-100957.

56. Gaylord B, Reed DC, Raimondi PT, Washburn L, McLean SR (2002) A physically based model of macroalgal spore dispersal in the wave and current-dominated nearshore. Ecology 83: 1239–1251.

57. Gaylord B, Reed DC, Washburn L, Raimondi PT (2004) Physical–biological coupling in spore dispersal of kelp forest macroalgae. J Mar Syst 49: 19–39. doi:10.1016/j.jmarsys.2003.05.003.

58. Rosman JH, Monismith SG, Denny MW, Koseff JR (2010) Currents and turbulence within a kelp forest (*Macrocystis pyrifera*): Insights from a dynamically scaled laboratory model. Limnol Oceanogr 55: 1145–1158. doi:10.4319/lo.2010.55.3.1145.

59. Lawrence JE, Chan AM, Suttle CA (2010) Viruses causing lysis of the toxic bloom-forming alga *Heterosigma akashiwo* are widespread in coastal sediments of British Columbia , Canada. Limnol Oceanogr 47: 545–550.

60. Clough J, Strom S (2005) Effects of *Heterosigma akashiwo* (Raphidophyceae) on protist grazers: laboratory experiments with ciliates and heterotrophic dinoflagellates. Aquat Microb Ecol 39: 121–134. doi:10.3354/ame039121.

61. Harvey EL, Menden-Deuer S (2011) Avoidance, movement, and mortality: The interactions between a protistan grazer and *Heterosigma akashiwo*, a harmful algal bloom species. Limnol Oceanogr 56: 371–378. doi:10.4319/lo.2011.56.1.0371.

62. Jeong HJ, Kim JS, Yoo Y Du, Kim ST, Kim TH, et al. (2003) Feeding by the heterotrophic dinoflagellate *Oxyrrhis marina* on the red-tide raphidophyte *Heterosigma akashiwo*: a potential biological method to control red tides using mass-cultured grazers. J Eukaryot Microbiol 50: 274–282.

63. Lakeman MB, von Dassow P, Cattolico RA (2009) The strain concept in phytoplankton ecology. Harmful Algae 8: 746–758. doi:10.1016/j.hal.2008.11.011.

Table 4.1 Average measures of cell survival, life-stage transitions and population growth within the experimental flasks, and cell distributions within the experimental filming tank.

		Flask				Tank		
Strain	**Day**	**Resting (%)**	**Viable (%)**	**Concentration (cells/mL)**	***k* * (div/day)**	**Hour 0 viable cells added**	**Hour 20 at bottom (%)**	**Hour 20 in top (%)**
CCMP 452	-18	0%	99%	45,873				
	1	99%	94%	15,903		13,536	**106%**	**60%**
	2	82%	75%	28,643	0.85	14,159	**73%**	**50%**
	3	58%	96%	36,640	0.36	17,941	41%	36%
	4	54%	94%	49,463	0.43	9,622	**105%**	**22%**
	5	41%	92%	54,027	0.13	10,627	60%	38%
UWC 13.03	-18	0%	98%	18,513				
	1	99%	51%	1,957		8,165	28%	28%
	2	95%	85%	1,487	- 0.40	7,644	17%	25%
	3	59%	93%	1,780	0.26	8,116	27%	24%
	4	42%	91%	5,950	1.74	10,481	15%	6%
	5	40%	88%	6,217	0.06	11,919	6%	10%

*Specific growth rates for algal cultures were calculated using the equation: $k = (\log_2 (N_1/N_0))/(t_1-t_0)$.

Table 4.2 Test statistics based on a Two-sample Kolmogorvo-Smirnov test ($\alpha = 0.05$) for differences in median vertical velocities between "newly emerged" and "previously emerged" cells.

Strain	**FOV***	**Z**	**P-value**	**N Previously Emerged**	**N Newly Emerged**
CCMP 452	Bottom	5.11	< .001	226	1403
	Below Halocline	3.57	< .001	24	526
	In Halocline	0.98	0.292	4	603
	Above Halocline	1.7	0.006	8	1312
UWC 13.03	Bottom	7.15	< .001	459	958
	Below Halocline	3.89	< .001	53	471
	In Halocline	3.53	< .001	56	1071
	Above Halocline	4.09	< .001	32	1346

* FOV = field of view.

Table 4.3 Proportions of upward and downward directed swimming cells during the light and dark periods for the two days of observation.

		Day 1					Day 2				
Strain	**Photo Period**	**N**	**Up (%)**	**Down (%)**	**X^2**	**P-value***	**N**	**Up (%)**	**Down (%)**	**X^2**	**P-value***
CCMP 452	Light	1446	69	31			497	60	40		
	Dark	746	56	44	36.5	< 0.001	1155	44	56	32.2	< 0.001
UWC 13.03	Light	1095	69	31			992	73	27		
	Dark	773	44	56	118.0	< 0.001	1013	46	54	147.8	< 0.001

*Significant differences in swimming direction between the light and dark were determined using a Chi-square Test for comparison of proportions (X^2).

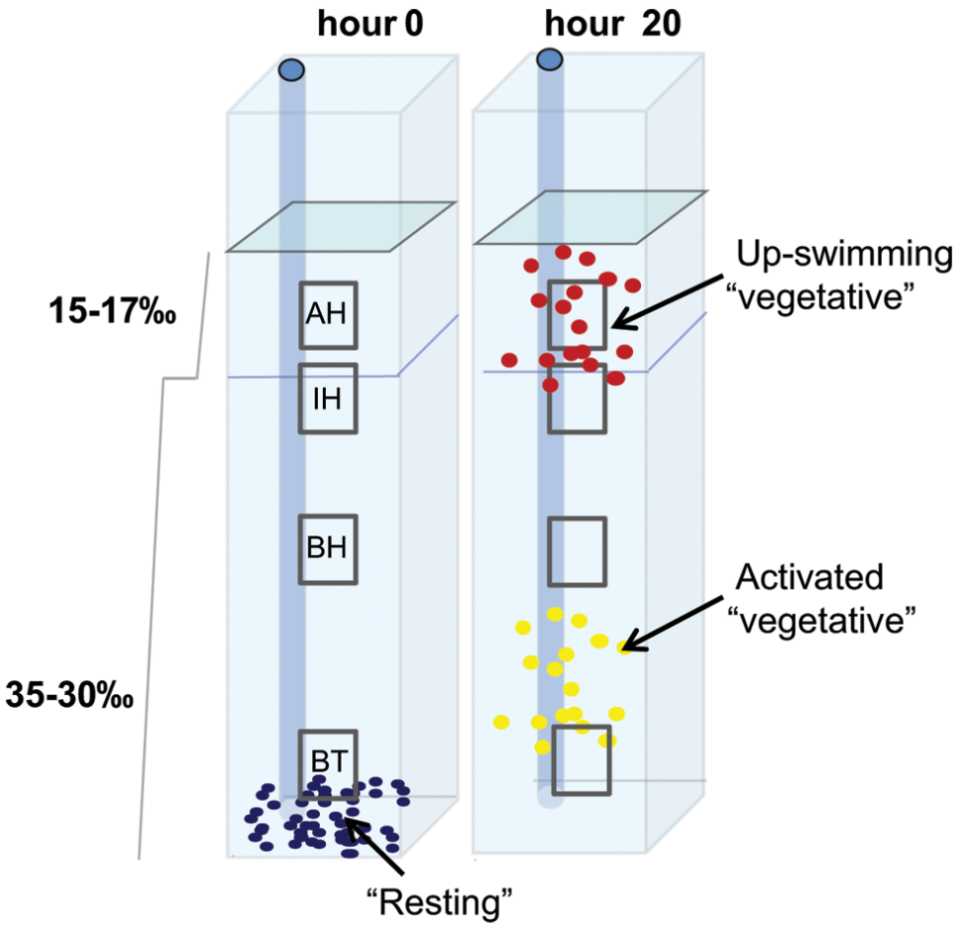

Figure 4.1 Schematics of the stratified water column within each replicate filming chamber of the experimental tank. Each chamber contained a two-layer water column separated by a 30-17 psu salinity transition (halocline). The four vertical fields of view are represented by the dashed boxes: bottom (BT), below the halocline (BH), in the halocline (IH) and above the halocline (AH). Schematics of initial (hour 0) and final (hour 20) cell distributions are shown.

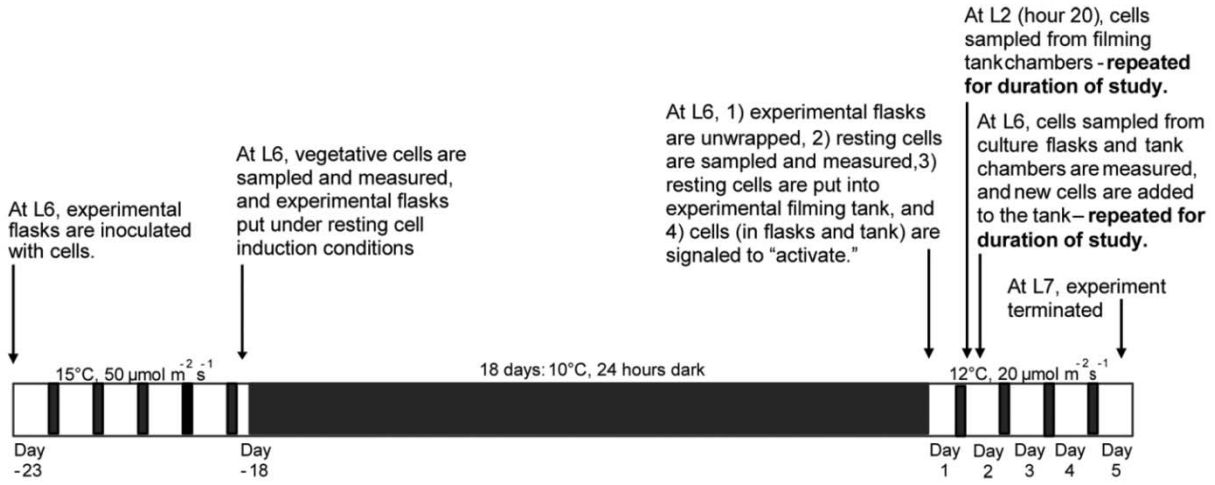

Figure 4.2 A timeline showing the environmental conditions and sampling periods over the duration of the study. The arrows indicate important sampling periods with an associated description. Experimental culture flasks were kept either in the dark for 24 hours per day, or on a 16 hour light: 8 hour dark photoperiod, as indicated on the timeline. "L6" refers to hour 6 of the light period.

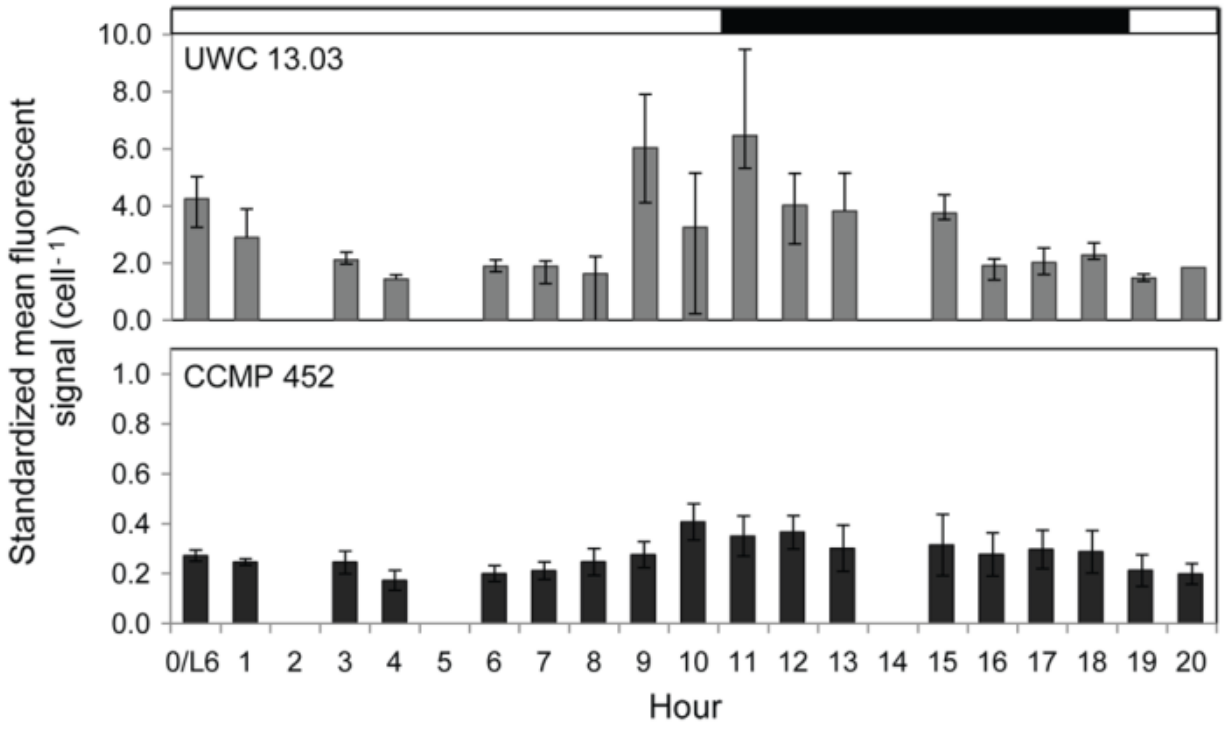

Figure 4.3 Mean DNA signal cell^{-1} following restoration of "activation" conditions for both *H. akashiwo* strains. Hour 0 indicates the signal expressed by resting cells just prior to exposure to the growth supporting, activation conditions. The triplicate cell culture flasks were unwrapped and exposed to activation conditions at L6 (see text and Fig. 2) of the 16 hour light: 8 hour dark photoperiod. Range in sample size (cell #): 3,040 – 11,770 (UWC 13.03) and 5,626 – 14,918 (CCMP 452). Errors bars show the standard error around the mean.

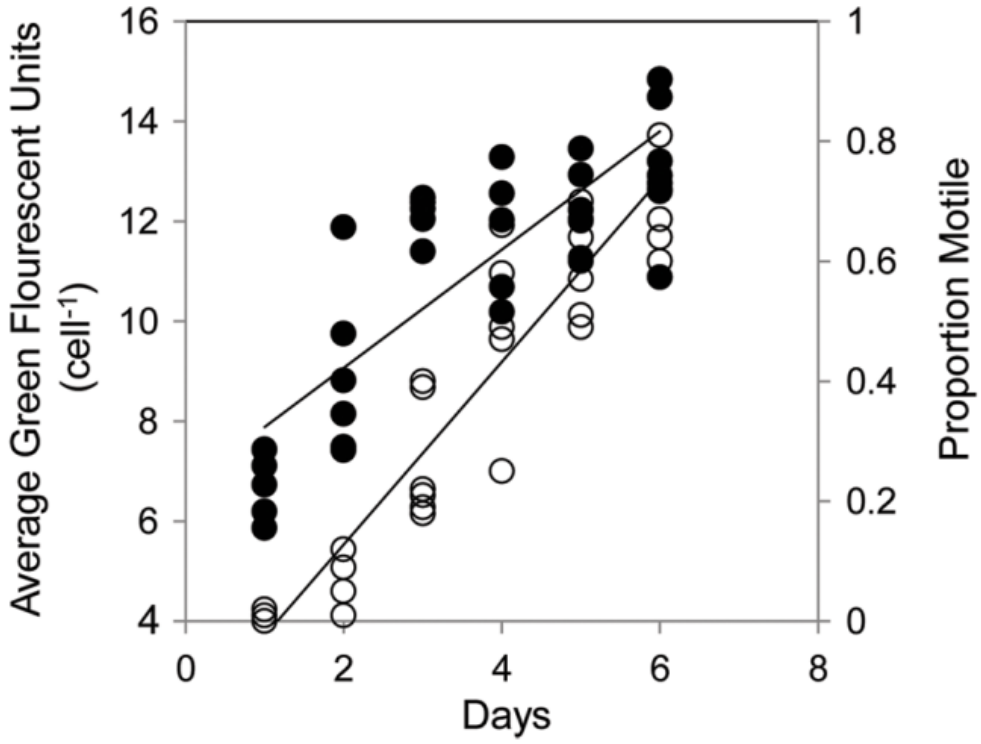

Figure 4.4 Changes in neutral lipid content cell^{-1} and cell motility following exposure to activation conditions. The scatter plot shows the association of average neutral lipid content cell^{-1} (BODIPY 505/515 signal; black circles) and the proportion of motile cells (open circles) with time under activation conditions (in days) for both *H. akashiwo* strains. A Spearman's rank correlation indicates that mean neutral lipid content (r = 0.676) and population motility (r = 0.824) both have significant, positive correlations with time under activation conditions (N = 65, p = < 0.001). Daily sample size (cell #): day 1 = 5358, day 2 = 9,039, day 3 = 11,526, day 4 = 16,624, day 5 = 18,073, and day 6 = 9,480.

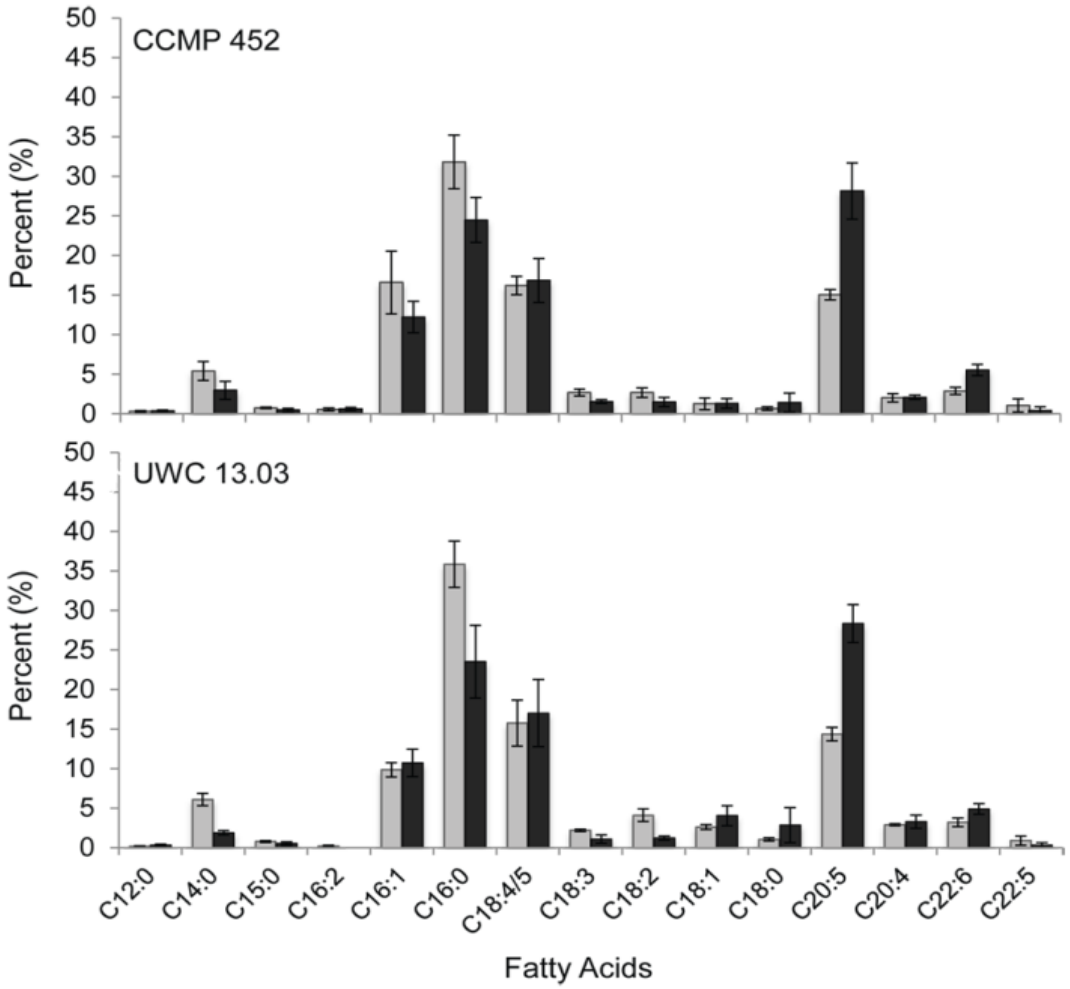

Figure 4.5 Fatty acid profiles of vegetative and resting *H. akashiwo* cells. The bar graphs show the average proportion (N = 3) of each fatty acid based on the total fatty acid content for strains CCMP 452 (top) and UWC 13.03 (bottom), during vegetative (grey bars) and resting (black bars) life-stages. Error bars represent the standard deviation around the mean.

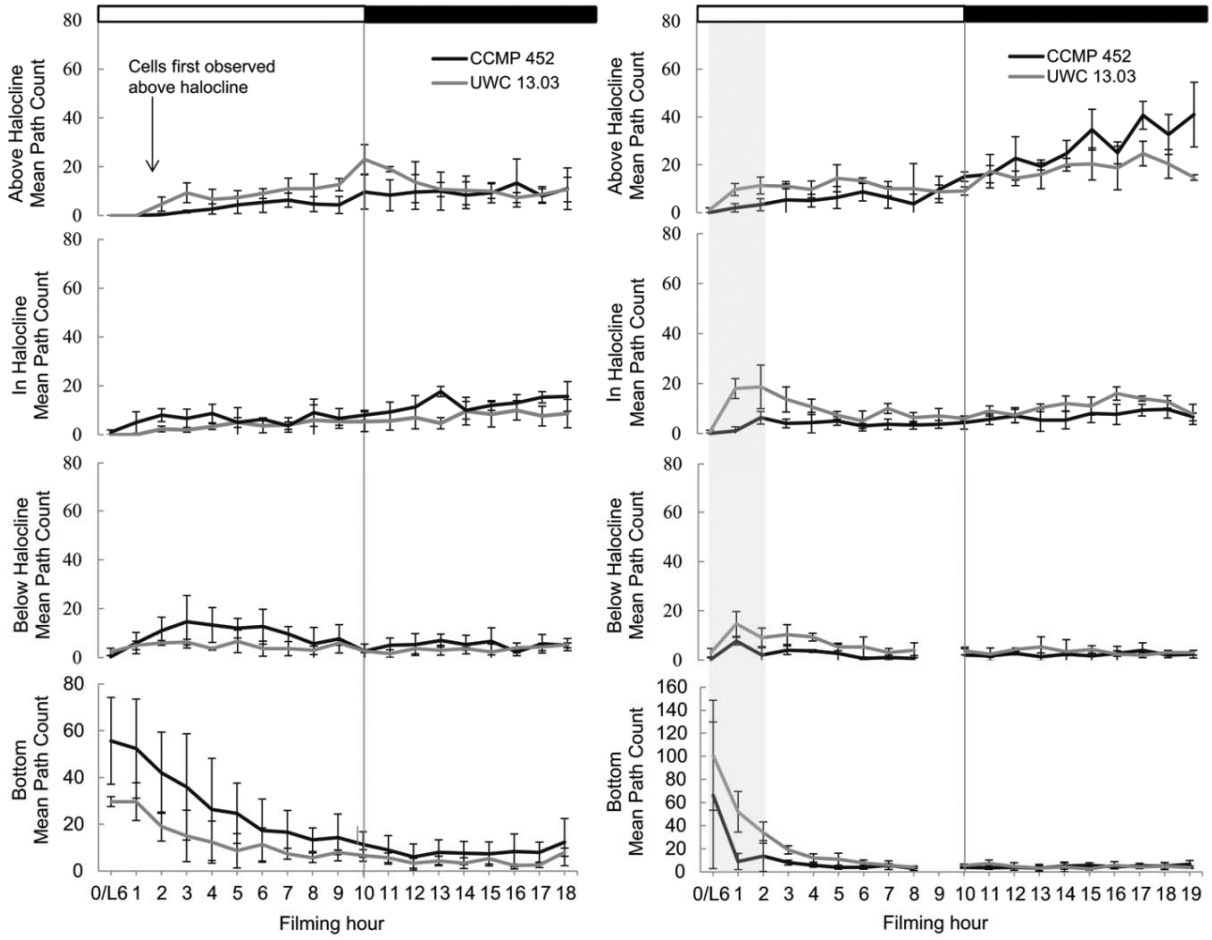

Figure 4.6 *H. akashiwo* cell distributions within the experimental tank. Distributions are based on the mean path count in each field of view for day 1 (left) and day 2 (right) filming observations. The grey shading on the day 2 plot represents vegetative cells determined to have previously activated on day 1. Error bars show the standard deviation around the mean.

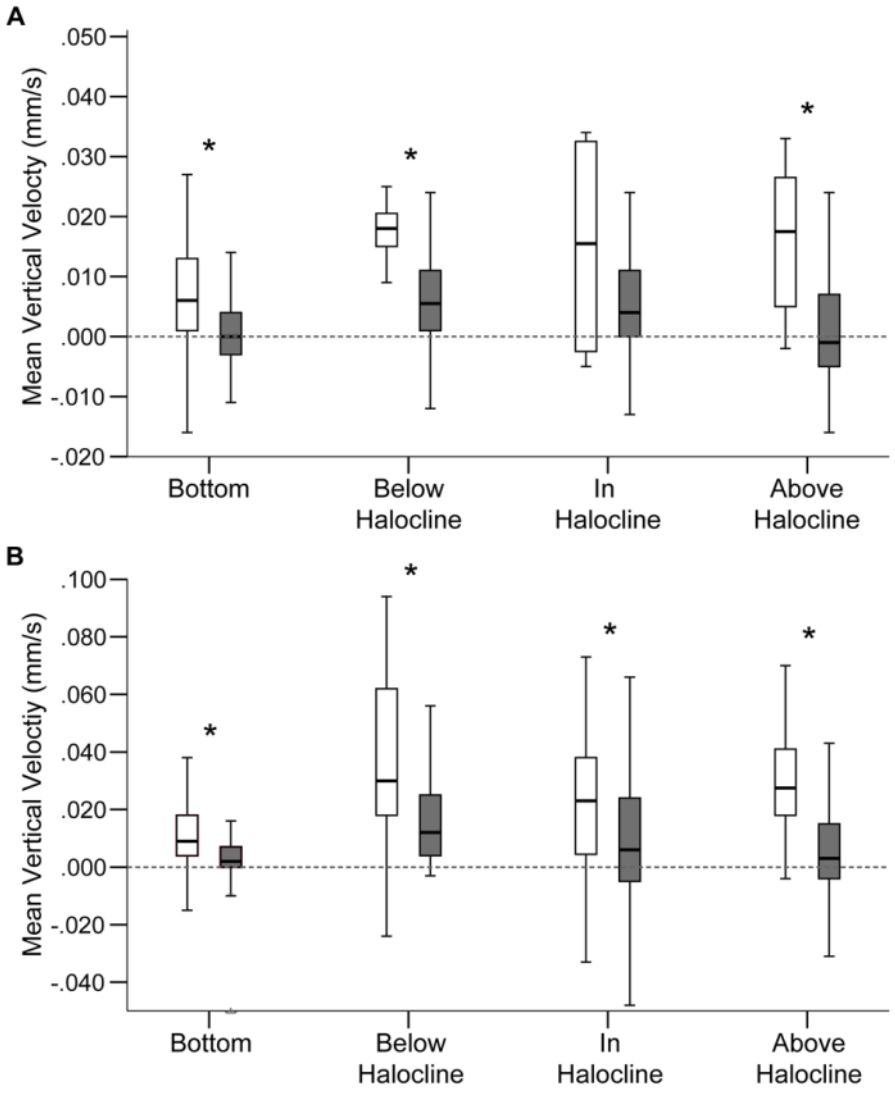

Figure 4.7 Vertical velocities observed for emerged *H. akashiwo* cells. Boxplots show the range of vertical velocities for "newly emerged" cells (■) and "previously emerged" (□) cells in each field of view for (**A**) CCMP 452 and (**B**) UWC 13.03. Asterisks indicate significantly different (p-value < 0.05) vertical velocity distributions based on a Two-sample Kolmogorvo-Smirnov test (see Table 2 for test statistics). Note the 2-fold difference in the *y*-axis scale between the two algal strains.

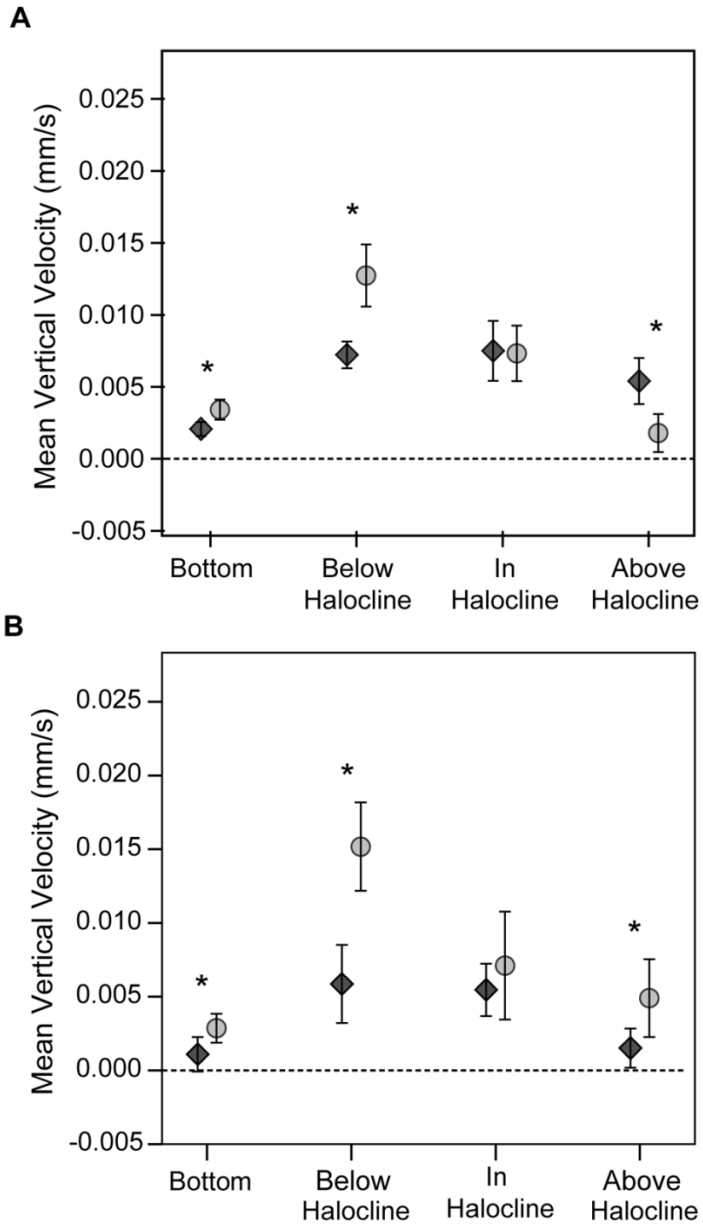

Figure 4.8 Mean vertical velocities of newly emerged *H. akashiwo* cells. The mean vertical velocity is plotted at each field of view for day 1 (A) and day 2 (B) for UWC 13.03 (grey circles) and CCMP 452 (black diamonds). Error bars show 95% confidence intervals. Asterisks indicate statistically significant differences in median vertical velocity based on a Mann Whitney U test – (**A**) BT: $Z = -5.00$, $p < 0.001$, $N = 565, 1130$ (UWC 13.03, CCMP 452), BH: $Z = -4.12$, $p < 0.001$, $N = 231, 414$ (UWC 13.03, CCMP 452), IH: $Z = -1.65$, $p = .100$, $N = 517, 296$ (UWC 13.03, CCMP 452), AH: $Z = -4.31$, $p < 0.001$, $N = 352, 1130$ (UWC 13.03, CCMP 452), (**B**) BT: $Z = -3.70$, $p < 0.001$, $N = 879, 499$ (UWC 13.03, CCMP 452), BH: $Z = -3.67$, $p < 0.001$, $N = 293, 136$ (UWC 13.03, CCMP 452), IH: $Z = -1.26$, $p = .206$, $N = 610, 311$ (UWC 13.03, CCMP 452), AH: $Z = -2.93$, $p = .003$, $N = 823, 968$ (UWC 13.03, CCMP 452).

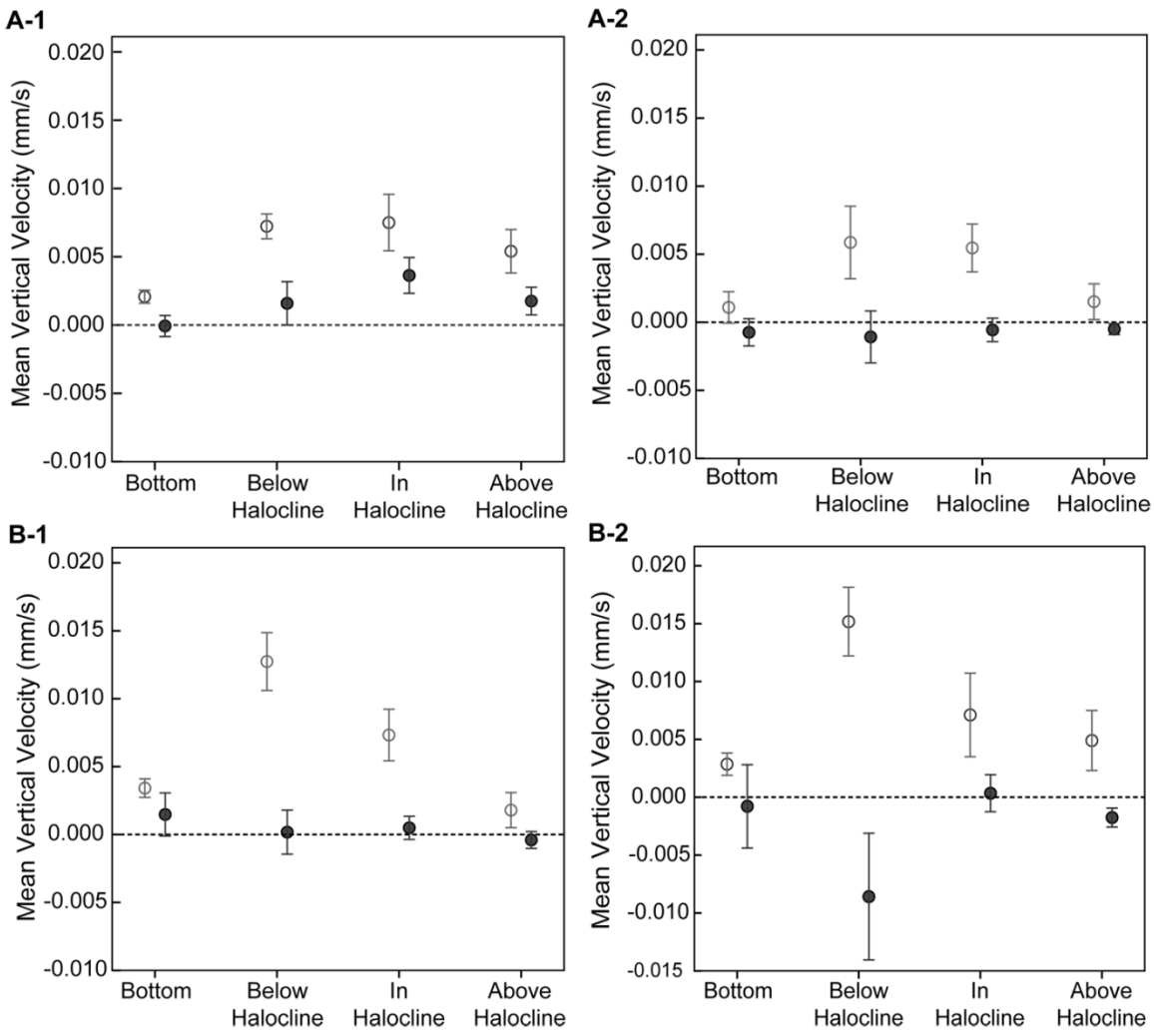

Figure 4.9 Light and dark comparisons of *H. akashiwo* mean vertical velocities. Mean vertical velocities are plotted for light (open circle) and dark (black circle) photoperiods for CCMP 452 (**A**) and UWC 13.03 (**B**) on day 1 (**1**) and day 2 (**2**) for each field of view. Error bars show the standard error around the mean. See Table 3 statistics for the Chi-square Test for comparison of proportions (X^2).

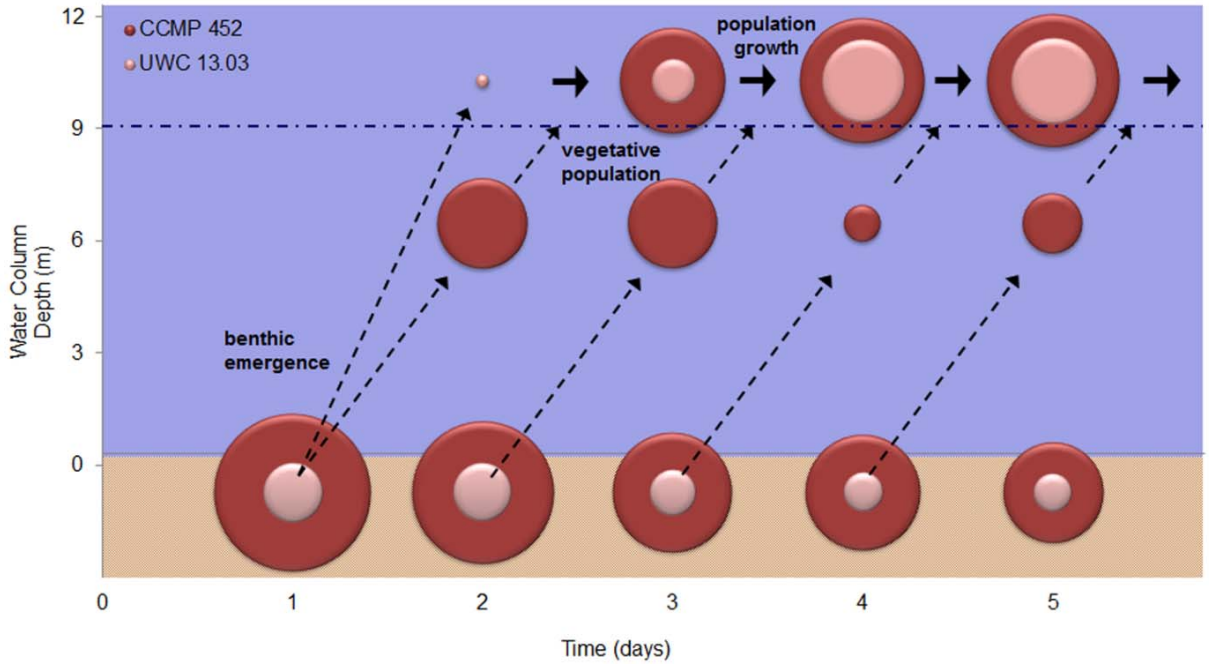

Figure 4.10 Heuristic model of *H. akashiwo* bloom formation (strains CCMP 452 and UWC 13.03). Observed values of cell viability and rates of resting cell activation, up-swimming and cell division (see Table 1 and Fig. 8) were used to calculate benthic and vegetative population densities (bubble plots) and their vertical distributions in the water column (*x*-axis) over time (*y*-axis). In the bubble plot, areas are proportional to population densities. The dashed arrows indicate upward swimming of daily cell "cohorts" leading to aggregation above the halocline (represented by the dot-dashed line at 9 m). Block arrows represent population growth of the near-surface cell aggregates.

Chapter 5. Novel optical remote sensing technology for early detection of Harmful Algal Blooms

5.1 Introduction

Harmful Algal Blooms (HABs) are outbreaks of planktonic algae that produce toxins or accumulate to densities sufficient to threaten public health, degrade aquatic ecosystems and/or cause major economic losses. HABs already affect nearly all coastal environments and are thought to be increasing worldwide in both frequency and severity [1,2]. Substantial progress has been made towards understanding algal bloom dynamics, yet the ecological mechanisms causing HABs remain poorly understood. New *in situ* methodologies for HAB cell detection and quantification would enhance capabilities to study bloom dynamics and enable improved prediction and management of HABs.

Early HAB detection via development of new, cost-effective technologies has been identified as a critical priority for HAB research and management [1,3]. Presently, most HABs are detected only after they reach an advanced stage, when they threaten to cause significant ecological and/or economic damage. Over the last decade, a number of field-deployable instruments have been developed for detection and monitoring of planktonic organisms (e.g., Underwater vision profiler, TowCam [4,5]). Examples of instruments specifically targeting HAB-forming species include the Environmental Sample Processor (ESP) and the Imaging FlowCytobot [6,7]. While such instruments have made great advancements in the detection of harmful algal species *in situ*, they are expensive, require skilled operators and are designed for intensive, localized sampling

of algal cells in near-surface environments. Thus, the need for inexpensive remote sensors capable of detecting and quantifying HAB cell populations remains unmet.

Detection and monitoring of pre-HAB cells within their natural environment require both detailed and sustained observations. Optical sensors that are based on new, low-cost microcomputers are potentially well suited for such long-term monitoring of widely dispersed algal cell populations. A network of these low-cost sensors could be distributed throughout a region to detect and quantify abundance and behaviors of harmful marine algae.

Another challenge to HAB detection and monitoring is that many HAB-forming species have complex life cycles with large cell populations overwintering or temporarily residing in the sediments [8–11]. Emergence of cells from these benthic populations likely initiates many HAB events, while transition of pelagic cells into the benthic resting stage can contribute to HAB termination (Fig. 5.1). Monitoring cells as they emerge from the benthos provides a promising strategy for early detection of potentially harmful blooms. Distribution of optical sensors to remotely detect, quantify and monitor cell emergence, coupled with geophysical circulation models to predict cell transport, could provide the crucial early warning information needed for improved HAB prediction. Monitoring emerging cells in combination with water column properties (e.g., , temperature, nutrients, light) would further enhance the basic understanding of the mechanisms promoting HABs under both present and future environmental conditions [12].

The required optical technology for this type of optical sensing network has never before been developed for a field-deployable sensor, but is well developed for laboratory use. Laboratory

methods have included novel video-based motion analysis methods to image and reconstruct detailed swimming trajectories of many types of small motile marine organisms [13–15]. From these cell-level swimming trajectories, fine-scale movement statistics can be calculated to quantify microorganism responses and behavior within their environment [16–19]. Swimming behavior can also serve as a diagnostic a tool for identification and/or physiological state [20].

Here, we report on the development of the first optical sensor designed to monitor *in situ* benthic emergence of small planktonic organisms (10 – 1000 μm). The sensor, called the Imaging Benthic Emergence Trap (IBET), integrates optical technology with a modified Plankton Emergence Trap [21] to enumerate and characterize the behaviors of HAB-forming algae as they emerge from shallow (< 30 m) benthic environments. Our primary goal was to develop, validate and field-test a prototype of the IBET to determine its suitability for monitoring pre-HAB populations and other field applications.

5.2 Methods and Procedures

Electrical/Optical/Mechanical

The IBET incorporates video imaging optimized for the detection of small planktonic organisms. It features a high resolution 5 Mp digital monochrome camera board (LI-5M03, Leopard Imaging Inc., Fremont, CA, USA) and an on-board 1GHz ARM microprocessor (BeagleBoard-xM, BeagleBoard.org Foundation, Richardson, TX, USA). Illumination of planktonic organisms is provided by a circular bank of 10 infrared (940 nm) light emitting diodes (TSAL6400, Vishay, Malvern, PA, USA). In the IBET prototype, all electrical components are enclosed in a 191.8 mm x 91.7 mm x 84.6 mm waterproof housing, designed for submersion to 30 meters (Otterbox

3500, Otter Products, LLC. USA). Electronics are powered by a 12V input, supplied by onboard high capacity rechargeable AA batteries (MAHA POWEREX, Thompson Distributing, USA; Fig 5.2a).

Planktonic organisms are imaged within a circular chamber ("imaging chamber") 50.8 mm in diameter and 4 mm deep. The imaging chamber is made from 2" (ID), schedule 80 PVC tubing with a back wall of mirrored acrylic. Opaque plastics were used to exclude external light from the imaging chamber. The housing is modified to have a clear, 12.7 mm thick window onto which the imaging chamber is sealed with a nitrile o-ring and fastened with a brace during deployment (Fig. 5.2b). The camera's focal plane is positioned in the center of the imaging chamber and the effective imaging volume is approximately 0.160 mL (see *Instrument Calibration*). The IR LED bank is distributed around the camera board, shining into the imaging chamber through the clear window. The IR light is reflected off of the mirrored back wall. Planktonic organisms within the camera's focal plane scatter the reflected IR light, illuminating them from behind in dark field.

A small reversible peristaltic pump, encased in a 152.4 mm x 63.5 mm PVC waterproof housing, flushes out the imaging chamber and corer after deployment and periodically collects water samples from the imaging chamber. The peristaltic pump is connected by tubing to the top of the imaging chamber (Fig. 5.2b). When the pump is turned on in the reverse direction, water is drawn out of the imaging chamber and is directed through one-way check valves into a clear container with 10 μm Nytex mesh-covered ventilation ports, allowing the imaged water sample to be collected for later microscope validation (Fig 5.3). The Nytex mesh permits the flow of

ambient seawater through the container while retaining the sampled microorganisms of ≥ 10 μm until instrument retrieval.

The imaging chamber is affixed to the top of a sediment corer so that upward swimming cells emerging from the sediments are funneled into the chamber. A 10 μm Nytex mesh filter is connected via an input check valve near the base of the corer above the sediment water interface. When the peristaltic pump is turned on in the forward direction, water is directed through one-way check valves out of the top of the sediment corer section and is replaced by the inflow of filtered ambient seawater (Fig. 5.3). This pumping design allows the sediment corer section to be flushed; purging any seawater that was trapped during deployment and ensuring that only microorganisms emerging from the sediments are observed in the imaging chamber.

The processor, camera, lights and peristaltic pump are controlled using a USB-based microcontroller (Teensy 2.0; https://www.pjrc.com/teensy/). The microcontroller is programmed using the open-source Arduino environment (http://arduino.cc/en/Main/Software) to control power supply and pump direction. Parameter files on a USB flash drive connected to the processor enable automatic video capture and system shutdown. These enable fully automated operation and while conserving battery power during deployment.

Instrument Deployment

For convenience in deployment, IBET components are assembled within and secured to a weighted wire crab pot. The crab pot, with additional weights, provides a sturdy frame so that the IBET sits securely on the seafloor, is protected from suspended debris and is not moved by tidal

currents. When fully assembled, the instrument package size is 610 mm x 610 mm x 330 mm and weighs approximately 25 lbs. The compact size and manageable weight of the IBET makes it easy for one or two people to deploy from a dock or small boat (Fig. 5.2c).

Instrument operation

In a typical benthic deployment, the IBET is pre-programmed to flush out water trapped during deployment, capture video data and collect a water sample from the imaging chamber at specified time intervals. The IBET can run autonomously for up to 30 hours when 2 minute video clips are collected every hour. Just prior to deployment, the instrument is turned on and the following operations are executed by the Teensy controller: 1) the instrument sleeps for 20 minutes while the instrument package is deployed; 2) power is supplied to the pump, turning it on in the forward direction for a 34 minute flush cycle to purge water trapped in the sediment corer during deployment (the flush time is based on calculating the e-folding time for 95% replacement[1] by 10 μm filtered sea water); 3) the pump is switched to the reverse direction for 3 minutes to clear air trapped in the imaging chamber and sample lines; 4) the instrument sleeps for 5 minutes; and 5) the 60 minute filming loop begins.

The IBET is programmed to collect a single video clip and subsequent water sample from the imaging chamber every hour. The filming loop repeats the following steps on a 60 minute interval: 1) power is supplied to the processor and the IR LED bank; 2) a two minute video clip is collected and stored on the USB flash drive; 3) the processor shuts itself down; 4) the power to

[1] The e-folding time is defined as the time it takes for concentration in a fixed volume to reduce 1/e its original value by gradual replacement with a new solution. The e-folding time is defined as, $\frac{Vi}{Vf} = e^{-k(\frac{1}{k})}$, where k = exchange rate (~ 30 mL/min.), v = exchange volume (400 mL), at time, $t = {}^{1}/_{k}$.

the processor and lights turns off; 5) the pump is turned on in the reverse direction for 2 minutes to collect the water sample from the imaging chamber; and 6) the instrument sleeps for the duration of the 60-minute cycle.

Video Analysis

Video data stored on the USB flash drive is processed using the specialized software package, Frugal Ocean Science Image Daemon/Capture Analysis (FOSID/FOSICA), developed by Wallingford Imaging Systems (http://www.wallingford-imaging-systems.com/). The FOSID software runs on the on-board microprocessor to capture, loosely compress and store the raw video. FOSID interfaces with the image sensor hardware to configure the video resolution, region of interest (ROI) and frame rate, providing fully programmable and automated video capture. The video analysis software (FOSICA) performs user-specified image processing on previously captured video, including removal of the background, equalizing the lighting and thresholding frames, to enhance detection of microorganisms. Individual microorganisms are identified in the software as "particles". The size range of the detected particles (in pixel area) can be adjusted to clearly resolve microorganisms of interest.

Once particles of interested are identified, the pixel position of each individual is determined and converted into physical units (in mm). Individual observations are assembled across successive video frames into complete 2D movement trajectories using the motion analysis software, Tracker 3D (Grünbaum, unpublished data). Statistical analysis can be performed on the observed movement patterns to determine fine scale movements that can be used to assist in particle classification and identify rates of benthic emergence [19,20].

5.3 Instrument Validation

Calibration

To assess cell quantification by the IBET, we analyzed replicate samples of known cell concentrations and cell size range of a laboratory culture of *Alexandrium catenella*, a harmful dinoflagellate. A two-fold serial dilution, using seawater filtered through a Whatman GF/F Glass Microfiber Filter (GE Whatman, Pittsburgh, PA, USA) to remove organisms > 0.7 μm, was performed to obtain five concentrations (1x, 1/2x, 1/4x, 1/8x and 1/16x) of *Alexandrium*. The average cell concentration for each dilution factor was determined by counting horizontal transects in a Sedgwick-Rafter slide (a known area relative to the 1000 mm^2 of the entire chamber), ensuring no less than 75 cells were counted. The cells were counted under transmitted light at 120x magnification using a Zeiss standard microscope. Microscope-based cell counts were done in triplicate. The count data were combined and treated as one sample from a Poisson distribution to calculate the cell concentration and 95% confidence intervals [22].

Cell size range for the *A. catenella* culture was determined using a Zeiss Axiovert microscope equipped with a digitizer pad and Microbiota software [23]. Five mL of cells were fixed with 0.5% gluteraldehyde and allowed to settle for 1 hour in a settling chamber. Cell lengths (diameter) of 75 individual cells were measured within the settling chamber under transmitted light and magnification of 200x.

Thirty second video clips of each known *A. catenella* cell concentration were collected in the IBET imaging chamber. The video data were processed using the FOSICA analysis software, yielding particle counts and particle dimensions for each frame in the video. Cell diameters (μm)

determined by microscopy-based measurements were compared to the diameters of targeted *Alexandrium*-sized particles (pixel area: 12 – 42; see Table 5.1) in the 1x concentration video clip. Pixel units for each particle detected were converted to physical units based on the camera sensor's known pixel size of 2.2 μm and a magnification factor of 0.4. Microscope-based cell measurements and *Alexandrium*-sized particles from video observations had similar physical size ranges and median diameters (μm) that were not significantly different (Mann-Whitney U-test: U = 27773, p = 0.114). Figure 5.4 shows *A. catenella* swimming trajectories generated from of the calibration files, demonstrating that the cells were successfully targeted by optical size.

The instrument calibration shows that the median number of *Alexandrium*-sized particles (pixel area: 12 – 42) observed by the IBET are strongly correlated with mean cell concentrations from microscope-based counts (Pearsons Correlation, r = 0.992, df = 3, p <0.001; Fig. 5). Error bars indicate 2.5% and 97.5% quantiles (middle 95%) of the number of *Alexandrium* size particles detected in each video (vertical) and 95% confidence intervals for the microscopy-based mean cell concentrations (horizontal). The equation $V = {\bar{N}}/{\bar{C}}$ was used to calculate the effective imaging volume (V) of the IBET, where $\bar{N}$ is the average of the median number of video particles for each video and $\bar{C}$ is the average of the mean cell concentrations. Using the above equation, we calculated V as 0.160 mL with 95% confidence intervals of ± 0.0115. Using the calculated imaging volume (V), Figure 5.5 shows the relationship between N and C bounded by the 95% confidence intervals.

Field Deployments

The IBET was field tested off a floating dock in Quartermaster Harbor – an embayment in Puget Sound, WA known to have annual *A. catenella* blooms seeded by a persistent *A. catenella* cyst bed [24–26]. The instrument was fully functional down to the maximum testing depth of 15 meters. The IBET was pre-programmed to autonomously capture video data and collect water samples on hourly intervals over a deployment duration of 30 hours.

Initial testing of the IBET was focused on determining if the instrument could detect *A. catenella* and other HAB cells of interest in the plankton if they were present. To accomplish this, we deployed the IBET at a time when we knew (based on plankton net tows) that HAB-forming algae were present in the water column. The water column sampling protocol was modified to eliminate the initial 34 minute sediment core flush cycle. The instrument package was deployed to a depth of approximately 5 meters. Air trapped in the imaging chamber and sample lines was first purged by the pump, then the 60 minute filming/sampling loop began. The instrument was retrieved after a 28 hour sampling duration. The IBET was able to quantify and detect diverse plankton, including two HAB-forming species – *Alexandrium catenella* and *Akashiwo sanguinea* – in field sampling of natural seawater communities (Fig. 5.6 & 5.7). All plankton detected and analyzed from the IBET video data were validated by microscopic observation of the water samples collected from the sampling chamber.

Environmental data collected by the IBET showed a high abundance of particles in the whole seawater sample in late summer. Figure 5.6 demonstrates how video data with high particle abundances can be sorted by size class using FOSICA. As validated by the instrument

calibration, particles can be categorized by optical size (pixel area) to target organisms of interest. For example, we were able to detect and track the unique swimming behavior of the chain-forming harmful alga, *A. catenella,* by excluding the smaller optical size fraction (pixel area < 300) of detected particles (Fig. 5.6b).

Our field deployments also captured *in situ* data during the early onset of a late-summer bloom of the HAB-forming dinoflagellate, *Akashiwo sanguinea.* Using this environmental data, we demonstrated how the IBET, and the associated particle tracking software, can be used to detect planktonic organisms in a whole seawater sample, target HAB-forming species of interest by optical size/shape and monitor cell swimming characteristics (Fig. 5.7 and Table 5.1). To target *Akashiwo sanguinea* cells in our video observations of natural seawater communities, optical size was used to excluded particles that fell outside of typical cell size range of *A. sanguinea* (approximately 40 to 150 pixel area) using the FOSICA software (Fig. 5.7 a, b). The pixel coordinates for each *A. sanguinea*-sized particle were converted into physical coordinates using a standard calibration grid of known dimensions. Particles were then tracked (using Tracker3D) over consecutive frames to generate the cell swimming trajectories (Fig. 5.7c, d). Each individual swimming trajectory was fitted with two smoothing splines, short-interval and long-interval splines, to eliminate noise and to distinguish directed movement from oscillatory motion.

Swimming statistics critical for distinguishing between passive vs. active particles and identifying cell-level rates of transport to surface waters (e.g., gross speed, vertical and horizontal velocities, oscillatory movement and frequency of directional changes) were calculated from the smoothed swimming trajectories. Directed movements (e.g., vertical

velocity) indicate upward and downward migration in the water column, while oscillatory motion can provide diagnostic information for cell identification and/or physiological state [13,19,20]. Examples of these swimming statistics are reported in Table 5.2 for the two HAB-forming species detected by the IBET during field deployments. This is the first study to quantify *A. sanguinea* cell-level swimming behaviors *in situ*. These swimming statistics indicate that *A. sanguinea* cells are capable of greater swimming speeds (maximum speed = 231 μm s^{-1}) and vertical velocities compared to single cells of *A. catenella* (maximum speed = 120 μm s^{-1}). Within *A. catenella,* the swimming statistics show that chain formation greatly enhances both gross swimming speed (maximum speed = 241 μm s^{-1}) and oscillatory motion, yet vertical velocities are slower when compared to single cells.

After we confirmed that the IBET was fully functional and capable of detecting HAB-forming cells of interest, we made several deployments attempting to capture benthic emergence of *A. catenella*. However, by the time the instrument was ready for benthic testing it was late in the summer season (September/October). Benthic emergence of *A. catenella* is generally known to occur in April through August in Quartermaster Harbor [27], and therefore, we believe that we were not able to deploy the IBET in time to capture benthic emergence. Several deployments of the IBET made in Quartermaster Harbor in late summer did not detect emerging cells of any kind.

5.4 Discussion and Recommendations

There is strong evidence that cell-level swimming plays a crucial role in algal distributions and bloom dynamics by regulating vertical fluxes and interactions with different water masses

[16,28,29]. While a number of studies have examined swimming of cells in culture, swimming behaviors in the field are rarely quantified, particularly those associated with benthic-pelagic life stage transitions. Advancements in field-deployable sensors will greatly improve our ability to detect and quantify real-world algal movement behaviors that regulate distributions of HABs and other planktonic organisms. Optical sensors like the IBET provide a unique opportunity to acquire new environmental information about fundamental ecological mechanisms that regulate HAB occurrences.

From the preliminary behavioral data collected by the IBET, we can begin to gain some insights on characteristic swimming behaviors among and within HAB species in their natural environment. For example, we observed that *A. sanguinea* cells are capable of greater swimming speeds and vertical velocities compared to single cells of *A. catenella.* Dinoflagellates often exhibit a diel vertical migration behavior to acquire nutrients at depth [30,31]. The observed greater vertical velocities of *A. sanguinea* suggests that this dinoflagellate species has the potential to vertically migrate through the water column more rapidly than single cells of *A. catenella,* which could provide a potential competitive advantage for resource acquisition. In our *in situ* observations, *A. catenella* chain formation greatly enhanced both gross swimming speed and oscillatory motion. This observation is in agreement with previous laboratory studies on *Alexandrium* motility [32,33]. Interestingly, this increase in gross speed is not associated with an increase in vertical movement rates. It has been suggested that chain formation helps *Alexandrium* conserve energy needed for motility, improves navigation in water masses with greater mixing, and may enhance retention within the euphotic zone [28]. Hence, our observation suggests the hypothesis that rates of transport to sunlit surface waters may be driven

by recent emergence of single cells, while chain formation may help *Alexandrium* cells maintain their position within the photic zone.

Direct *in situ* measurements are needed to improve understanding of the role of benthic-pelagic life stage transitions in algal population dynamics. Yet, few studies have successfully quantified *in situ* rates of benthic emergence. Prior observations of benthic emergence rates have primarily been limited to laboratory studies of samples transported from the field. A few *in situ* devices have been designed to sample benthic emergence, trapping cells at the sediment-water interface [e.g., 25–27]. However, those sampling devices are not automated, and hence, not capable of collecting fine-scale temporal data, nor are they capable of characterizing *in situ* cell-level behaviors. The IBET is the first instrument specifically designed to provide *in situ* detection, quantification and behavioral monitoring of emerging meroplanktonic organisms. While we have not been able to directly show IBET-detected algal emergence, we believe that the video data collected from whole seawater samples provides compelling evidence that the instrument is capable of detecting disperse HAB-forming cells at relatively low concentrations (the lowest concentration observed was 2 cells per video observation, approximately 10 cells mL^{-1}) and monitoring their abundance and behavior when present.

The IBET has been rigorously calibrated and field tested, validating the effective use of the instrument for future HAB detection, monitoring and prediction efforts. The IBET calibration protocols can be used to easily convert video particle observations to true cell concentrations and sizes. While we have not yet had the opportunity to detect benthic emergence of HAB-forming species with the IBET, initial field testing has demonstrated that the IBET can run autonomously

for 30 hours on an hourly sampling interval and is effective at detecting and monitoring behaviors of HAB-forming algae, as well as other microorganisms (e.g., benign algal species and copepod naupli; data not shown), over extended deployments. Because the IBET is easily programmable, it provides great flexibility in adjusting sampling frequency, and hence deployment duration, to meet specific detection and monitoring needs.

The true innovation of the IBET is the compact size and low cost of production for a highly capable optical sensor. Advancements in upcoming generations of the IBET and its accompanying software will further improve its ease of use so that the sensor can be readily deployed by other researchers and stakeholders (e.g., aquaculture managers) for more comprehensive temporal and spatial monitoring. The low cost (approximately $1000 per sensor) and ease of transport and deployment allows the IBET to be easily integrated into region-wide remote sensing networks that will improve spatial and temporal scales of detection. A network of optical sensors to remotely detect and monitor benthic emergence of algal cells throughout Puget Sound, WA is currently being developed in the Grünbaum laboratory in collaboration with the Northwest Association of Networked Ocean Observing Systems (NANOOS) and the Suquamish Tribe's Chief Kitsap Academy. This network will provide a unique tool for biologists, engaged citizens, and stakeholders to gain crucial early warning information on HAB formation.

The IBET can provide quantitative information that is immediately useful to those concerned with predicting and mitigating HAB impacts. For example, paralytic shellfish toxin testing efforts in Puget Sound by the Washington State Department of Heath could be better targeted if the timing, rates of emergence and subsequent transport of *Alexandrium* cell populations (the

causative organism) were available. When deployed with other marine environmental sensors (e.g., CTD or ACDP), the IBET could provide new insights into the physical factors that regulate benthic emergence and subsequent bloom formation. Quantitative data obtained by the IBET can be directly incorporated into rapidly improving geophysical models to simulate cell transport in coastal regions and provide more accurate biological data to inform biophysical modeling efforts. New field-deployable technologies, such as the IBET, have the potential to significantly improve HAB prediction and general understanding of plankton ecology.

5.5 References

1. Ramsdell J., Anderson D., Gilbert P. (2005) Harmful algal research and response: A national environmental science strategy 2005-2015. Washington DC.

2. Bauer M (2006) Harmful algal research and response: A human dimensions strategy. In: Bauer M, editor. National Office for Marine Biotoxins and Harmful Algal Blooms, Woods Hole Oceanographic Institution, Woods Hole, MA. p. 58.

3. Jewett EB, Lopez CB, Dortch Q, Etheridge S., Backer LC (2008) Harmful algal bloom management and response: Assessment and plan. Interagency Working Group on Harmful Algal Blooms, Hypoxia and Human Health of the Joint Subcommittee on Ocean Science and Technology. Washington, DC.

4. Picheral M, Guidi L, Stemmann L, Karl DM, Iddaoud G, et al. (2010) The Underwater Vision Profiler 5: An advanced instrument for high spatial resolution studies of particle size spectra and zooplankton. Limnol Oceanogr Methods 8: 462–473. doi:10.4319/lom.2010.8.462.

5. Fornari DJ (2003) A new deep-sea towed digital camera and multi-rock coring system. Eos, Trans Am Geophys Union 84: 69. doi:10.1029/2003EO080001.

6. Greenfield DI, Doucette GJ, Mikulski C, Jones K, Jensen S, et al. (2008) Field applications of the second-generation Environmental Sample Processor (ESP) for remote detection of harmful algae: 2006-2007. Limnol Oceanogr Methods 6: 667–679. doi:10.4319/lom.2008.6.667.

7. Olson RJ, Sosik HM (2007) A submersible imaging-in-flow instrument to analyze nano- and microplankton: Imaging FlowCytobot. Limnol Oceanogr Methods 5: 195–203. doi:10.4319/lom.2007.5.195.

8. Figueroa RI, Bravo I, Garcés E (2006) Multiple routes of sexuality in *Alexandrium taylori* (Dinophyceae) in culture. J Phycol 42: 1028–1039. doi:10.1111/j.1529-8817.2006.00262.x.

9. Figueroa RI, Rengefors K (2006) Life cyle and sexuality of the freshwater raphidophyte *Gonyostomum semen* (Raphidophyceae). J Phycol 42: 859–871. doi:10.1111/j.1529-8817.2006.00240.x.

10. Han M, Kim Y, Cattolico RA (2002) *Heterosigma akashiwo* (Raphidophyceae) resting cell formation in batch culture: Strain identity versus physiological response. J Phycol 317: 304–317. doi:10.1046/j.1529-8817.2002.01087.x.

11. Taylor FJ., Trainer VL (2002) Harmful algal blooms in the PICES region of the North Pacific. PICES Scientific Report. B.C. Canada.

12. Moore SK, Trainer VL, Mantua NJ, Parker MS, Laws E a, et al. (2008) Impacts of climate variability and future climate change on harmful algal blooms and human health. Environ Heal 7: S4. doi:10.1186/1476-069X-7-S2-S4.

13. Bearon R., Grunbaum D, Cattolico R. (2004) Relating cell-level swimming behaviors to vertical population distributions in *Heterosigma akashiwo* (Raphidophyceae), a harmful alga. Limnol Oceanogr 49: 607–613. doi:10.43119/lo.2004.49.2.0607.

14. Chan KY., Grünbaum D (2010) Temperature and diet modified swimming behaviors of larval sand dollar. Mar Ecol Ser 415: 49–59.

15. Menden-Deuer S, Grünbaum D (2006) Individual foraging behaviors and population distributions of a planktonic predator aggregating to phytoplankton thin layers. Limnol Oceanogr 51: 109–116.

16. Bearon RN, Grünbaum D, Cattolico RA (2006) Effects of salinity structure on swimming behavior and harmful algal bloom formation in *Heterosigma akashiwo*, a toxic raphidophyte. Mar Ecol Prog Ser 306: 153–163. doi:10.3354/meps306153.

17. Chan KYK., Grünbaum D, O'Donnell MJ (2011) Effects of ocean-acidification-induced morphological changes on larval swimming and feeding. J Exp Biol 214: 3857–3867.

18. Clay TW, Grünbaum D (2010) Morphology-flow interactions lead to stage-selective vertical transport of larval sand dollars in shear flow. J Exp Biol 213: 1281–1292.

19. Tobin ED, Grünbaum D, Patterson J, Cattolico RA (2013) Behavioral and physiological changes during benthic-pelagic transition in the harmful alga, *Heterosigma akashiwo*: Potential for rapid bloom formation. PLoS One 8.10: e76663. doi:10.1371/journal.pone.0076663.

20. Tobin ED, Grünbaum D, Cattolico RA (2011) Pelagic-benthic transition of the harmful alga, *Heterosigma akashiwo*: Changes in swimming and implications for benthic cell distributions. Harmful Algae 10: 619–628. doi:10.1016/j.hal.2011.04.014.

21. Ishikawa A, Hattori M, Imai I (2007) Development of the "plankton emergence trap/chamber (PET Chamber)", a new sampling device to collect in situ germinating cells from cysts of microalgae in surface sediments of coastal waters. Harmful Algae 6: 301–307. doi:10.1016/j.hal.2006.04.005.

22. Venrick E (1978) How many cells to counts? In: Sournia A, editor Phytoplankton Manual. Paris: UNESCO. pp. 167–180.

23. Roff JC, Hopcroft RR (1986) High precision microcomputer based measuring system for ecological research. Can J Fish Aquat Sci 43: 2044–2048.

24. Horner R., Greengrove CL, Davies-Vollum KS, Gawel JE, Postel JR, et al. (2011) Spatial distribution of benthic cysts of *Alexandrium catenella* in surface sediments of Puget Sound, Washington, USA. Harmful Algae 11: 96–105. doi:10.1016/j.hal.2011.08.004.

25. Nishitani L, Chew KK (1984) Recent developments in paralytic shellfish poisoning research. Aquaculture 39: 317–329. doi:10.1016/0044-8486(84)90274-6.

26. Greengrove CL, Masura JE, Moore SK, Bill BD, Hay LR, et al. (2012) *Alexandrium catenella* cyst distribution and germination in Puget Sound, WA USA. In: Kim HG, editor. International Confrence on Harmful Algae 15th Proceedings. Changwong, Korea.

27. Tobin ED, Horner RA (2011) Germination characteristics of *Alexandrium catenella* cysts from surface sediments in Quartermaster Harbor, Puget Sound, Washington, USA. Harmful Algae 10: 216–223. doi:10.1016/j.hal.2010.10.002.

28. Smayda TJ (2002) Turbulence, watermass stratification and harmful algal blooms: An alternative view and frontal zones as "pelagic seed banks." Harmful Algae 1: 95–112. doi: 10.1016/S1568-9883(02)00010-0.

29. Durham WM, Kessler JO, Stocker R (2009) Disruption of vertical motility by shear triggers formation of thin phytoplankton layers. Science (80-) 323: 1067–1070. doi:10.1126/sciencce.1167334.

30. Cullen, JJ (1985) Diel vertical migration by dinoflagellates: roles of carbohydrate metabolism and behavioral flexibility. Contr. Mar. Sci. 27 (Suppl.): 135-152. (1985). 27: 135–152.

31. Anderson DM, Stolzenbach K (1985) Selective retention of two dinoflagellates in a well-mixed estuarine embayment: The importance of diel vertical migration and surface avoidance. Mar Ecol Prog Ser 25: 39–50.

32. Karp-Boss L, Boss E, Jumars PA (2000) Motion of dinoflagellates in a simple shear flow. Limnol Oceanogr 45: 1594–1602.

33. Fraga S, Gallager SM, Anderson DM (1989) Chain-forming dinoflagellates: An adaption to red tides. In: Okaichi T, Anderson DM and Nemoto T, editors Red Tides: biology, environmental science and toxicology. New York: Elsevier. pp. 281–284.

34. Ishikawa A, Fujita N, Taniguchi A (1995) A sampling device to measure in situ germination rates of dinoflagellate cysts in surface sediments. J Plankton Res 17: 647–651.

35. Ishikawa A, Taniguchi A (1996) Contribution of benthic cysts to the population dynamics of *Scrippsiella* spp . (Dinophyceae) in Onagawa Bay, northeast Japan. Mar Ecol Prog Ser 140: 169–178. doi:10.3354/meps140169.

36. Thistle D, Sedlacek L, Carman KR, Fleeger JW, Barry JP (2007) Emergence in the deep sea: Evidence from harpacticoid copepods. Deep Sea Res Part I Oceanogr Res Pap 54: 1008–1014. doi:10.1016/j.dsr.2007.03.002.

37. Horner RA (2002) A taxonomic guide to some common marine phytoplankton. Bristol, England: Biopress Ltd.

Table 5.1 Recommendations for FOSICA pixel area settings to target single cells of HAB-forming species commonly observed in Puget Sound from IBET video data. Cell size data obtained from Horner [37].

Motile HAB-forming cells of interest	Approximate cell size range (μm)	Associated optical length (pixels)	Suggested particle area range (pixels)
Heterosigma akashiwo	10 – 20	1.8 – 3.6	2.5 – 10.2
Alexandrium sp.	22 – 40	4.0 – 7.3	12.5 – 41.8
Akashiwo sanguinea	40 – 80	7.3 – 14.5	41.8 – 165.1
Dinophysis sp.	38 – 100	6.9 – 18.2	37.4 – 260.1

Table 5.2 Examples of *in situ* swimming statistics calculated for two HAB species detected during field deployments in Quarter Master Harbor, WA. The numbers in parentheses are the median values for each swimming statistic.

HAB species	Gross Swimming Speed (μm/s)	Vertical Velocity (μm/s)	Oscillatory Speed (μm/s)
Akashiwo sanguinea	5 – 231 (58)	-160 – 219 (35)	4 – 77 (37)
Alexandrium sp.			
Single cells	23 – 120 (74)	-97 – 144 (24)	4 – 79 (39)
Chains	36 – 241 (138)	-11 – 90 (39)	54 – 173 (114)

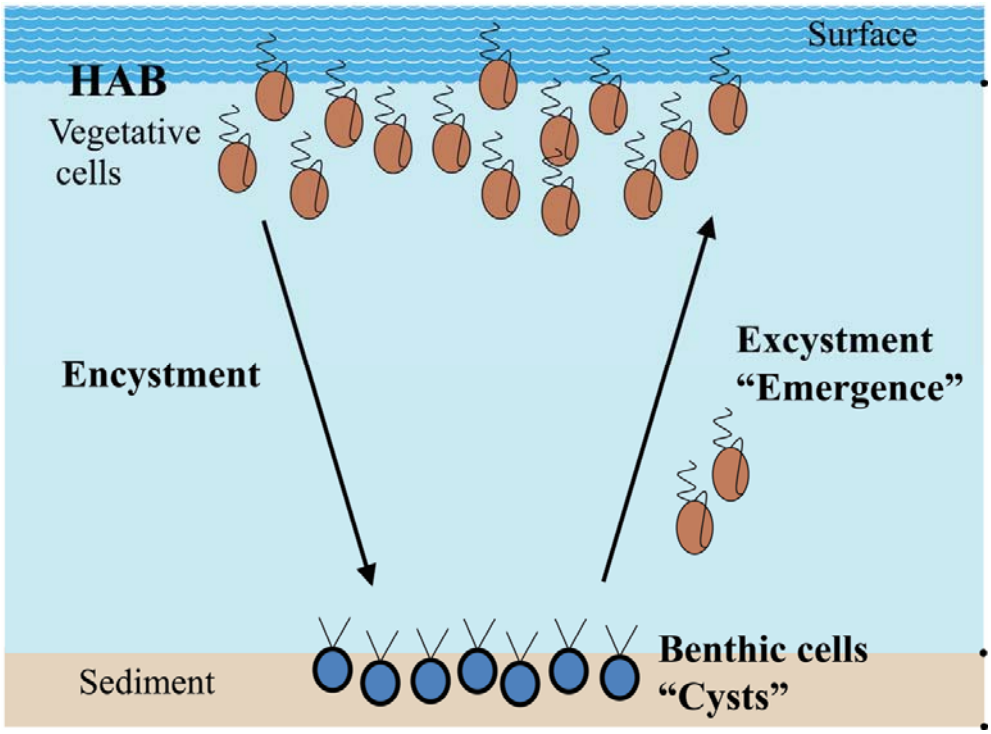

Figure 5.1 Generalized schematic of the dual-stage life cycle of many harmful algae. Figure modified from Han et al. 2002 [10]

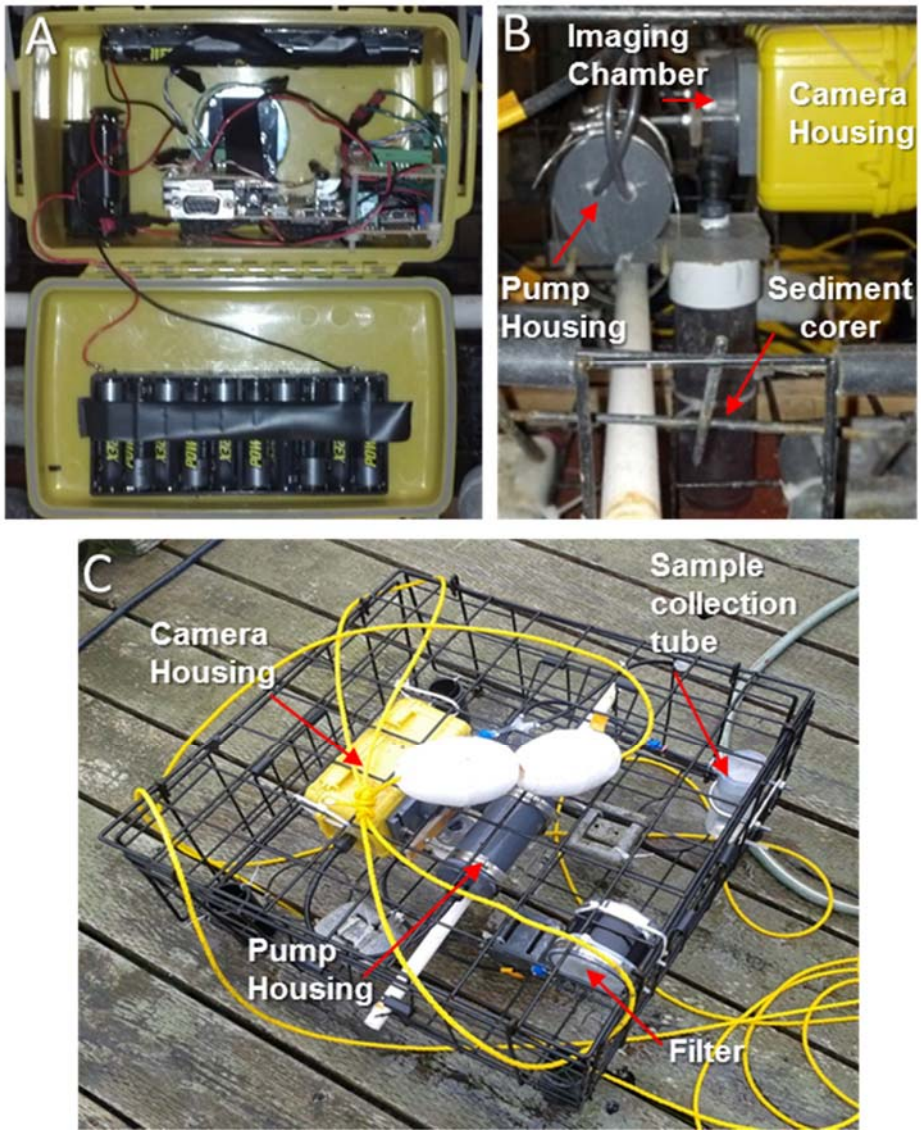

Figure 5.2 Photographs of the Imaging Benthic Emergence Trap (IBET). (A) The optical and electrical components housed in a waterproof casing. (B) Side profile of the primary IBET components assembled: pump, imaging chamber, camera housing and the corer. (C) The entire IBET instrument package assembled and ready for a dock-based deployment.

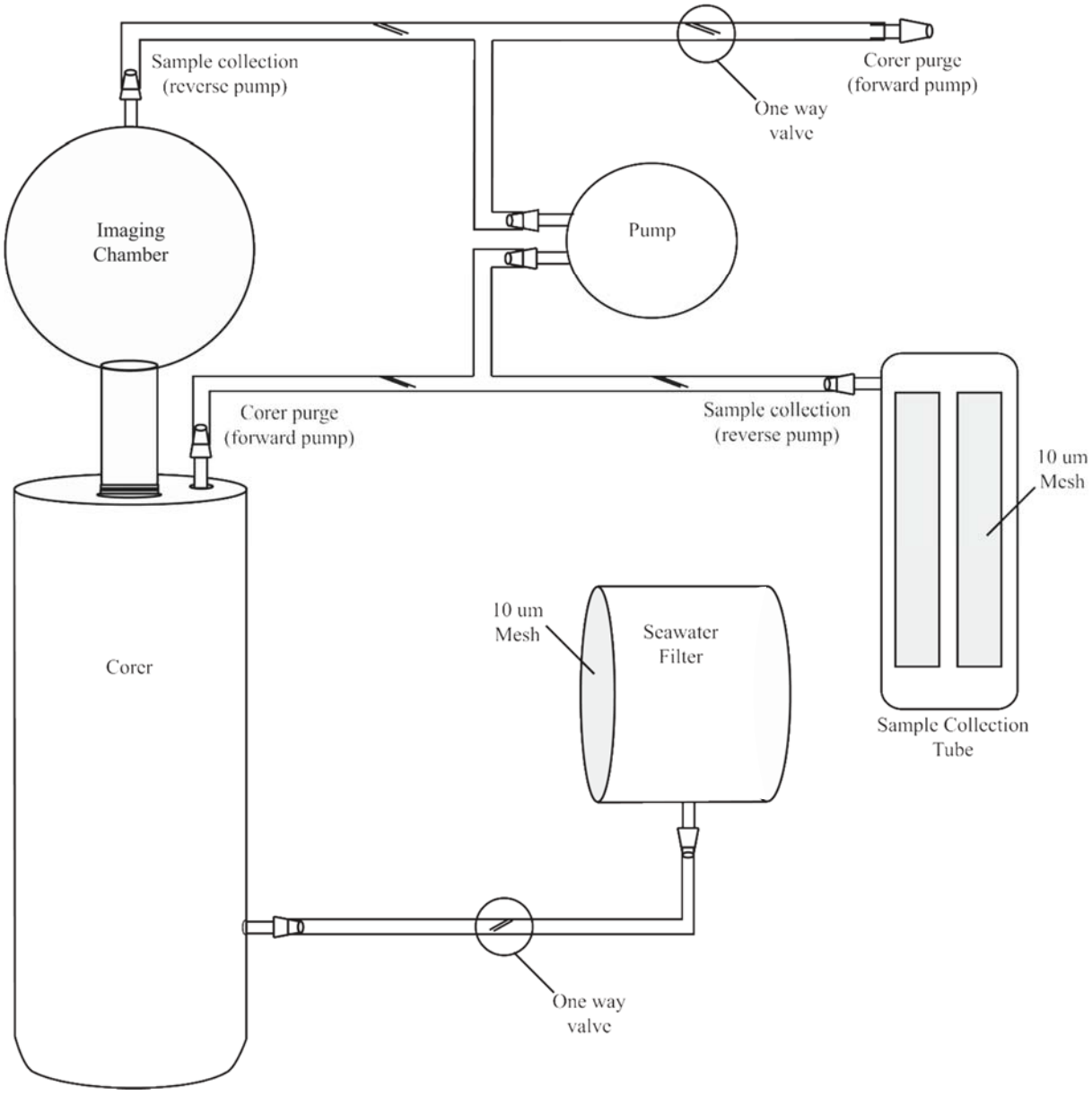

Figure 5.3 Illustration of the IBET's pumping system to control instrument flushing and sample collection.

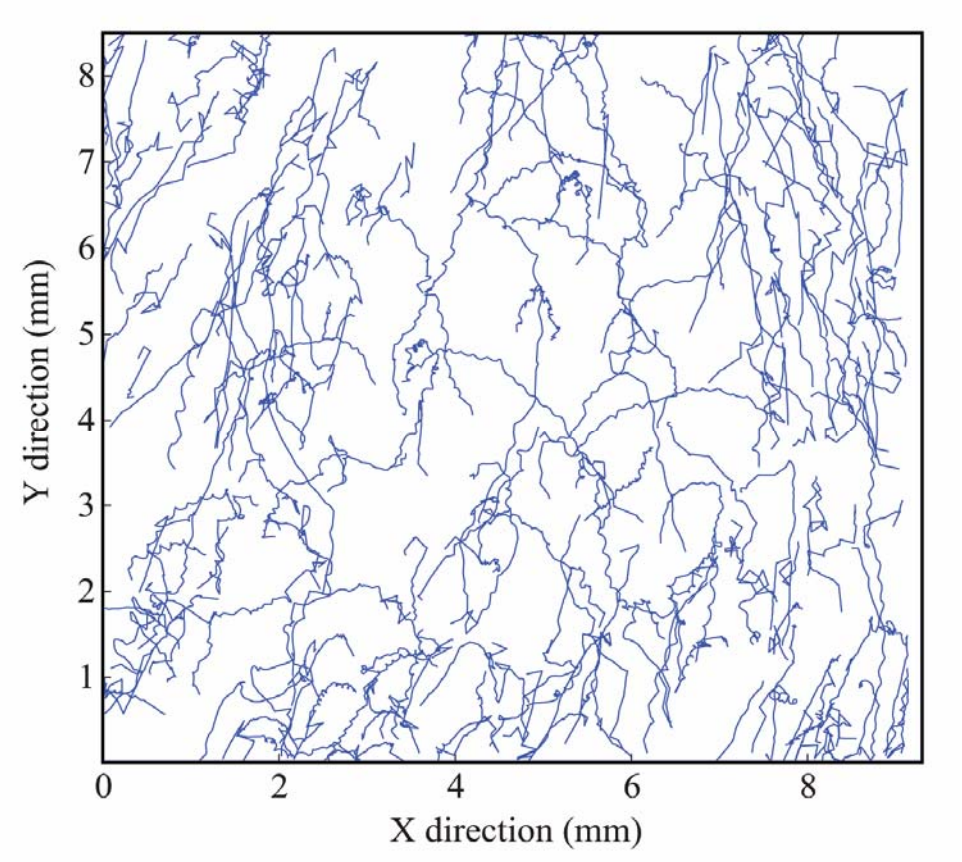

Figure 5.4 Trajectories of *Alexandrium*-sized particles over the duration of one 30s video clip (1/4x culture dilution) used to calibrate the IBET. The oscillatory movement (deviation from the central axis of the trajectory) observed for nearly all paths is a distinguishing feature of motile algal cells.

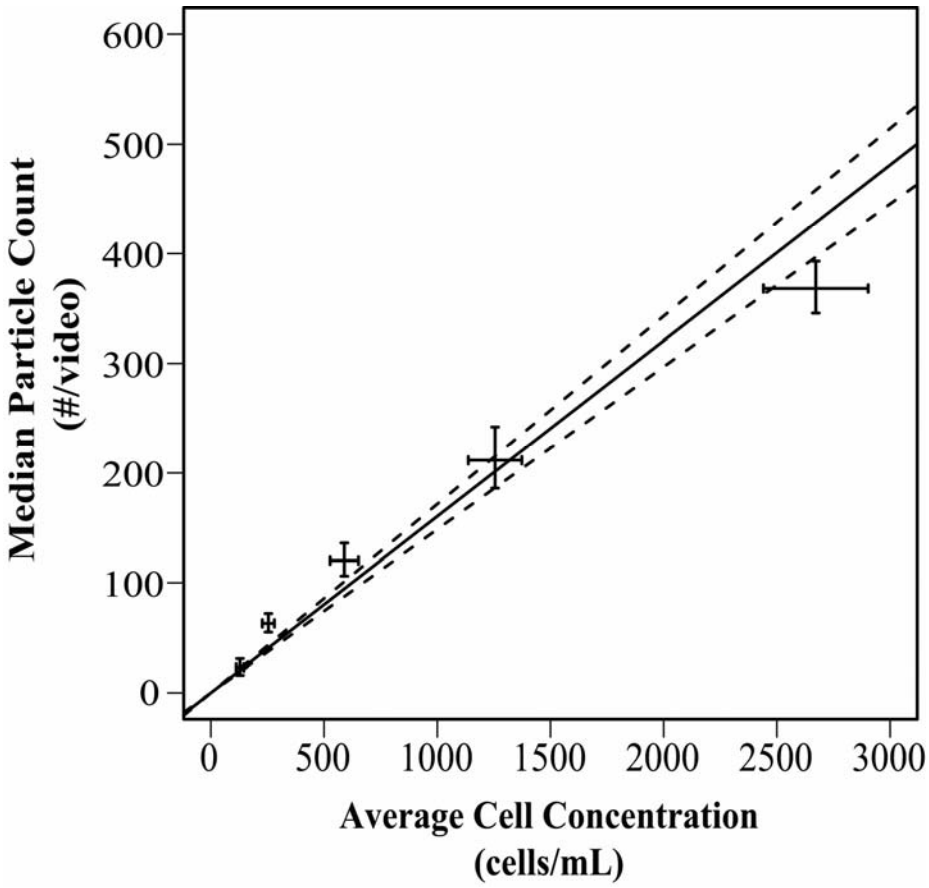

Figure 5.5. **The IBET calibration plot**. Video cell-sized particle counts (y – axis) and microscope cell concentrations (x – axis) are significantly correlated (Pearson's r = 0.992, df = 3, $p \leq 0.001$). Error bars represent 95% confidence intervals for the cell concentrations (horizontal) and the 2.5% and 97.5% quantiles of the video counts (vertical). The solid line (—) shows the relationship between IBET video particle counts (N) and true cell concentrations (C) bounded by 95% confidence intervals, dotted lines (- - -).

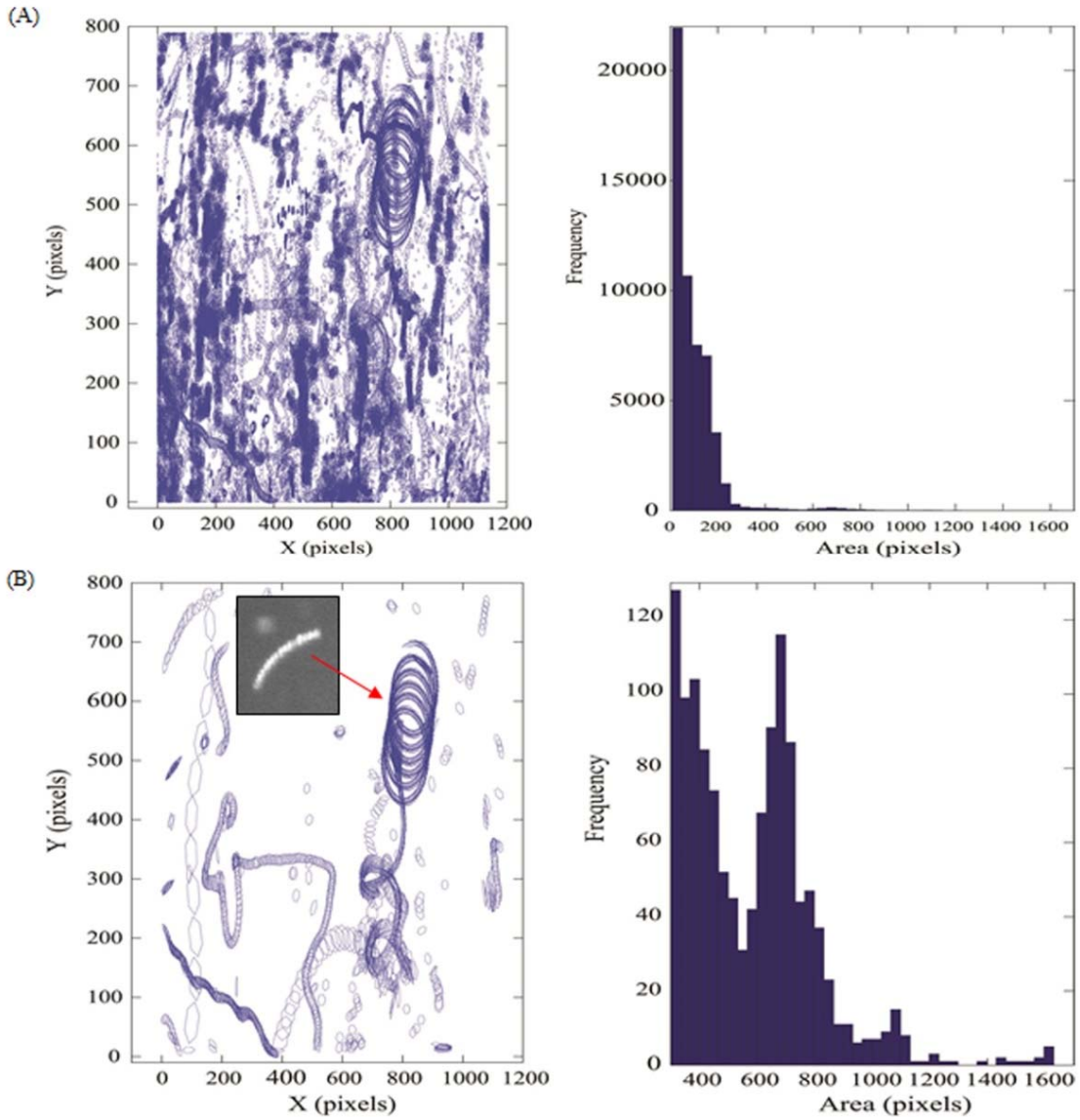

Figure 5.6 Sample field data collected by the IBET. (A) Example of the total abundance of plankton-like particles detected by the IBET in a single video clip. (B) Larger particle size fraction (300-1600 pixels) only. Plots on the left show best-fit ellipses for each organism tracked over the duration of the video. Plots on the right show the frequency of optical size (in pixel area). The red arrow (with video picture insert) points to the unique swimming pattern of a long *Alexandrium sp.* chain.

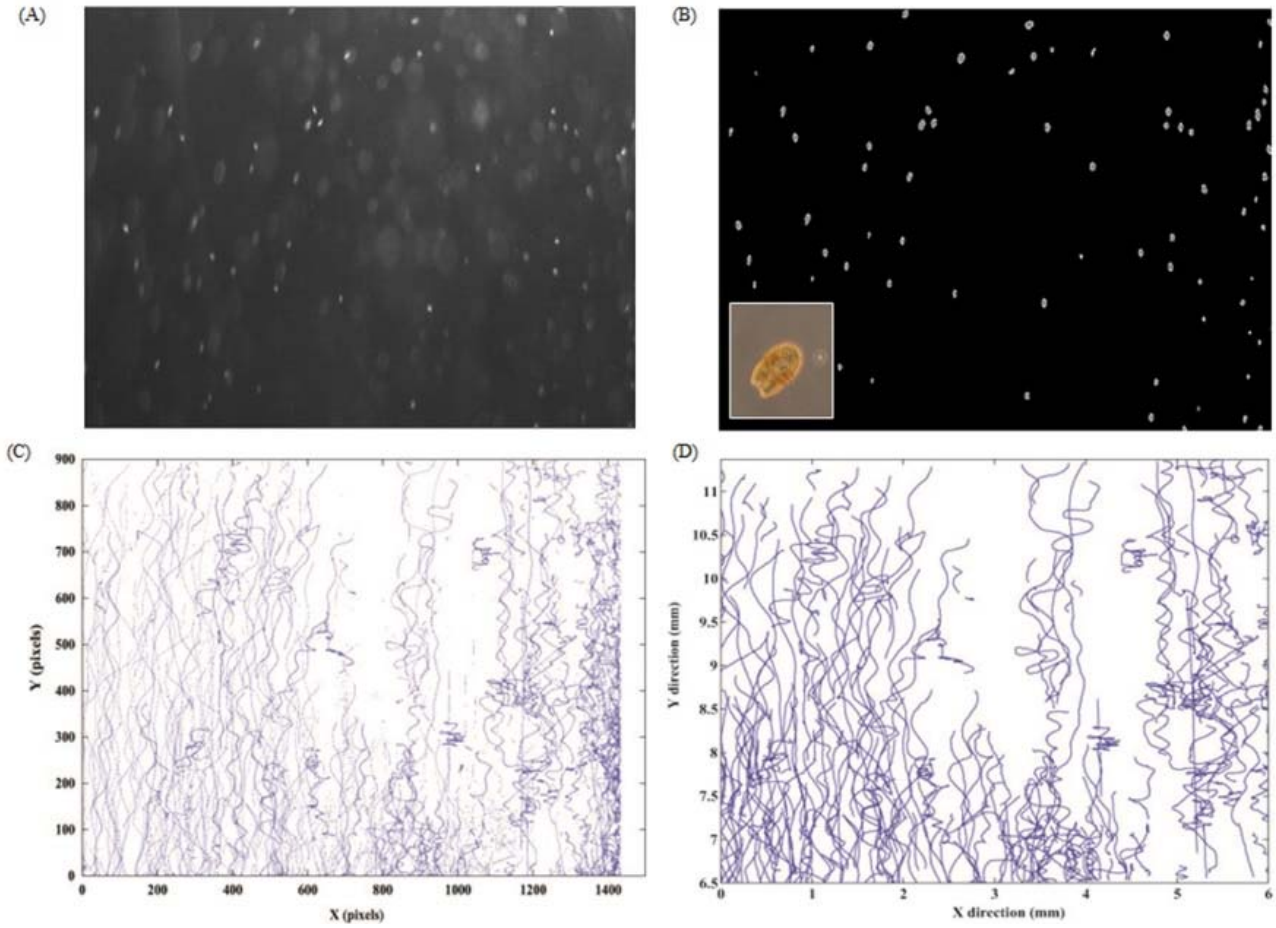

Figure 5.7 Example of data analysis steps from *in situ* video data collected by the IBET in Quartermaster Harbor, WA**.** (A) Image of the raw video footage collected by the IBET. (B) *A. sanguinea* cells targeted based on optical size. The inserted photo is *of A. sanguinea* cell collected from the sampling chamber for video validation. (C) Pixel positions of each cell plotted over the duration of the video clip. (D) Cell swimming trajectories are generated by converting pixel positions to physical coordinates.

Chapter 6. Summary and Conclusions

Quantifying biological and physical characteristics that influence algal cells' survival, growth and distributions is critical for understanding the fundamental ecological mechanisms that regulate HAB dynamics. Biological characteristics involve algal cell behavior (e.g. swimming) and physiology (e.g. life histories, metabolic processes, maintenance of energy reserves) which interact with physical characteristics (e.g., ambient currents and turbulence) to determine the location, magnitude and frequency of blooms [1,2]. Physiological traits expressed during life-stage transitions directly influence algal survival and growth. While algal distributions are largely determined by advection from ambient flows, cell-level swimming behaviors directly influence vertical positioning, and hence, interactions with different water masses. This dissertation has explored and quantified several key aspects of algal cell biology expressed during benthic and pelagic life stage transitions with the goal of improving knowledge about the mechanisms that regulate HABs in dynamic estuarine systems.

This research clearly demonstrated that quantification of behaviors expressed during pelagic and benthic life stage transitions can improve understanding of regional HAB dynamics. For example, the slow sedimentation rate observed for transitional *Heterosigma* cells in Chapter 3 verified that benthic distributions of *Heterosigma* are ultimately controlled by physical processes, suggesting that benthic distributions could be predicted by modeling interactions between cell sedimentation rates and geophysical flow patterns. Rapid variation in speed and direction of mean flows within deeper estuarine environments could cause interannual variability in benthic distributions, providing one explanation for the seemingly stochastic nature of *Heterosigm*a blooms in the Salish Sea [3,4].

It remains uncertain if such a simple mechanism of passive transport to the benthos can be applied to other HAB-forming species. However, it is unlikely for species with more complex life cycles, such as dinoflagellates that account for approximately 75% of known HAB species [1]. The sexually formed intermediate stage ("planozygote") of many dinoflagellates, distinct in morphology and swimming behavior, has been reported to remain motile in the water for days to weeks before undergoing encystment [5,6]. Planozygote swimming behaviors therefore have the potential to actively influence benthic distributions in ways that are currently not understood. More research is needed to improve understanding of how transitional behaviors expressed by different HAB species, particularly those with complex life cycles, influence distributions of benthic populations.

Examination of benthic-pelagic transitions for *A. catenella* in Chapter 2 and *Heterosigma* in Chapter 4 showed distinct species and strain-specific variation in fundamental biological traits that have the potential to regulate the timing and location of HABs. The results from Chapter 2 indicated that *Alexandrium* populations may operate under different benthic emergence ("germination") strategies. Variations in germination rates were observed within the Puget Sound *A. catenella* population and across geographically distinct *Alexandrium* populations. Similarly, results from Chapter 4 suggested that regionally distinct strains of *Heterosigma akashiwo* may operate under different population growth strategies during benthic-pelagic transition. Distinct strategies utilized by *Heterosigma* were shown to have the potential to influence vertical fluxes to surface waters, thereby governing the timescales over which *Heterosigma* blooms form.

The presence of both inter- and intra-specific variation during algal life stage transitions, as exhibited by both *Alexandrium* and *Heterosigma*, is likely to facilitate survival under a wide range of environmental conditions [7]. Such phenotypic diversity is widespread among many species of marine algae. Future consideration and quantification of variability in fundamental biological traits, such as those expressed during algal life stage transitions, will enhance our understanding of regional bloom dynamics and improve the biological accuracy of predictive modeling efforts.

While laboratory experiments allow researchers to obtain controlled and detailed information critical to understanding fundamental aspects of algal cell biology, it is often difficult to accurately infer the results of laboratory findings within the context of the organism's natural environment. Hence, *in situ* environmental measurements of algal abundances, behaviors and distributions are also needed to truly understand the ecological mechanisms that promote or repress HABs. This type of field-based detection and monitoring of harmful algae will require the development of inexpensive field-deployable sensors, such as the Imaging Benthic Emergance Trap (IBET) described in Chapter 5, capable of collecting data on disperse populations. Sensors to monitor algal abundance and behaviors in combination with molecular-based techniques to accurate identify algal species and/or strains (e.g., Environmental Sample Processor (ESP) [8] or genetic "fingerprinting" on collected water samples [Black and Cattolico pers. comm.]) will provide powerful tools for improved HAB detection and monitoring.

Future efforts towards improved HAB prediction and effective management and mitigation strategies will require interdisciplinary research initiatives and strong science-management partnerships. Comprehensive scientific understanding of regional HAB dynamics and assessment of future bloom scenarios will require integration of controlled laboratory experiments on algal cell biology, new technologies for environmental detection and monitoring of algal cells, and modeling approaches to simulate biophysical and trophic interactions. Sound science-based management of HABs and their impacts will require implementation of cooperative partnerships between scientific researchers, stakeholders (e.g., shellfish/fin-fish growers, managers, tribes) and policy makers [9]. Such integrative and multidisciplinary approaches will help meet present and future challenges in prediction and management of HABs.

6.1 References:

1. Smayda TJ (1997) Harmful algal blooms: Their ecophysiology and general relevence to phytoplankton blooms in the sea. Limnol Oceanogr 42: 1137–1153. doi:10.4319/lo.1997.42.5_part_2.1137.

2. Smayda TJ (2002) Turbulence, watermass stratification and harmful algal blooms: An alternative view and frontal zones as "pelagic seed banks." Harmful Algae 1: 95–112. doi:10.1016/S1568-9883(02)00010-0.

3. Connell L, Jacobs M (1998) Anatomy of a bloom: *Heterosigma carterae* in Puget Sound 1997. Puget Sound Res: 830–834.

4. Rensel JJE (2007) Fish kills from the harmful alga *Heterosigma akashiwo* in Puget Sound: Recent blooms and review. Prepared by Rensel Associates Aquatic Sciences for the National Oceanic and Atmospheric Administration Center for Sponsored Coastal Ocean Research (CSCOR), Washington, DC (2007): pp. 58.

5. Figueroa RI, Bravo I, Garcés E (2005) Effects of nutritional factors and different parental crosses on the encystment and excystment of *Alexandrium catenella* (Dinophyceae) in culture. Phycologia 44: 658–670. doi:10.2216/0031-8884(2005)44[658:eonfad]2.0.co;2.

6. Brosnahan ML (2011) Life cycle studies of the red tide dinoflagellate species complex *Alexandrium tamarense*. Doctoral dissertation, Massachusetts Institute of Technology.

7. Anderson DM (1998) Physiology and bloom dynamics of toxic *Alexandrium* Species, with emphasis on life cycle transitions. In: Anderson DM, Cembella AD, Hallefraeff GM, editors. Physiological Ecology of Harmful Algal Blooms. Springer-Verlag Berline Heidelberg. pp. 29–48.

8. Greenfield DI, Doucette GJ, Mikulski C, Jones K, Jensen S, et al. (2008) Field applications of the second-generation Environmental Sample Processor (ESP) for remote detection of harmful algae. Limnol Oceanogr: Methods 6: 667-679. doi:10.4319/lom.2008.6.667.

9. Chadsey M, Trainer VL, Leschine TM (2012) Cooperation of science and management for harmful algal blooms: Domoic acid and the Washington coast razor clam fishery. Coast Manag 40: 33–54. doi:10.1080/08920753.2011.639865.